Cluster radioactivity: exotic process or dominant nuclear decay

Michał Warda

Uniwersytet Marii Curie-Skłodowskiej
w Lublinie

Warszawa, 21.05.2026

Collaboration:

- Krzysztof Pomorski, UMCS, Lublin
- Luis M. Robledo, UAM, Madrid
- Rayner Rodriguez-Guzman, Nazarbayev University, Astana
- Anna Zdeb, UMCS, Lublin

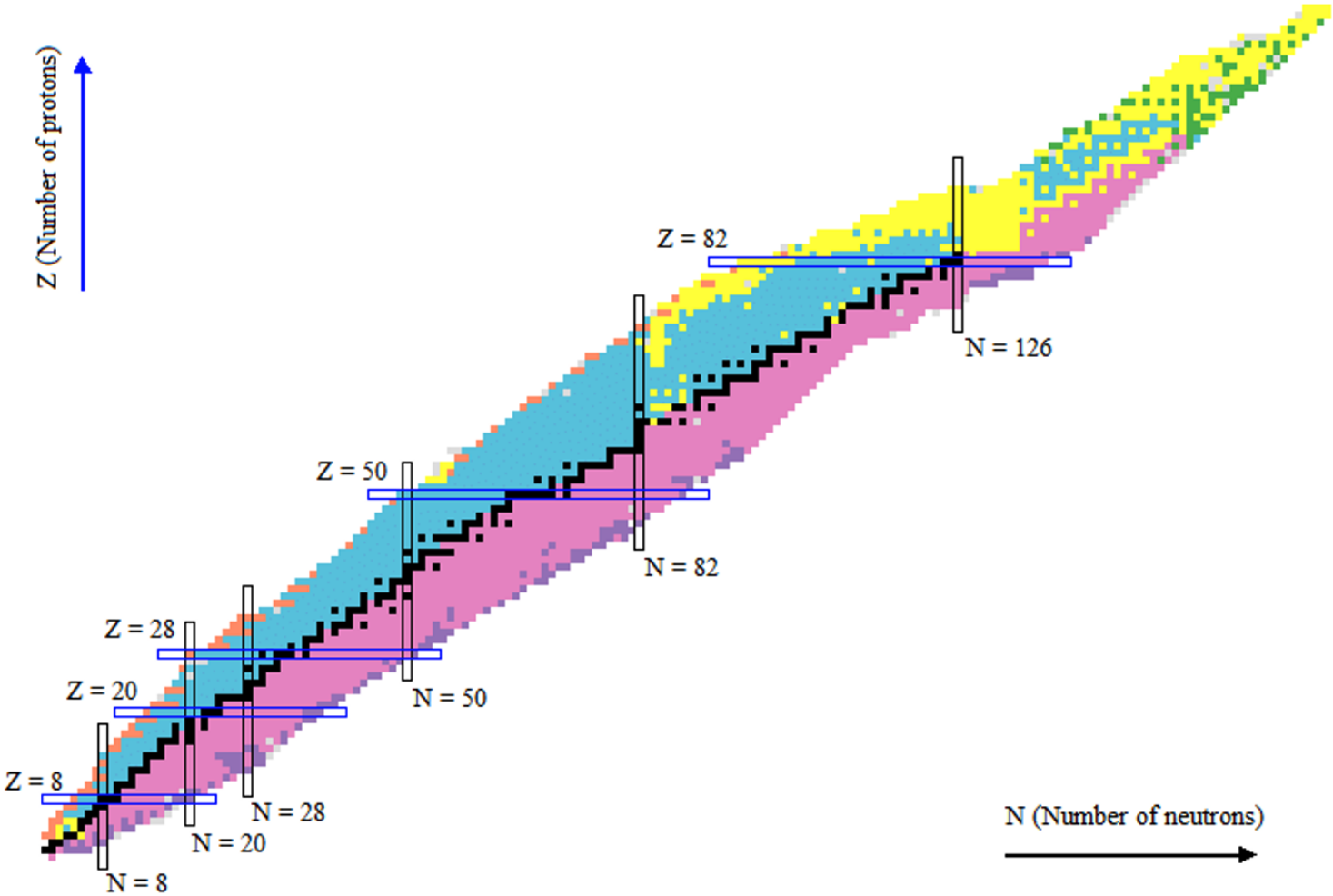
Z (Number of protons)
Z = 82
N = 126
Z = 50
N = 82
Z = 28
Z = 20
N = 50
Z = 8
N = 28
N = 20
N = 8
N (Number of neutrons)

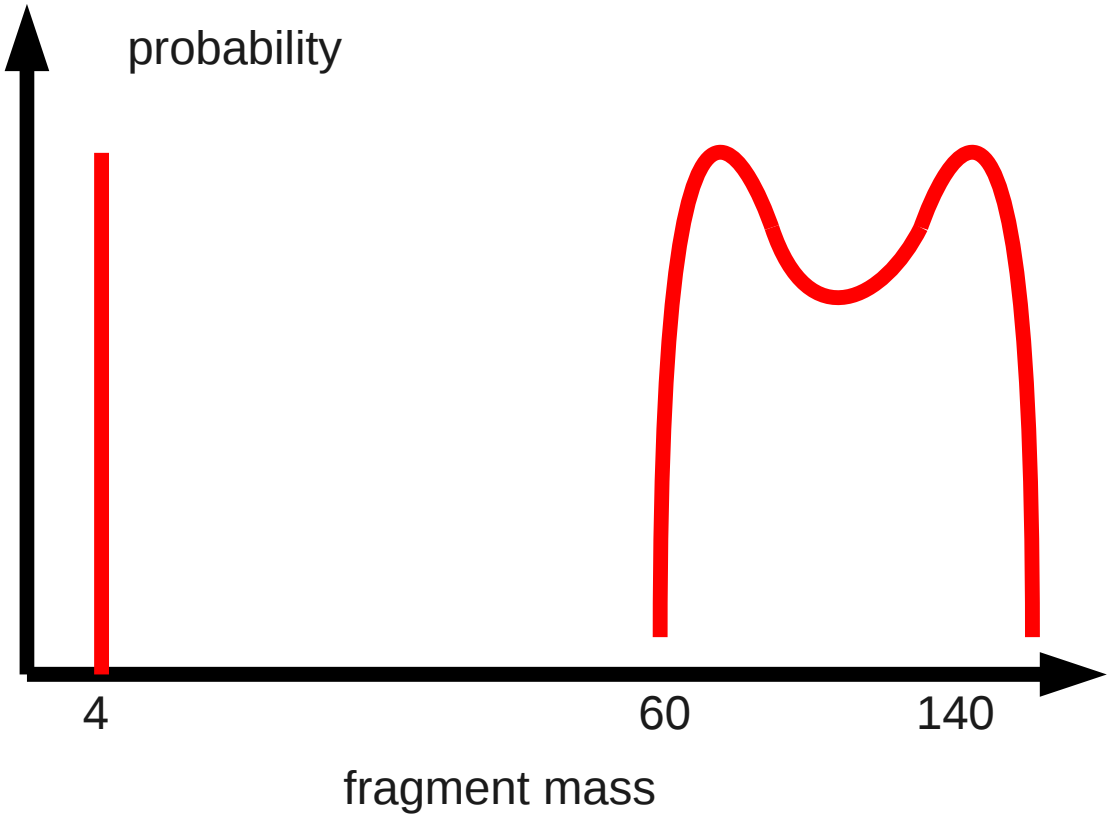
probability
4
60
140
fragment mass

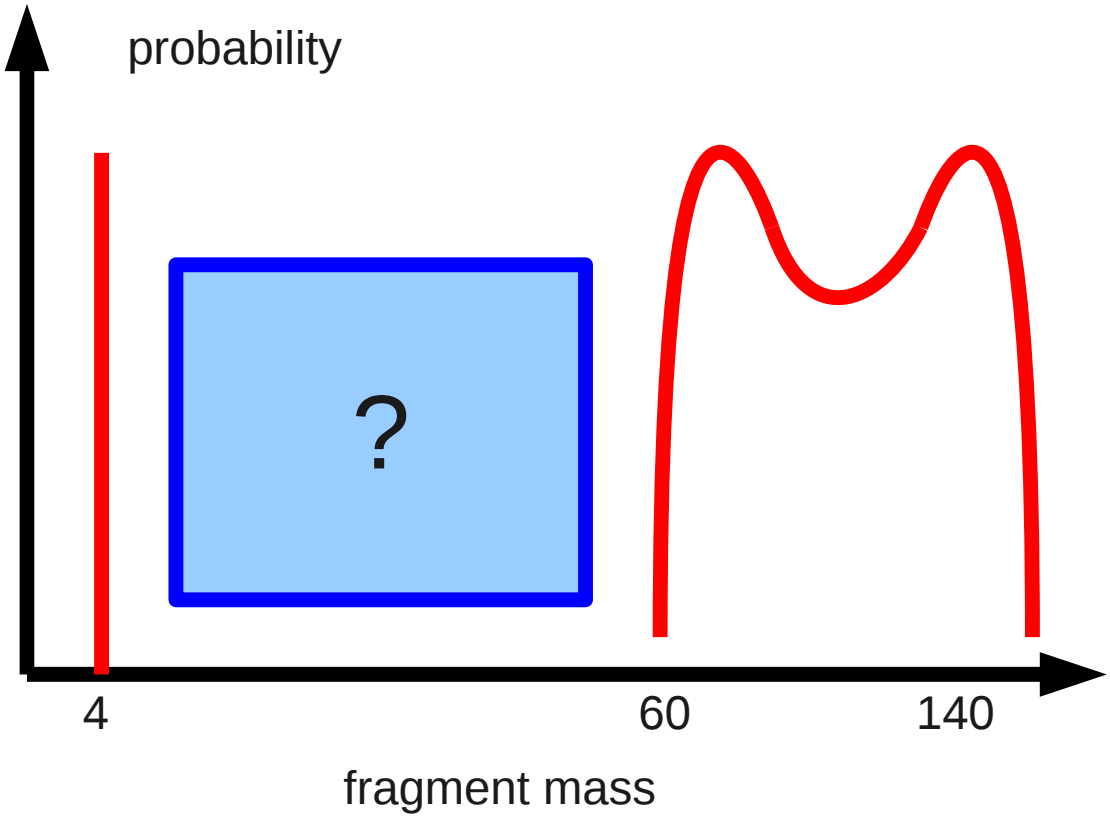
probability
?
4
60
140
fragment mass

Discovery of cluster radioactivity

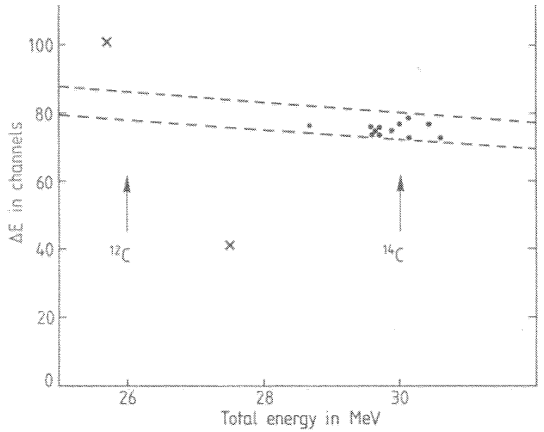

Fig. 1 Contents of the two-dimensional array ΔE versus E_{total} after a run of 189 days. The dotted line indicates the allowed region for carbon ions and the arrows indicate the total energies expected for ^{12}C and ^{14}C emissions in the decay of ^{223}Ra. The lower of the two crosses represents a quadruple pile-up. Below the total energy displayed, large numbers of triple and double α-pile-ups were recorded. Single α-events (and, in part, even double α-pile-ups) were biased out on the analogue side to avoid deadtime problems on the digital side. The upper cross is an event which was recorded during a thunderstorm which affected the mains badly. A run of 194 days was made before this one, yielding 8 events and, in addition, a run of approximately half a year was performed to investigate possible cosmic ray-induced events. Channel 77 in $\Delta E \cong 6.7$ MeV, which is exactly as expected for 30 MeV ^{14}C. Detector characteristics: The dead layer of the ΔE detector (200 mm^2 active area, 8.2 μm sensitive thickness) was determined to lie between 0.3 and 0.8 μm. In addition a protective layer of gold of thickness 20 μg cm^{-2} was evaporated on the source and 15 μg cm^{-2} carbon film inserted between the source and the ΔE detector. An extra 30–40 μg cm^{-2} of gold is present on the E-detector (300 mm^2 active area). This gives a total of 150–250 μg cm^{-2} of effective dead layer (Si equivalent) and an energy loss of ^{14}C ions of 0.5–0.8 MeV. The source of strength 3.3 μCi gave a counting rate of ≈4,000 s^{-1}, corresponding to an effective solid angle of detection of ≈1/3 sr.

$$^{223}_{88}\text{Ra} \longrightarrow {}^{14}\text{C} + {}^{209}\text{Pb}$$

H.J. Rose and G.A. Jones, *Nature* **307**, 245 (1984)
Sandulescu, Poenaru and Greiner, *Sov. J. Part Nucl.* **11**, 528 (1980)

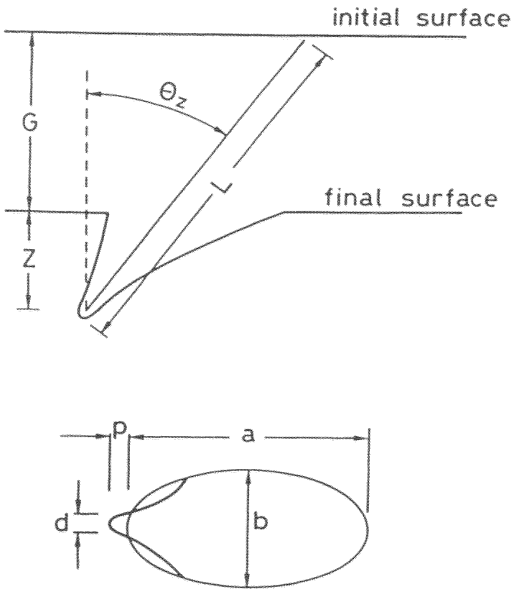

Fig. 1. Geometry of a track etched until the end of the particle range, L. G is the thickness of the material etched away, d the tip diameter, a and b the major and minor axes, p the overhang, Θ_z the zenith angle, z the track depth.

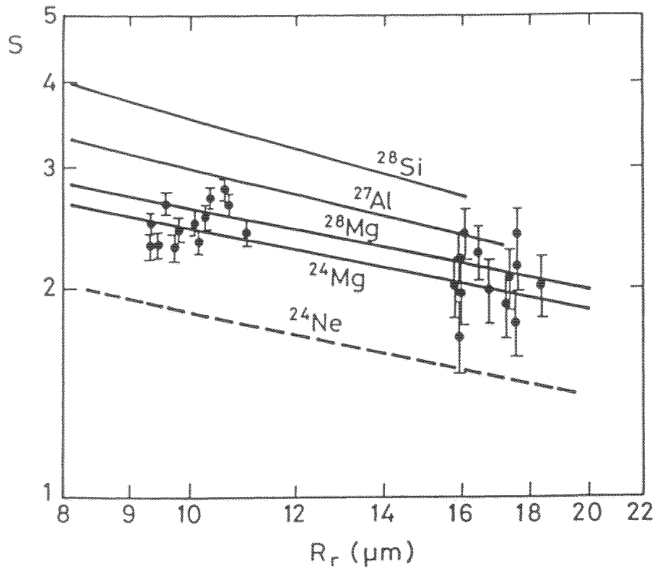

Fig. 6. Comparison of the sensitivity S measured at two stages of the etching process for the 15 events from the decay of ^{236}Pu with accelerator calibrations. Reprinted with permission from M. Hussonnois et al., "Cluster decay of ^{236}Pu and correlations of the probabilities of α decay, cluster decay and spontaneous fission of heavy nuclei" JETP Letters 62 (1995) p 701. Copyright 1995 American Institute of Physics.

R. Bonetti, A. Guglielmetti, in *Heavy Elements and Related New Phenomena Vol II, ed. W. Greiner and R.K. Gupta*, p.634, Word Scientific, 1999

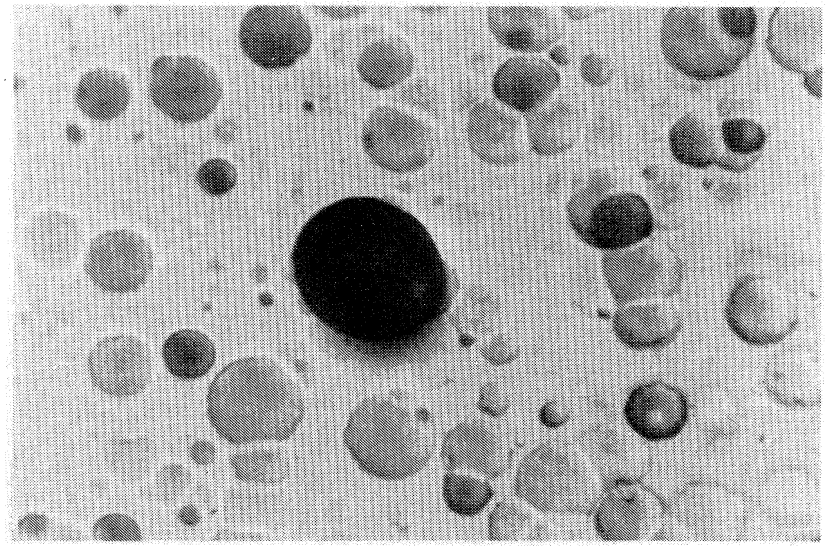

FIG. 1. Photomicrograph showing one etch pit due to a 56 MeV ^{24}Ne ion striking a Cronar detector nearly head on. About 3×10^6 alpha particles passed through this field of view.

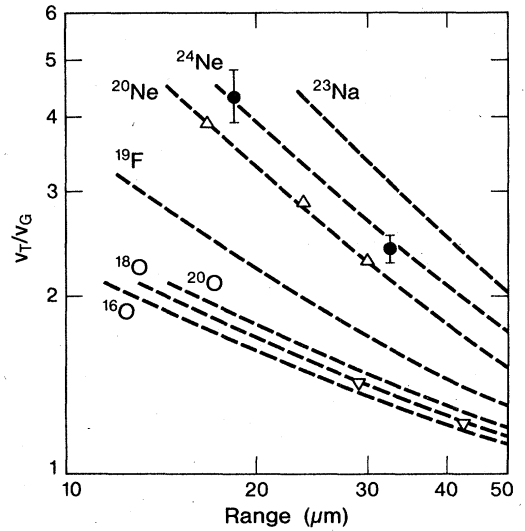

FIG. 2. Comparison of average signal of ^{24}Ne nuclei (●) emitted from ^{232}U with calibrations (dashed lines) obtained with ^{18}O (▽) and ^{20}Ne (△) ions at Lawrence Berkeley Laboratory accelerators. Ratio of etching rate along track to general etching rate v_T/v_G, is plotted as a function of residual range.

Barwick et al., PRC **31**, 1984 (1985)

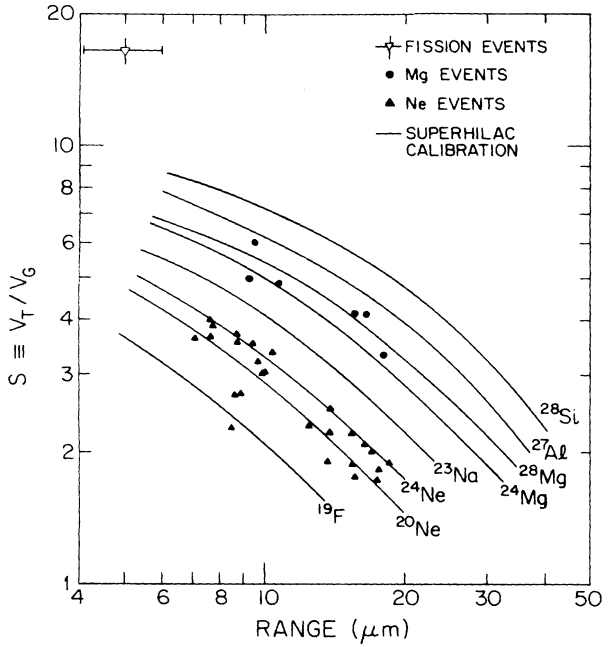

FIG. 1. Identification of ions emitted from ^{234}U as Ne and Mg. The curves are based on calibrations obtained with ^{28}Si, ^{24}Mg, and ^{20}Ne ions at Lawrence Berkeley Laboratory SuperHilac.

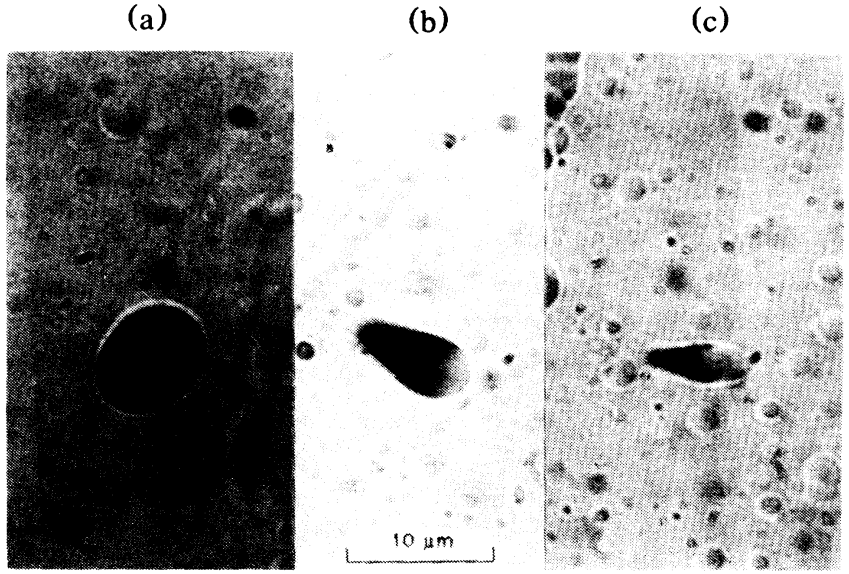

FIG. 2. Photomicrographs showing etch pits due to (a) spontaneous fission, (b) Mg emission, and (c) Ne emission from ^{234}U source.

Wang et al., PRC **36**, 2717 (1987)

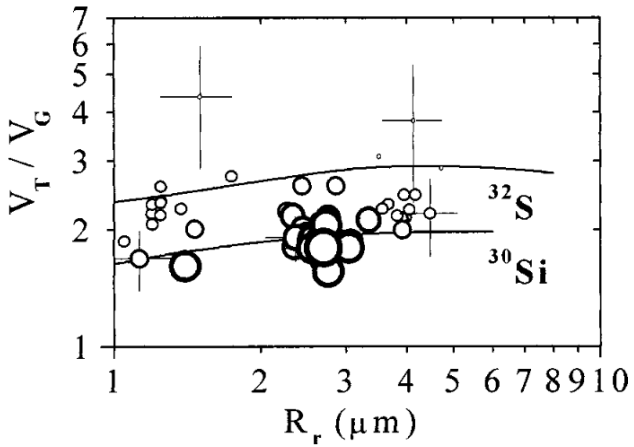

FIG. 2. Ratio of etching rates $\mathbf{S}=V_T/V_G$ versus the residual range for tracks registered after exposition of the detectors to ^{242}Cm. The diameters of the circles are inversely related with the error values of **S**. The solid lines are the results of calibration with ^{30}Si and ^{32}S ions. The smallest and largest errors are shown as examples.

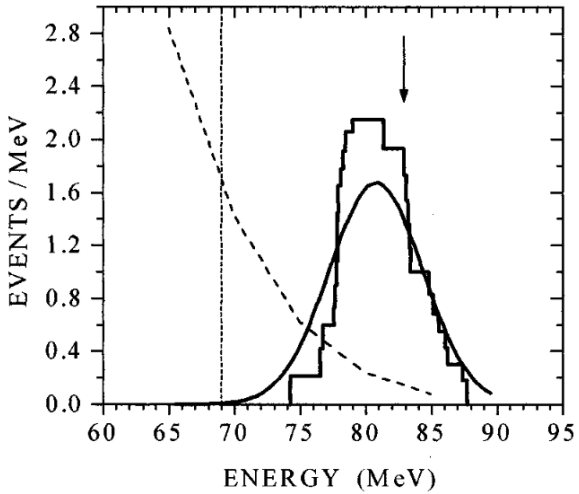

FIG. 4. Energy spectrum of the Si particles emitted from ^{242}Cm sources. The dashed line shows the possible effect due to ternary fission. The dotted line shows the registration threshold due to the combined effect of absorbers and the range deficit in the glass detector ($3.24\pm0.6\,\mu$m see text). The arrow shows the ^{34}Si cluster kinetic energy following from the decay Q value.

A.A. Ogloblin et al., PRC **61**, 034301 (2000)

Cluster radioactivity: key facts

- Emitters: $^{221}_{87}$Fr — $^{242}_{96}$Cm
  experimental evidence in 12 even-even, 9 odd nuclei
- Clusters: ^{14}C — ^{34}Si
- Heavy mass residue: doubly magic ^{208}Pb ± 4 nucleons
  "Lead radioactivity"
- Half lives: 10^{11} s – 10^{26} s
- α branching ratio: 10^{-9} – 10^{-16}

Cluster radioactivity: key facts

- Emitters: $^{221}_{87}$Fr — $^{242}_{96}$Cm
  experimental evidence in 12 even-even, 9 odd nuclei
- Clusters: ^{14}C — ^{34}Si
- Heavy mass residue: doubly magic ^{208}Pb ± 4 nucleons
  "Lead radioactivity"
- Half lives: 10^{11} s – 10^{26} s
- α branching ratio: 10^{-9} – 10^{-16}

Cluster radioactivity: key facts

- Emitters: $^{221}_{87}$Fr — $^{242}_{96}$Cm
  experimental evidence in 12 even-even, 9 odd nuclei
- Clusters: ^{14}C — ^{34}Si
- Heavy mass residue: doubly magic ^{208}Pb ± 4 nucleons
  "Lead radioactivity"
- Half lives: 10^{11} s – 10^{26} s
- α branching ratio: 10^{-9} – 10^{-16}

Cluster radioactivity: key facts

- Emitters: $^{221}_{87}$Fr — $^{242}_{96}$Cm
  experimental evidence in 12 even-even, 9 odd nuclei
- Clusters: ^{14}C — ^{34}Si
- Heavy mass residue: doubly magic ^{208}Pb $\pm$4 nucleons
  "Lead radioactivity"
- Half lives: 10^{11} s – 10^{26} s
- α branching ratio: $10^{-9} - 10^{-16}$

Cluster radioactivity: key facts

- Emitters: $^{221}_{87}$Fr — $^{242}_{96}$Cm
  experimental evidence in 12 even-even, 9 odd nuclei
- Clusters: ^{14}C — ^{34}Si
- Heavy mass residue: doubly magic ^{208}Pb $\pm$4 nucleons
  "Lead radioactivity"
- Half lives: 10^{11} s – 10^{26} s
- α branching ratio: 10^{-9} – 10^{-16}

Cluster radioactivity: key facts

- Emitters: $^{221}_{87}$Fr — $^{242}_{96}$Cm
  experimental evidence in 12 even-even, 9 odd nuclei
- Clusters: ^{14}C — ^{34}Si
- Heavy mass residue: doubly magic ^{208}Pb $\pm$4 nucleons
  "Lead radioactivity"
- Half lives: 10^{11} s – 10^{26} s
- α branching ratio: 10^{-9} – 10^{-16}

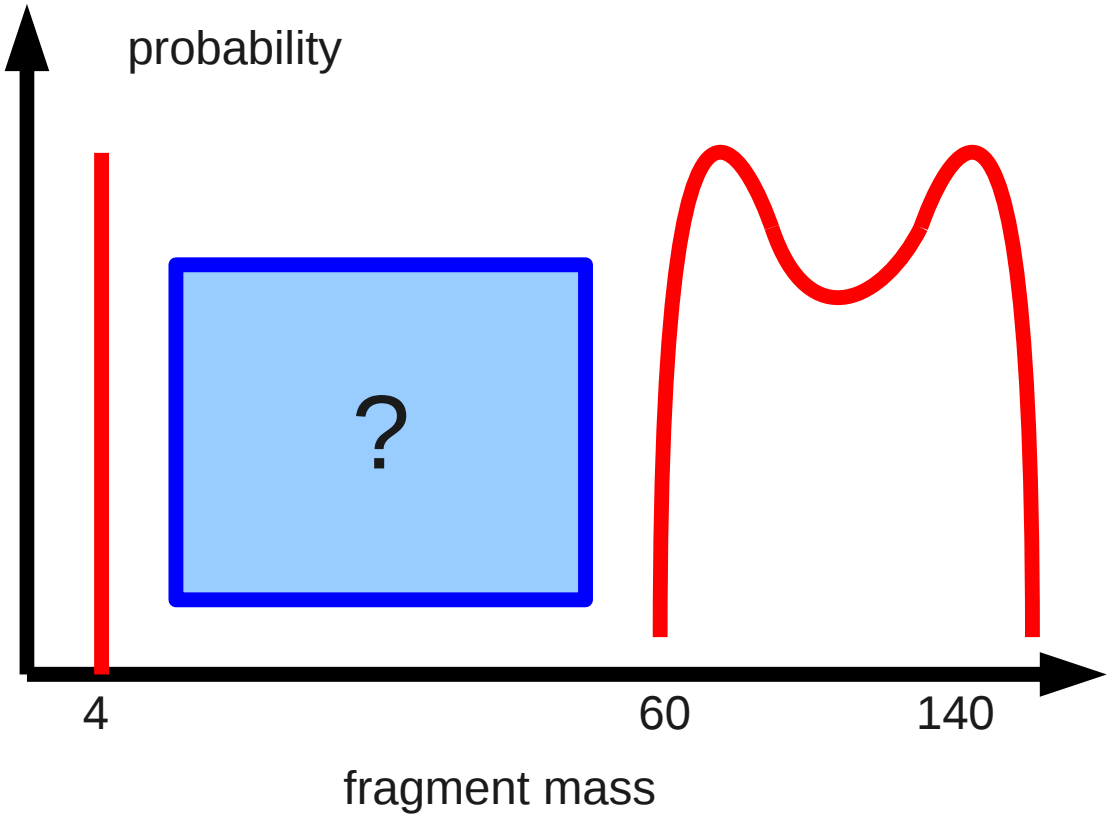
probability
?
4
60
140
fragment mass

Theoretical description

- Extrapolation of Gamov model of alpha emission
  Modified Geiger-Nuttall formula for half-lives

Theoretical description

- Extrapolation of Gamov model of alpha emission
  Modified Geiger-Nuttall formula for half-lives

$$\log_{10} T_{1/2}^{AZ} = \frac{aA_2\eta + bZ_2\eta_z}{\sqrt{Q}} + c.$$

$a = 10.603$, $b = 78.027$, and $c = -80.66$

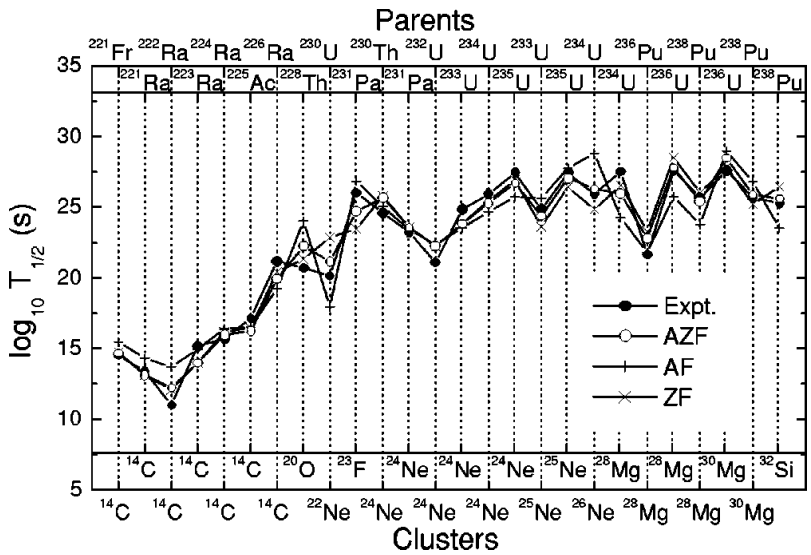

FIG. 1. $\log_{10} T_{1/2}$ (s) for different clusters emitted from various radioactive parents, calculated by using the AZ formula (AZF) and compared with experimental data. Also, the results of calculations for AF ($b=0$) and ZF ($a=0$) truncations of AZF are shown for comparisons.

Balasubramaniam et al., PRC **70**, 017301 (2004)

$$\log_{10} T_{1/2} = a\sqrt{\mu} Z_c Z_d Q^{-1/2} + b\sqrt{\mu}(Z_c Z_d)^{1/2} + c$$

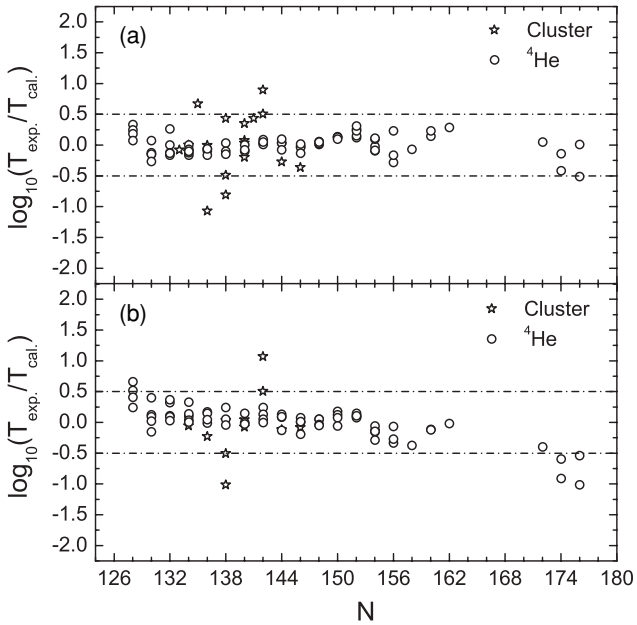

FIG. 4. Deviations between the logarithms of the experimental data and of the calculated values for even-even nuclei (a) when we use two sets of parameters to describe α decay and cluster radioactivity respectively and (b) when we use one set of parameters to describe both α decay and cluster radioactivity at the same time.

Ni et al., PRC **78**, 044310 (2008)

$$V(r) = \begin{cases} -V_0 & 0 \le r \le R \\ \frac{Z_1 Z_2 e^2}{r} & r > R \end{cases}$$

$$R = r_0(A_1^{1/3} + A_2^{1/3})$$

$$b = \frac{Z_1 Z_2 e^2}{E_k}$$

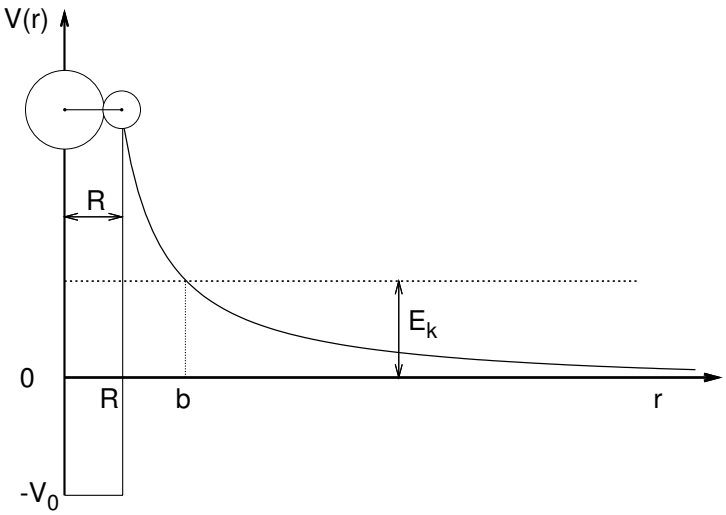

$$P = \exp\left[-\frac{2}{\hbar}\int_R^b \sqrt{2\mu(V(x) - E_k)}dx\right]$$

$$P = \exp\left\{-\frac{2}{\hbar}\sqrt{2\mu Z_1 Z_2 e^2 b}\left[\arccos\sqrt{\frac{R}{b}} - \sqrt{\frac{R}{b} - \left(\frac{R}{b}\right)^2}\right]\right\}$$

A. Zdeb, M. Warda, K. Pomorski, Phys. Rev. C87 024308 (2013)

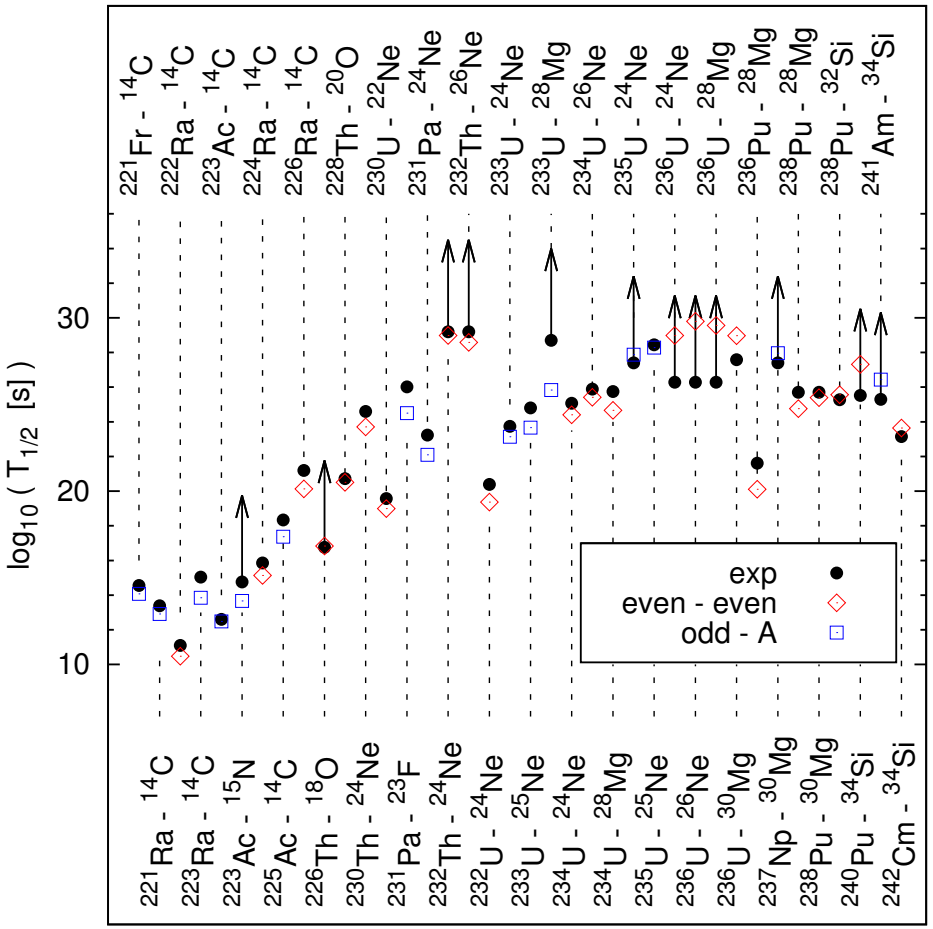

$$T_{1/2} = \frac{\ln 2}{P\nu} \cdot 10^h$$

$$\nu = \frac{\pi\hbar}{2\mu R^2}$$

$$r_0 = 1.21 \text{ fm}$$

$$h = 1.973$$

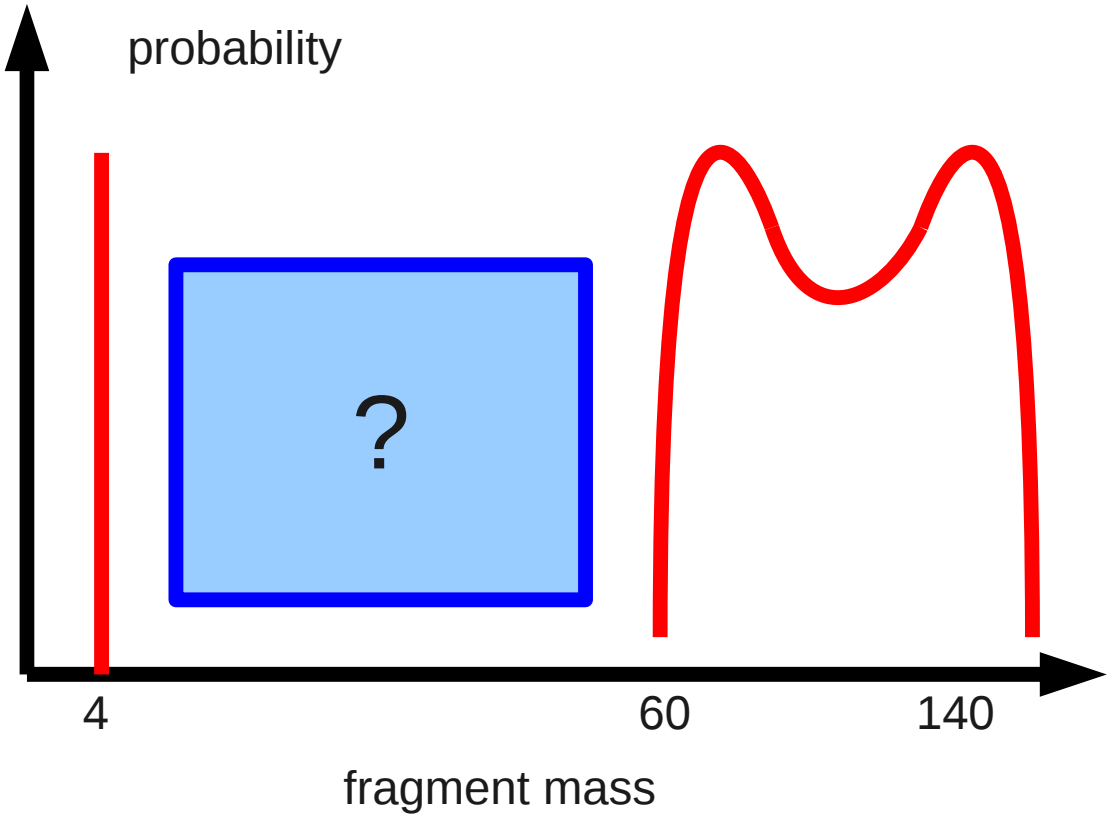
probability
?
4
60
140
fragment mass

Theoretical description

- **Super-asymmetric** fission
- Potential energy surfaces are determined in the self-consistent procedure in HFB theory with Gogny D1S force

Theoretical description

- **Super-asymmetric** fission
- Potential energy surfaces are determined in the self-consistent procedure in HFB theory with Gogny D1S force

Theoretical description

- **Super-asymmetric** fission
- Potential energy surfaces are determined in the self-consistent procedure in HFB theory with Gogny D1S force

Shape evolution: ^{238}Pu

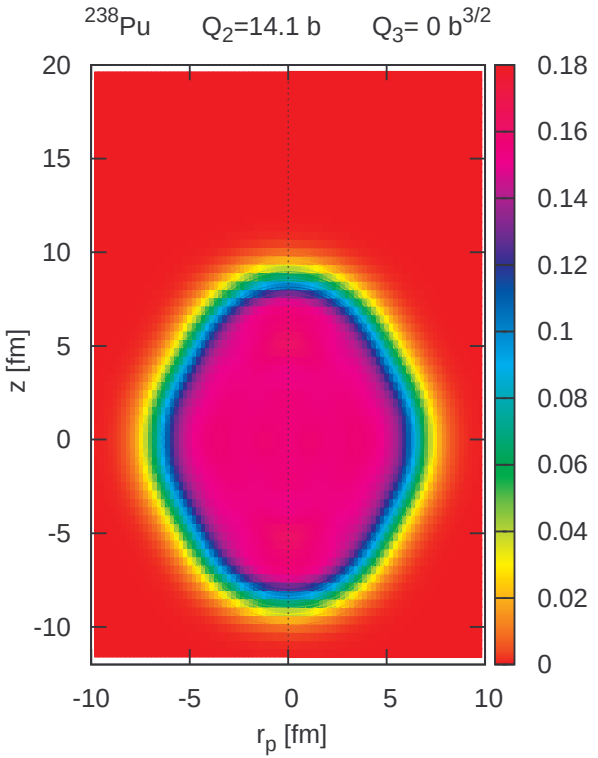

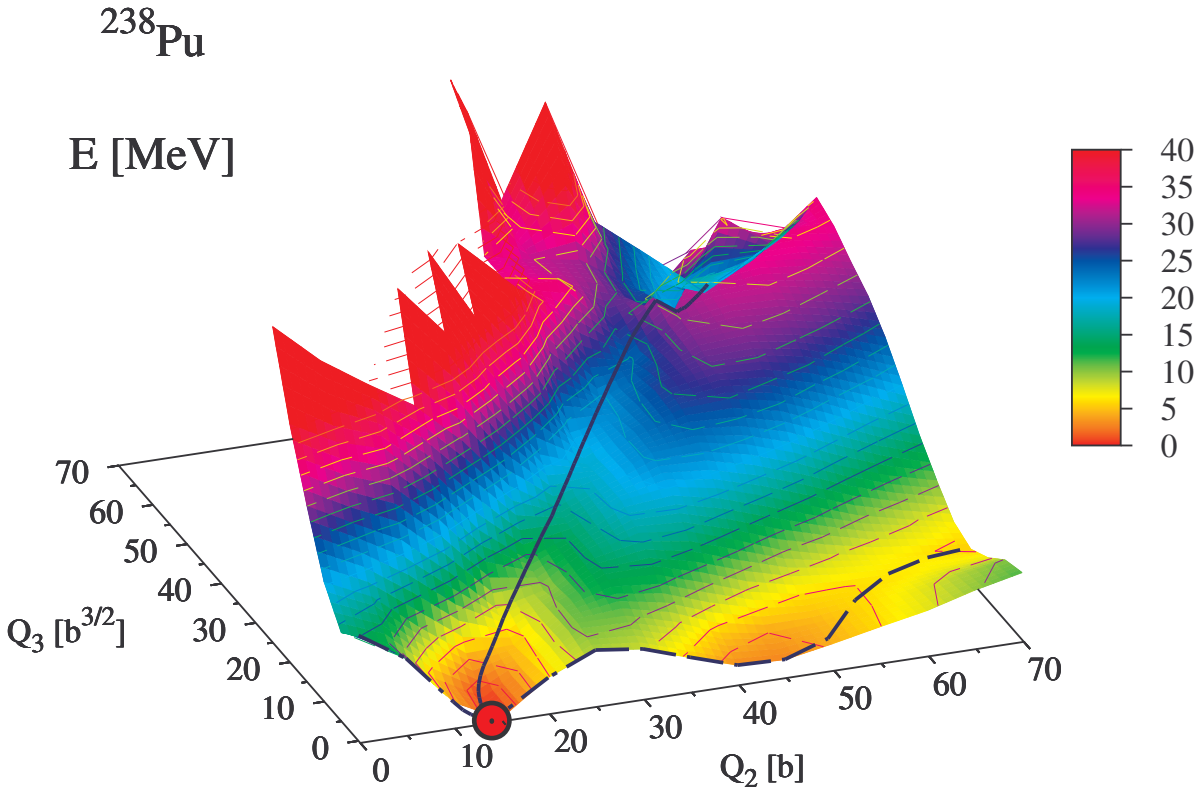

M. Warda and L. M. Robledo, Phys. Rev. C 84, 044608 (2011).

Shape evolution: ^{238}Pu

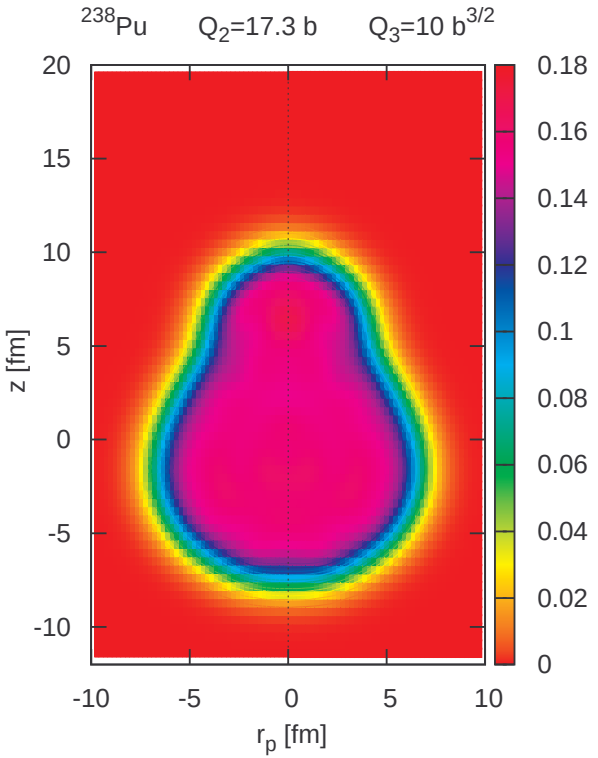

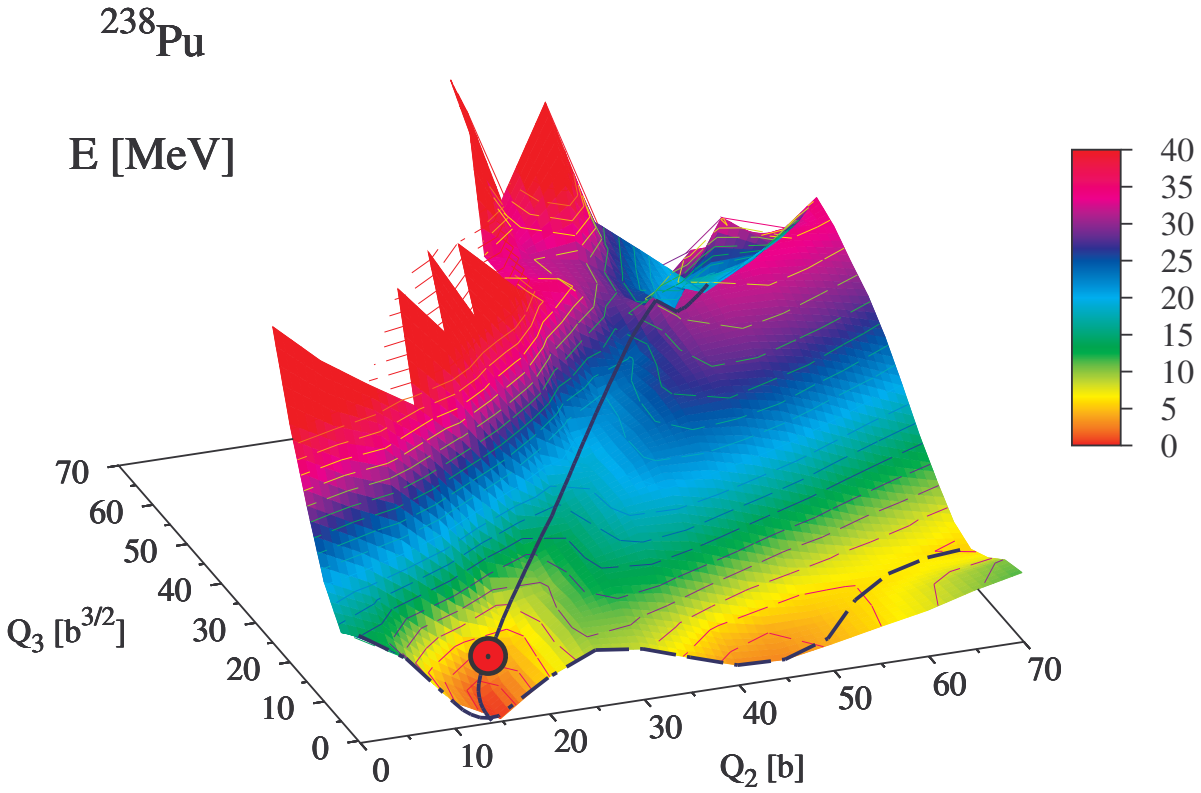

M. Warda and L. M. Robledo, Phys. Rev. C 84, 044608 (2011).

Shape evolution: ^{238}Pu

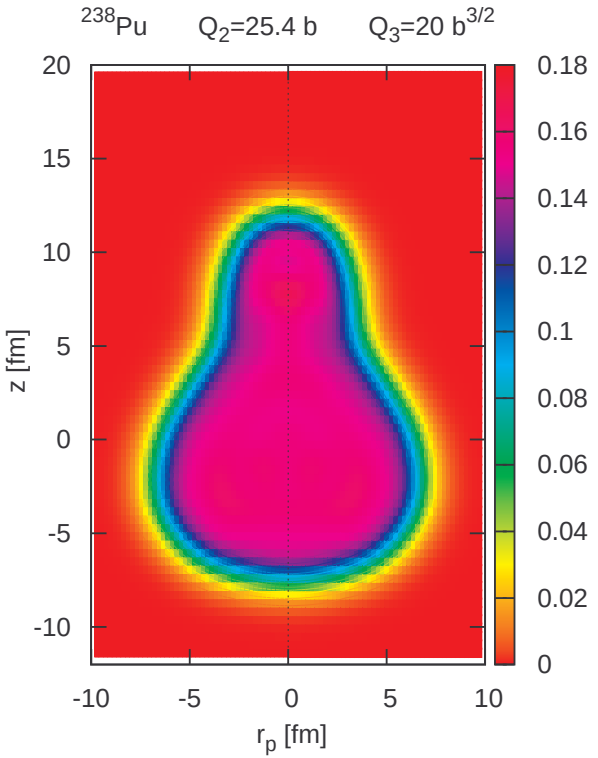

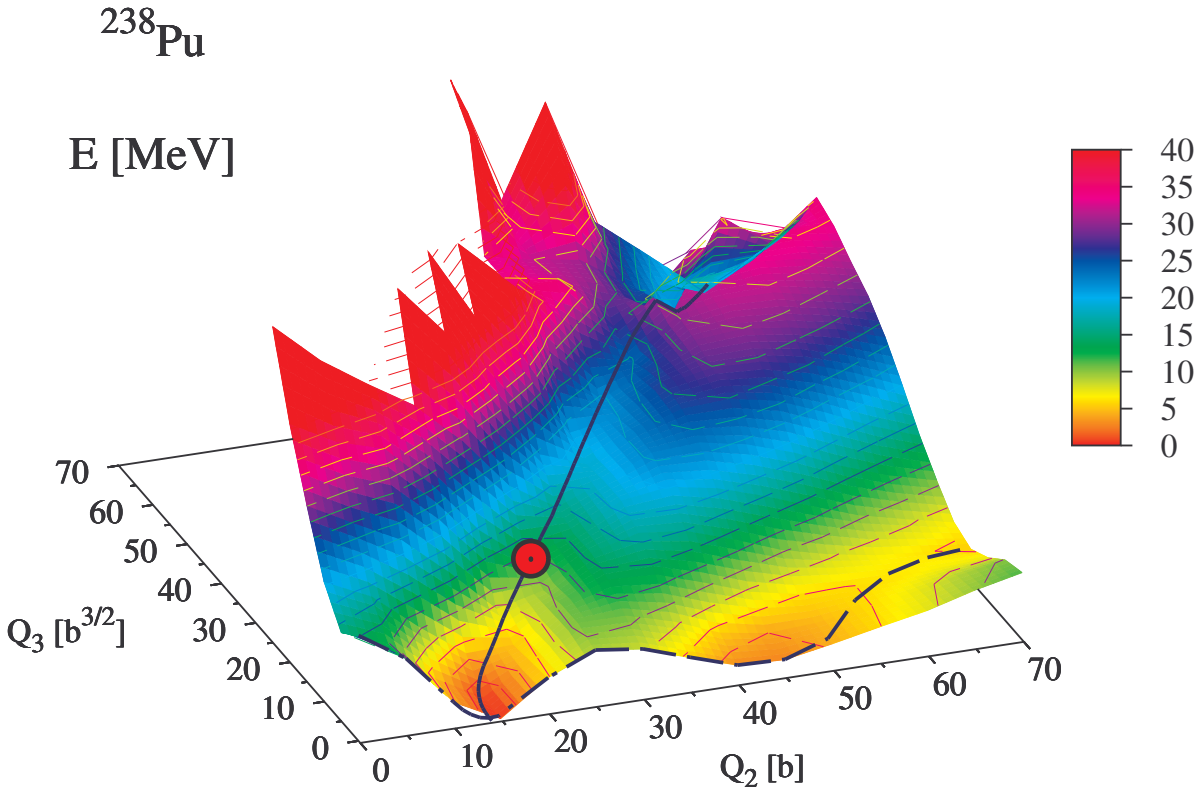

M. Warda and L. M. Robledo, Phys. Rev. C 84, 044608 (2011).

Shape evolution: ^{238}Pu

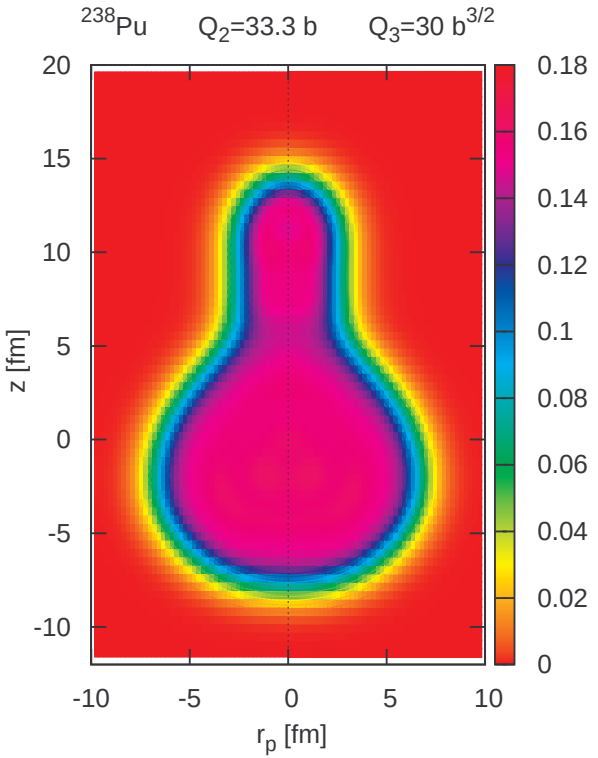

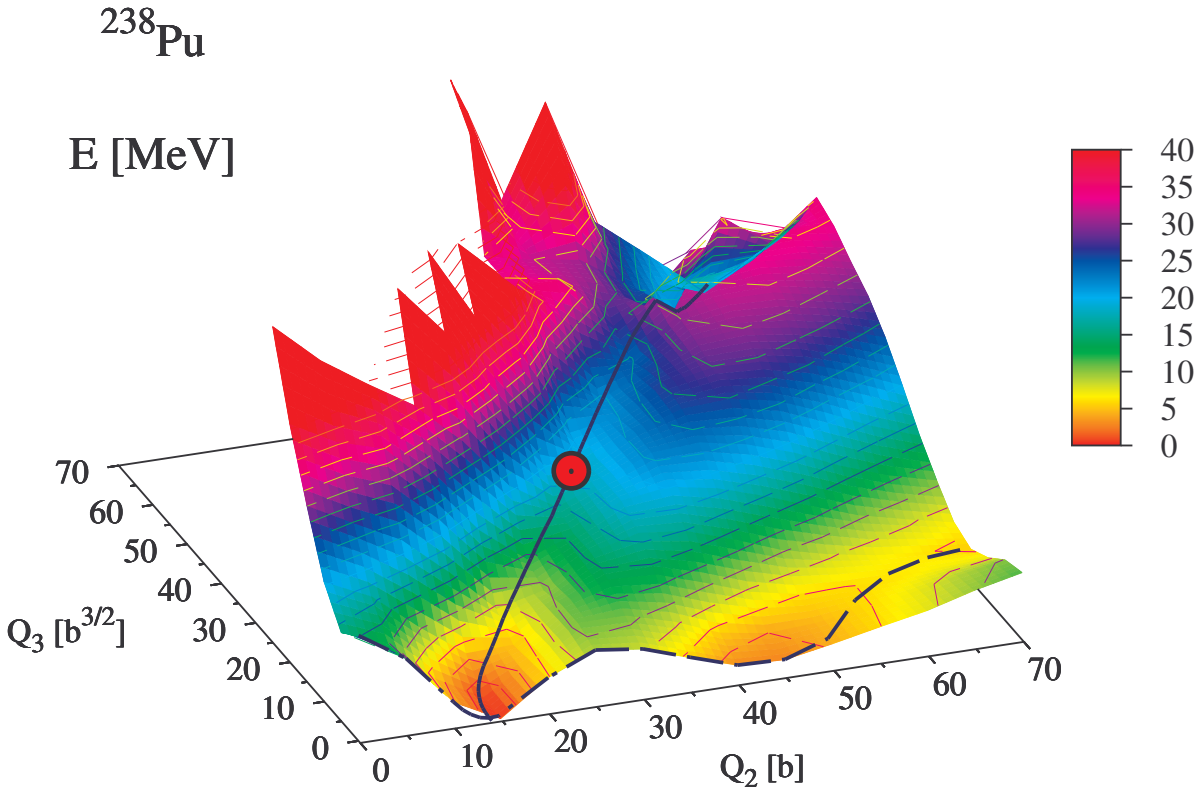

M. Warda and L. M. Robledo, Phys. Rev. C 84, 044608 (2011).

Shape evolution: ^{238}Pu

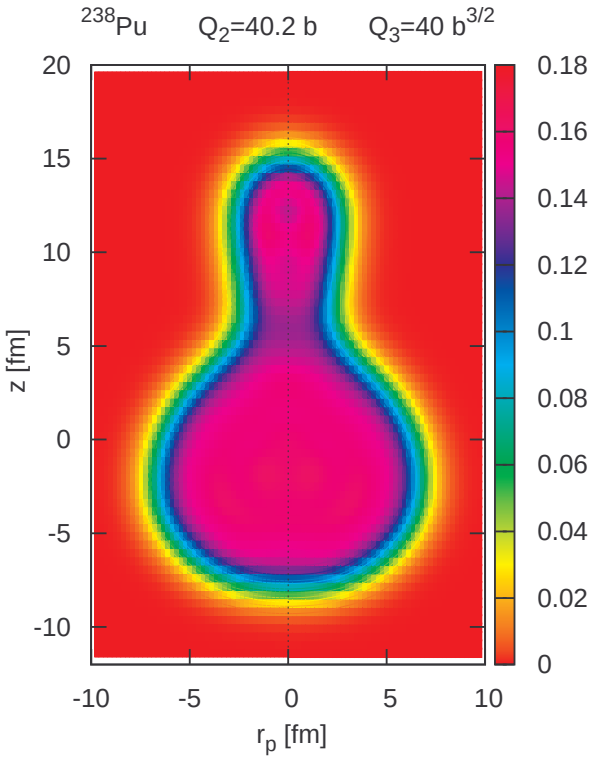

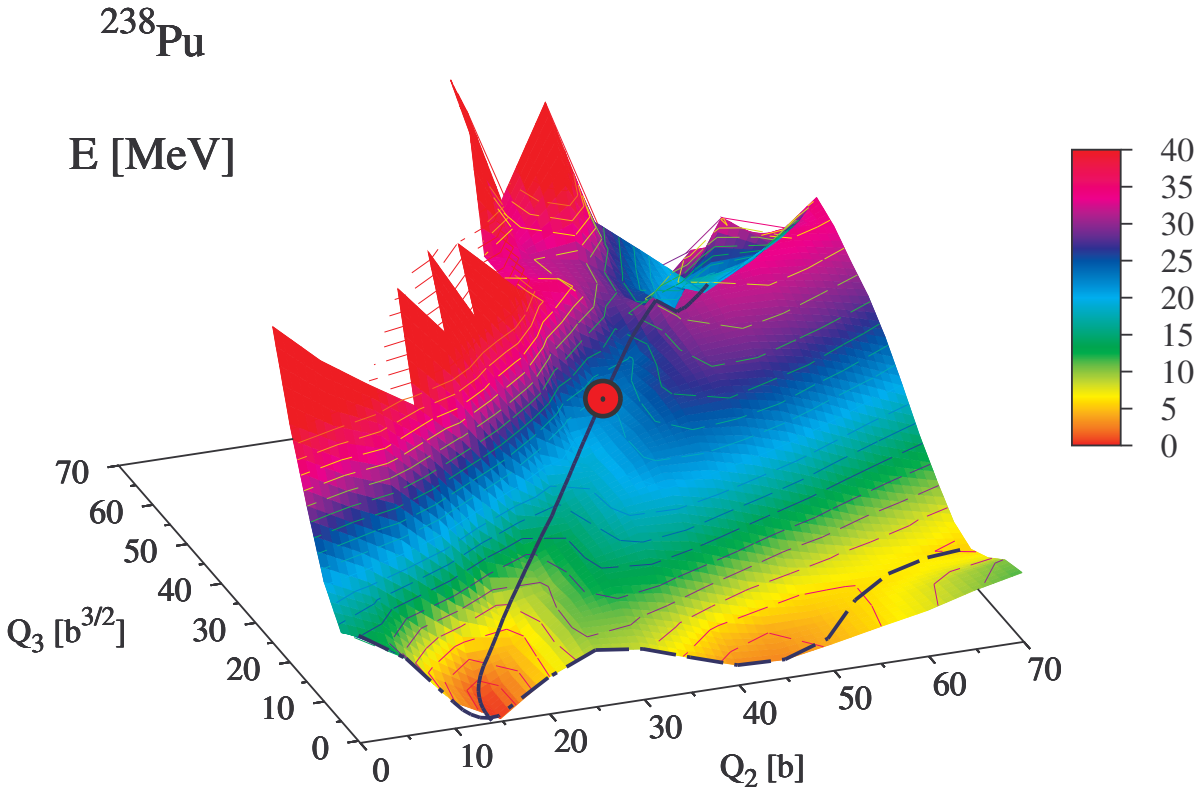

M. Warda and L. M. Robledo, Phys. Rev. C 84, 044608 (2011).

Shape evolution: ^{238}Pu

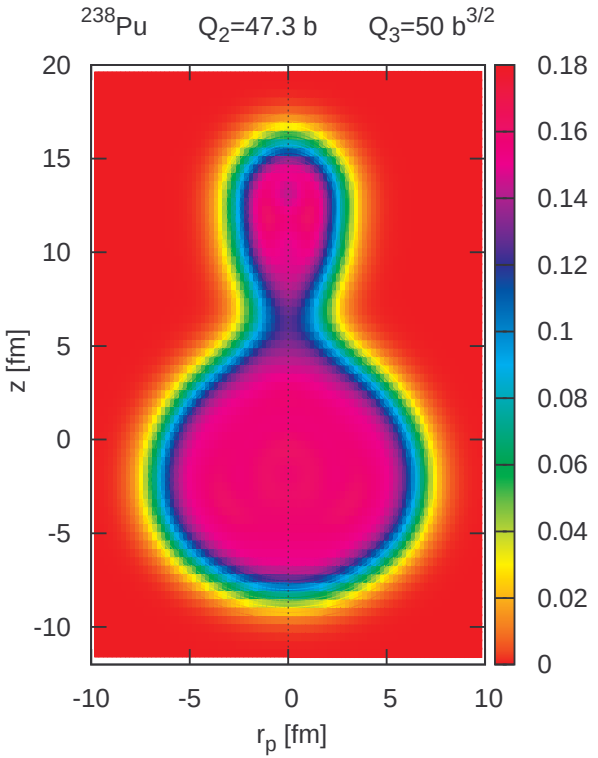

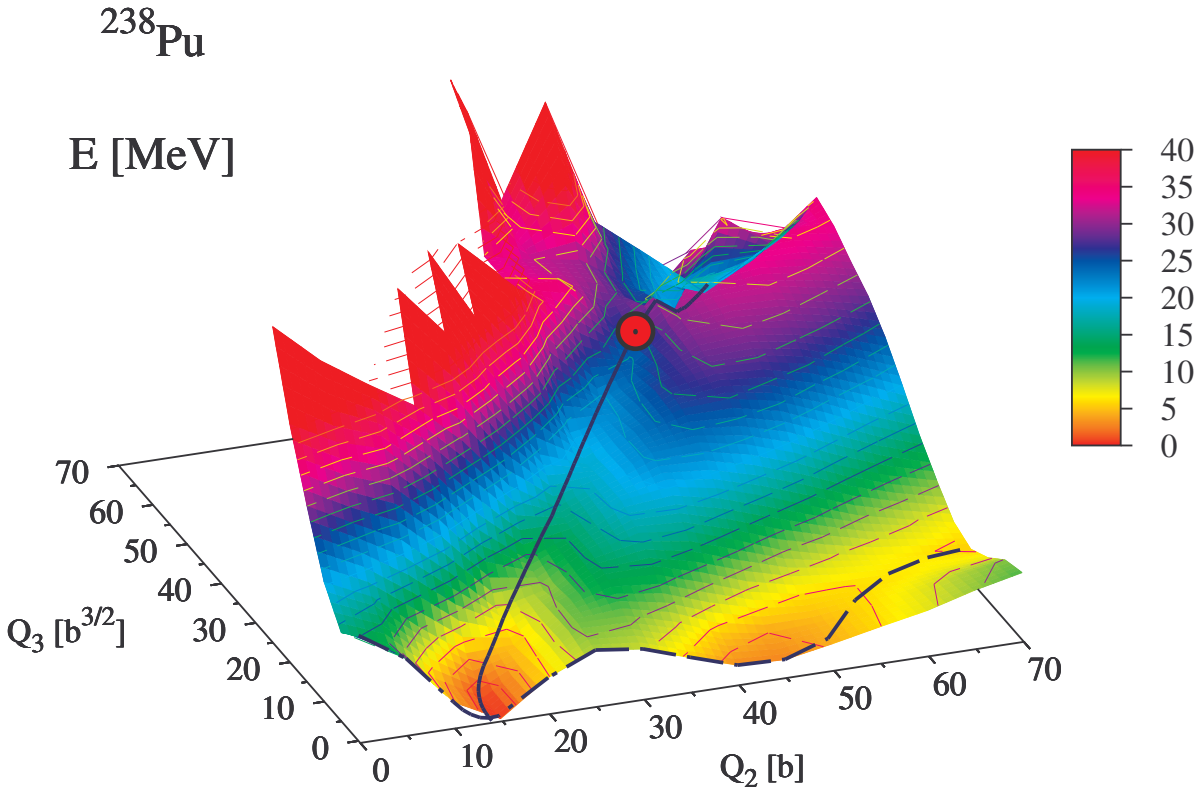

M. Warda and L. M. Robledo, Phys. Rev. C 84, 044608 (2011).

Shape evolution: ^{238}Pu

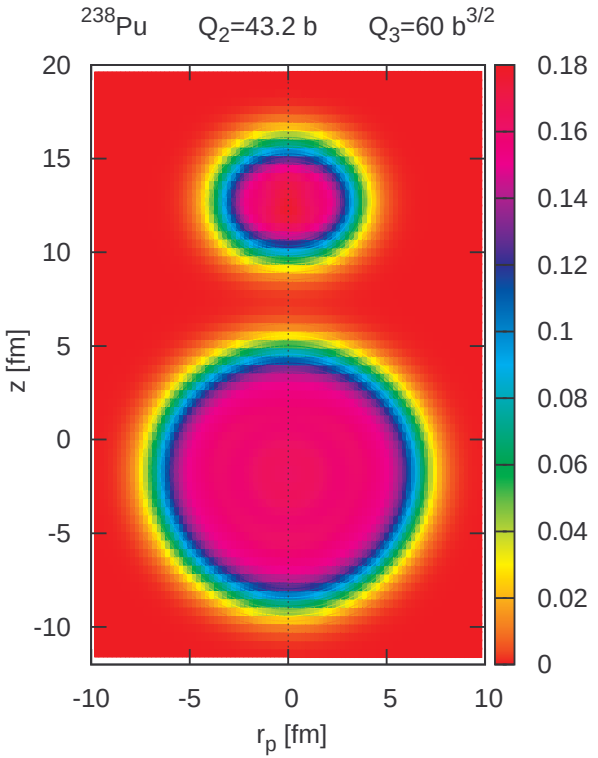

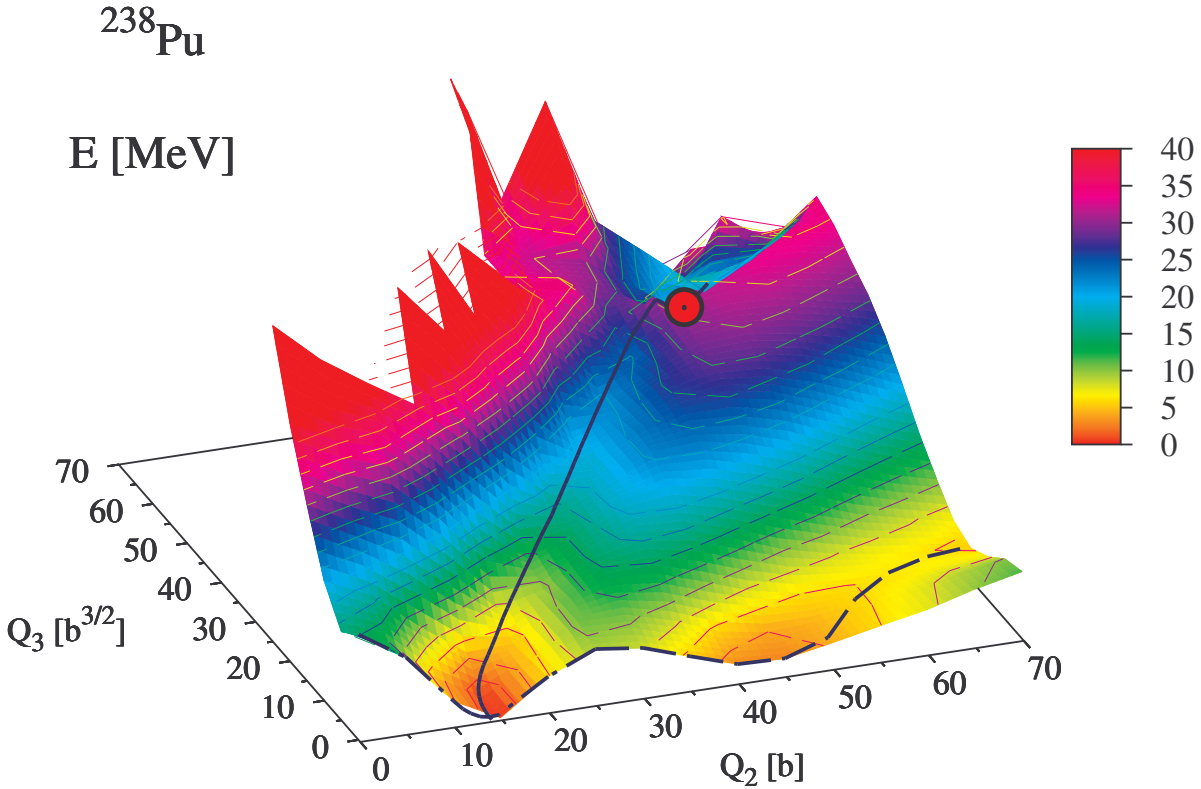

M. Warda and L. M. Robledo, Phys. Rev. C 84, 044608 (2011).

Shape evolution: ^{238}Pu

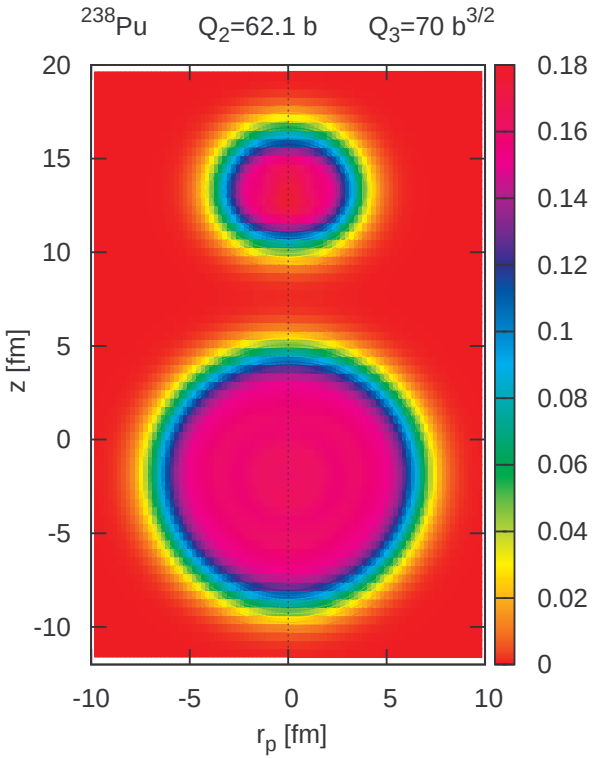

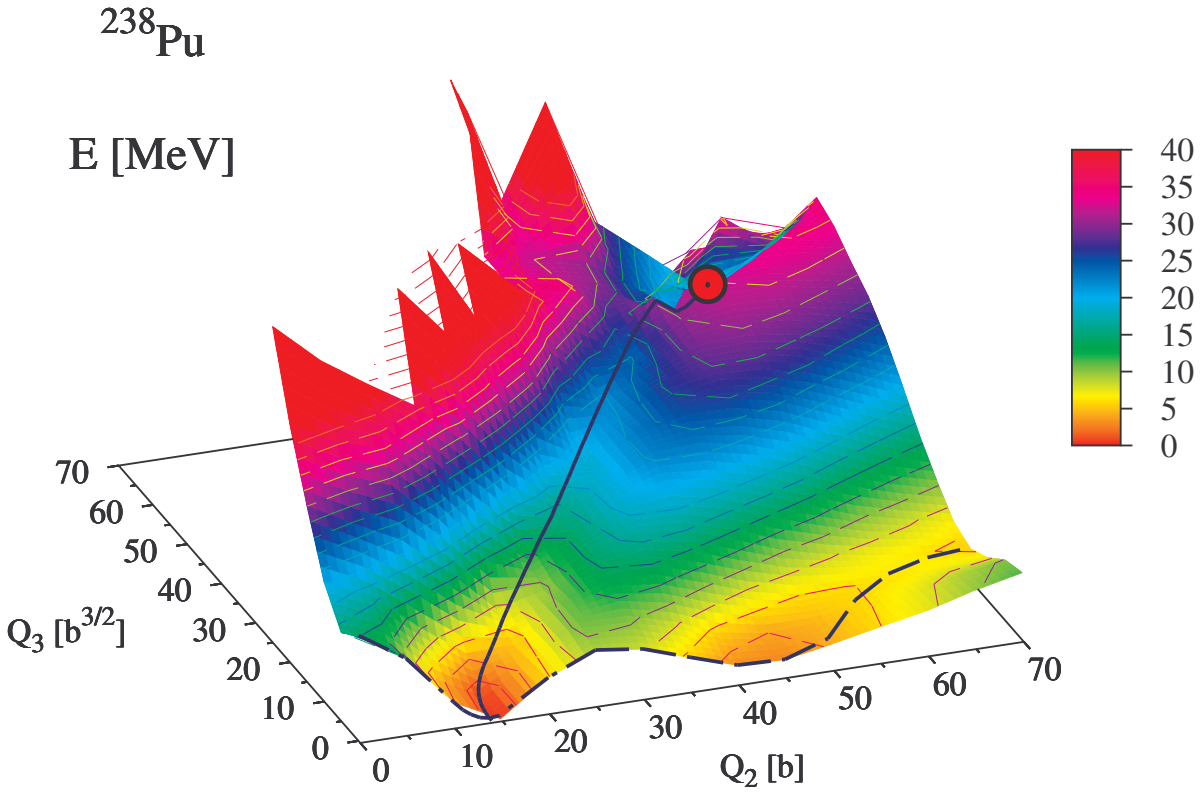

M. Warda and L. M. Robledo, Phys. Rev. C 84, 044608 (2011).

Shape evolution: ^{238}Pu

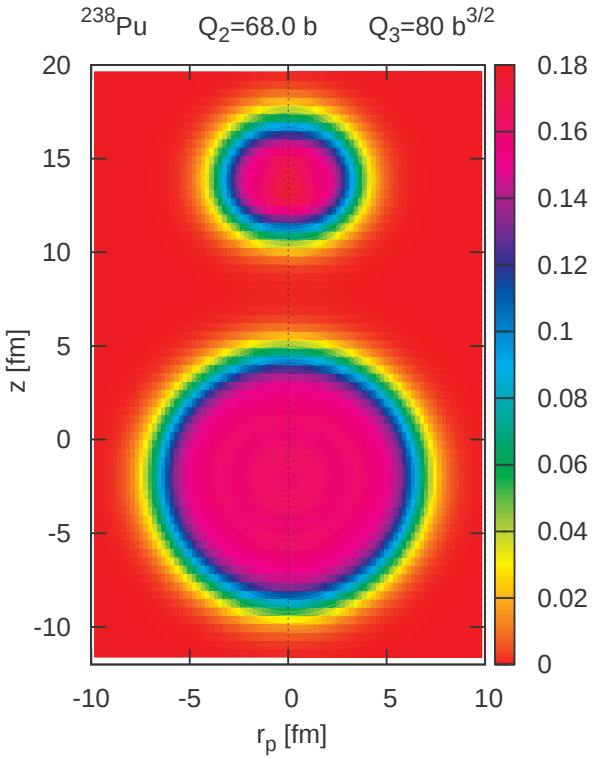

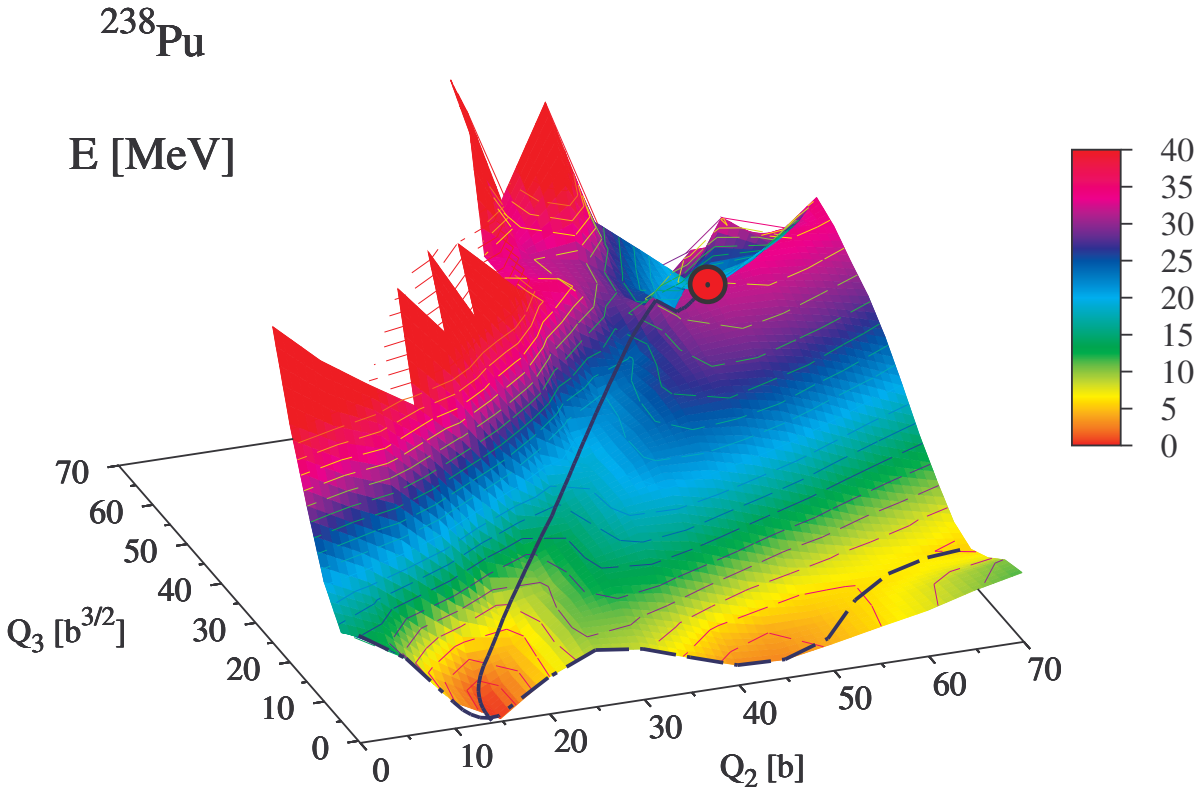

M. Warda and L. M. Robledo, Phys. Rev. C 84, 044608 (2011).

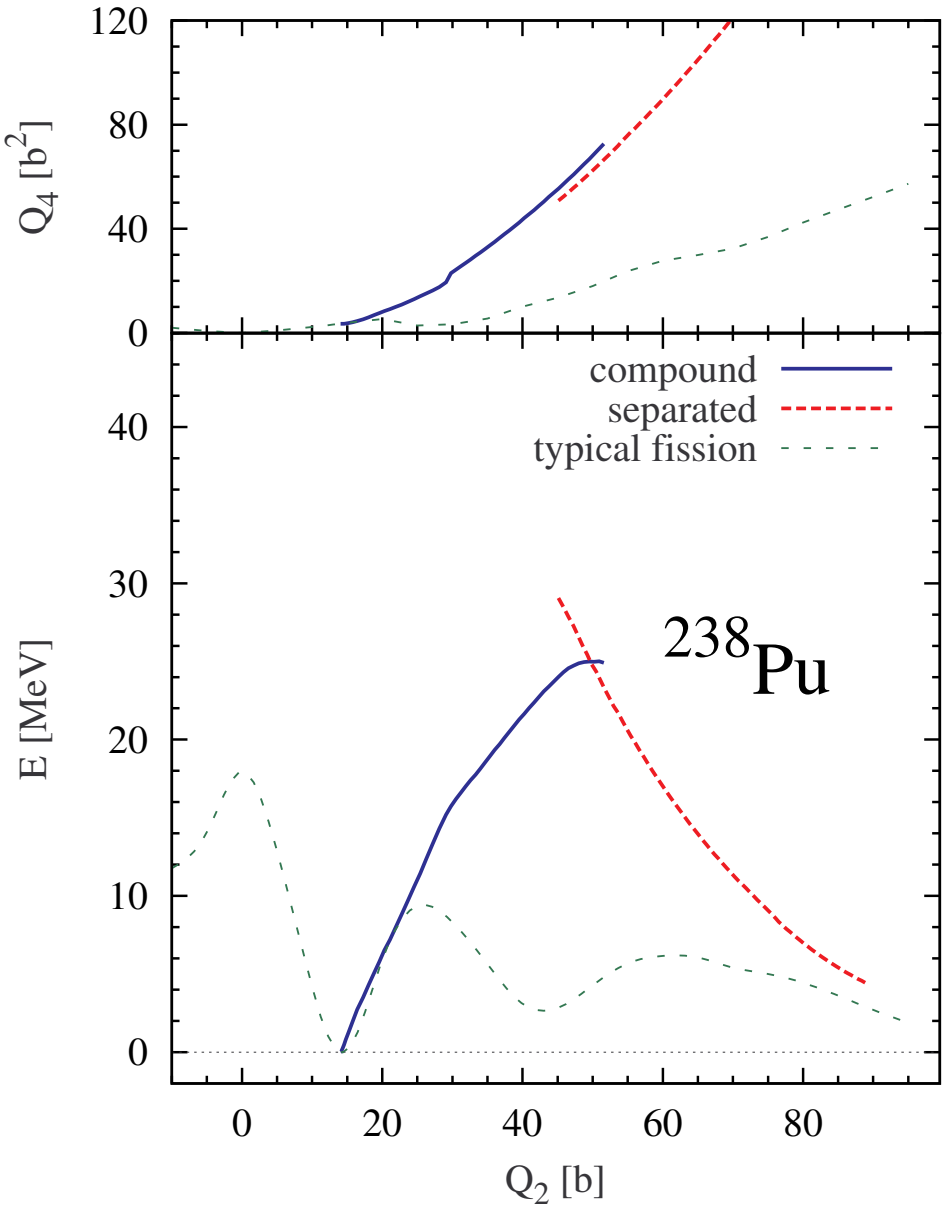
120
80
40
0
Q_4 [b^2]
compound
separated
typical fission
40
30
20
10
0
E [MeV]
^{238}Pu
0
20
40
60
80
Q_2 [b]

Half-lives

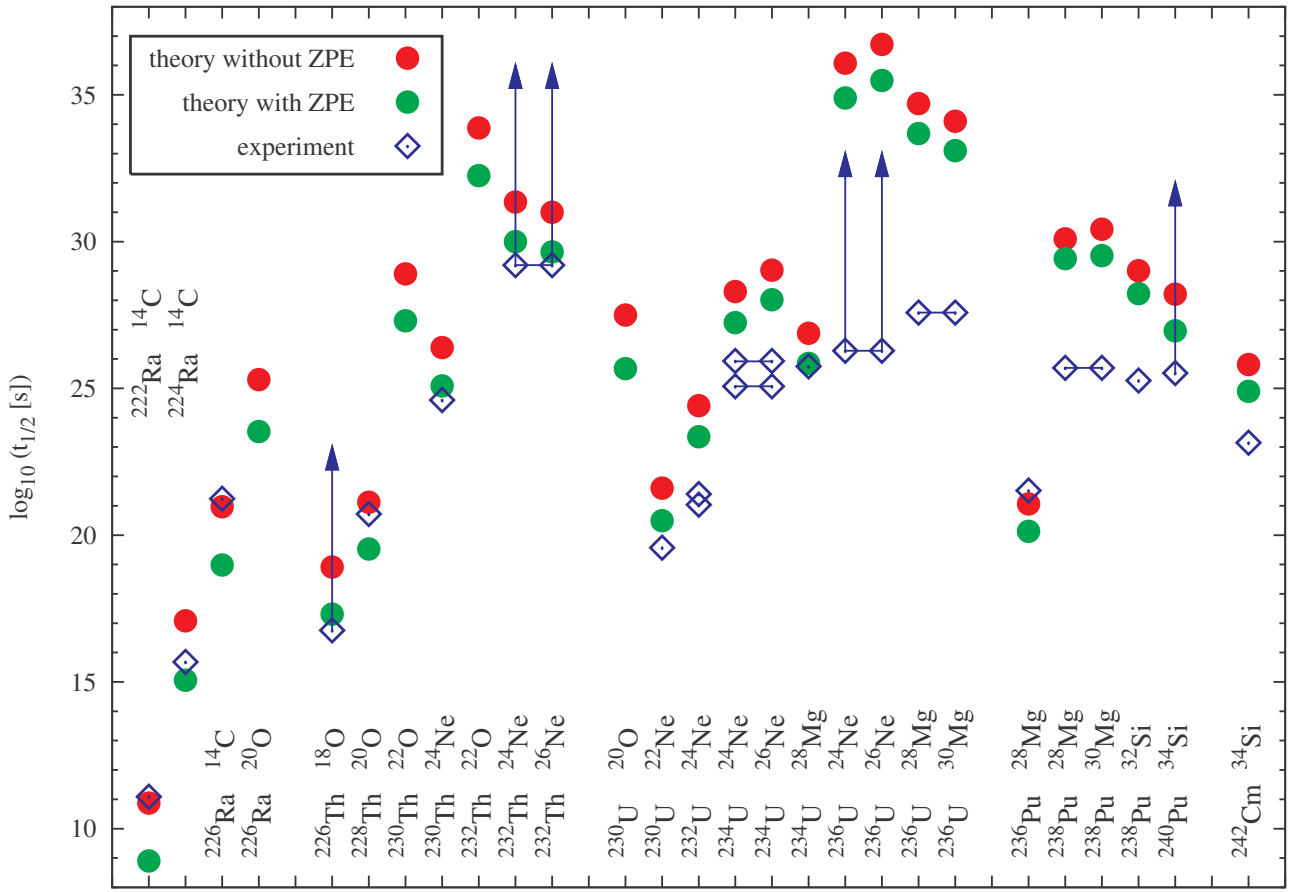
theory without ZPE
theory with ZPE
experiment
log10 (t1/2 [s])
35
30
25
20
15
10
222Ra
224Ra
14C
14C
14C
226Ra
226Ra
20O
18O
226Th
20O
228Th
22O
230Th
24Ne
230Th
22O
232Th
24Ne
232Th
26Ne
232Th
20O
230U
22Ne
230U
24Ne
232U
24Ne
234U
26Ne
234U
28Mg
234U
24Ne
236U
26Ne
236U
28Mg
236U
30Mg
236U
28Mg
236Pu
28Mg
238Pu
30Mg
238Pu
32Si
238Pu
34Si
240Pu
34Si
242Cm

Fission fragments - N/Z ratio

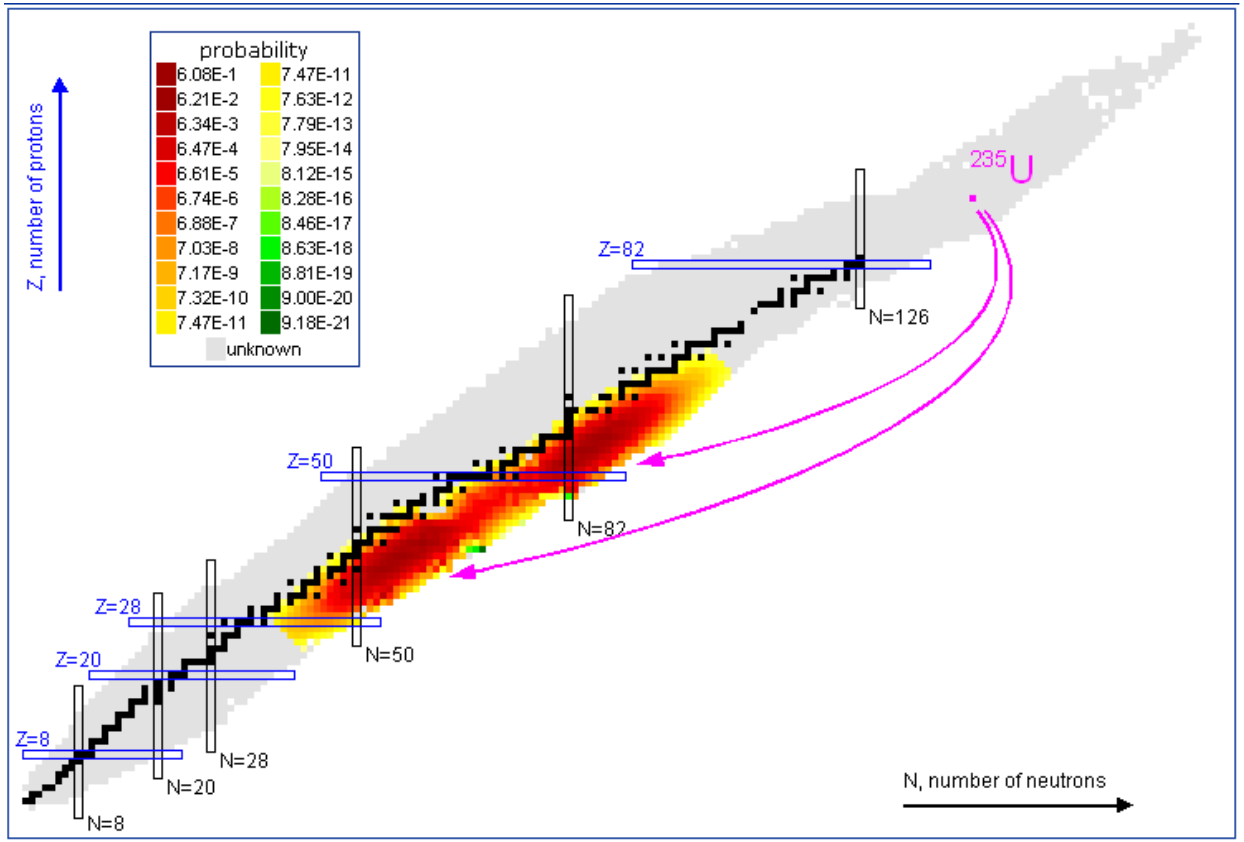

http://lablemminglounge.blogspot.com/2011/03/why-fuel-rods-are-radioactive.html

Fission fragments - N/Z ratio

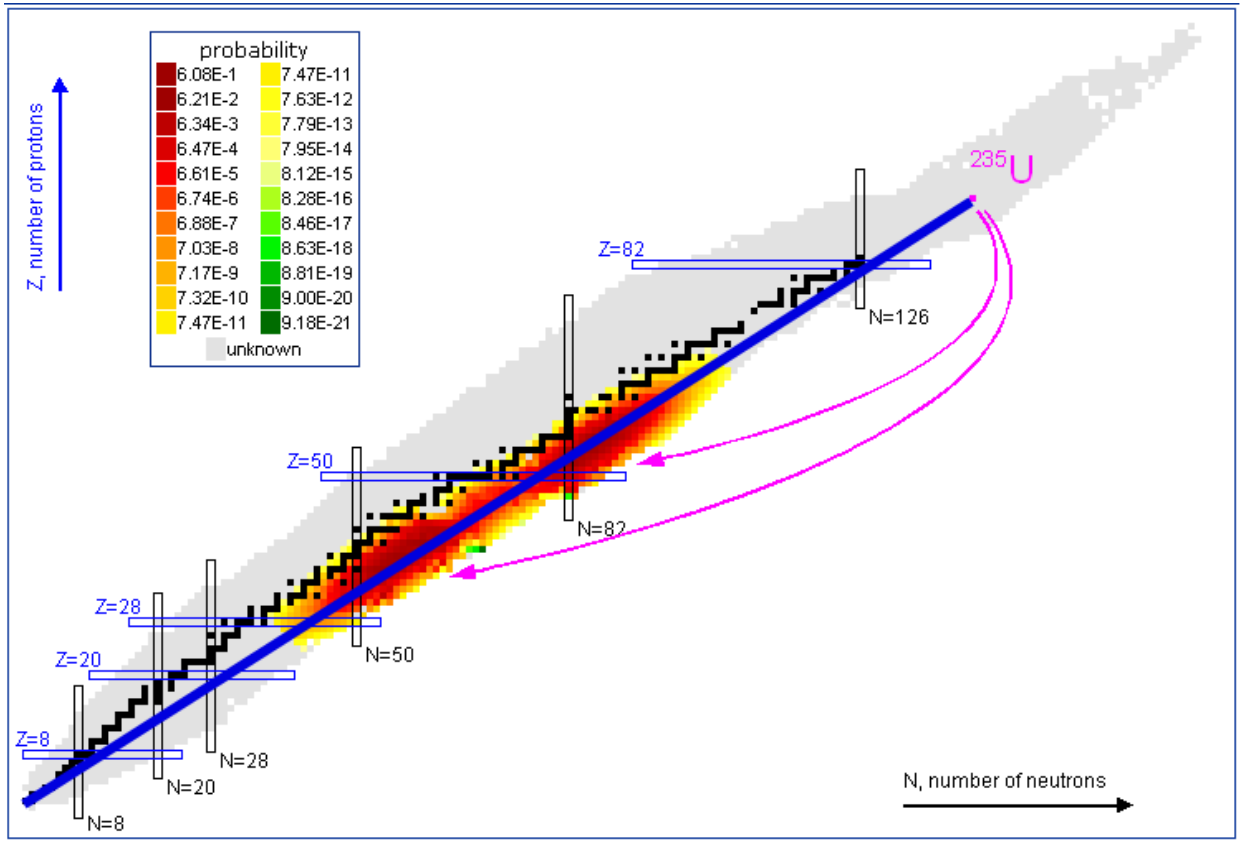

http://lablemminglounge.blogspot.com/2011/03/why-fuel-rods-are-radioactive.html

Cluster radioactivity - chart of nuclides

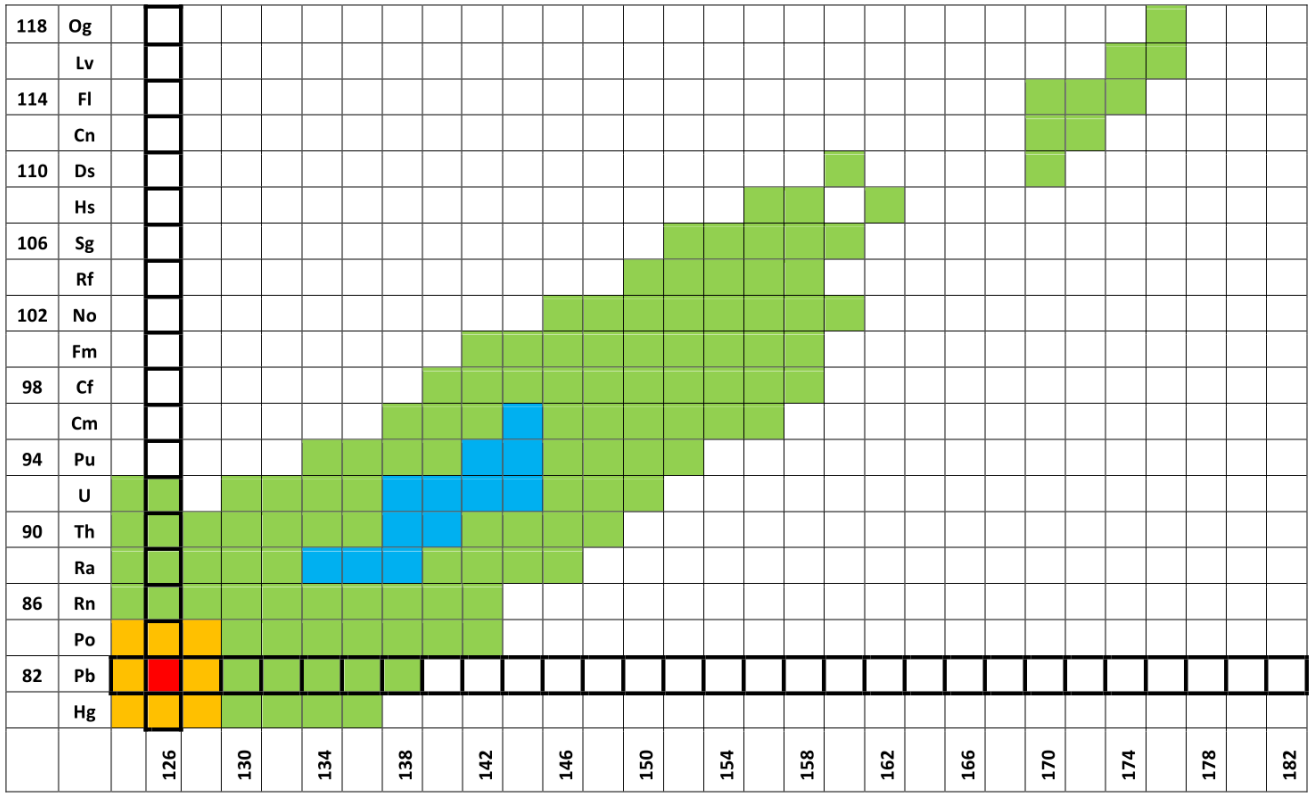

Cluster radioactivity - chart of nuclides

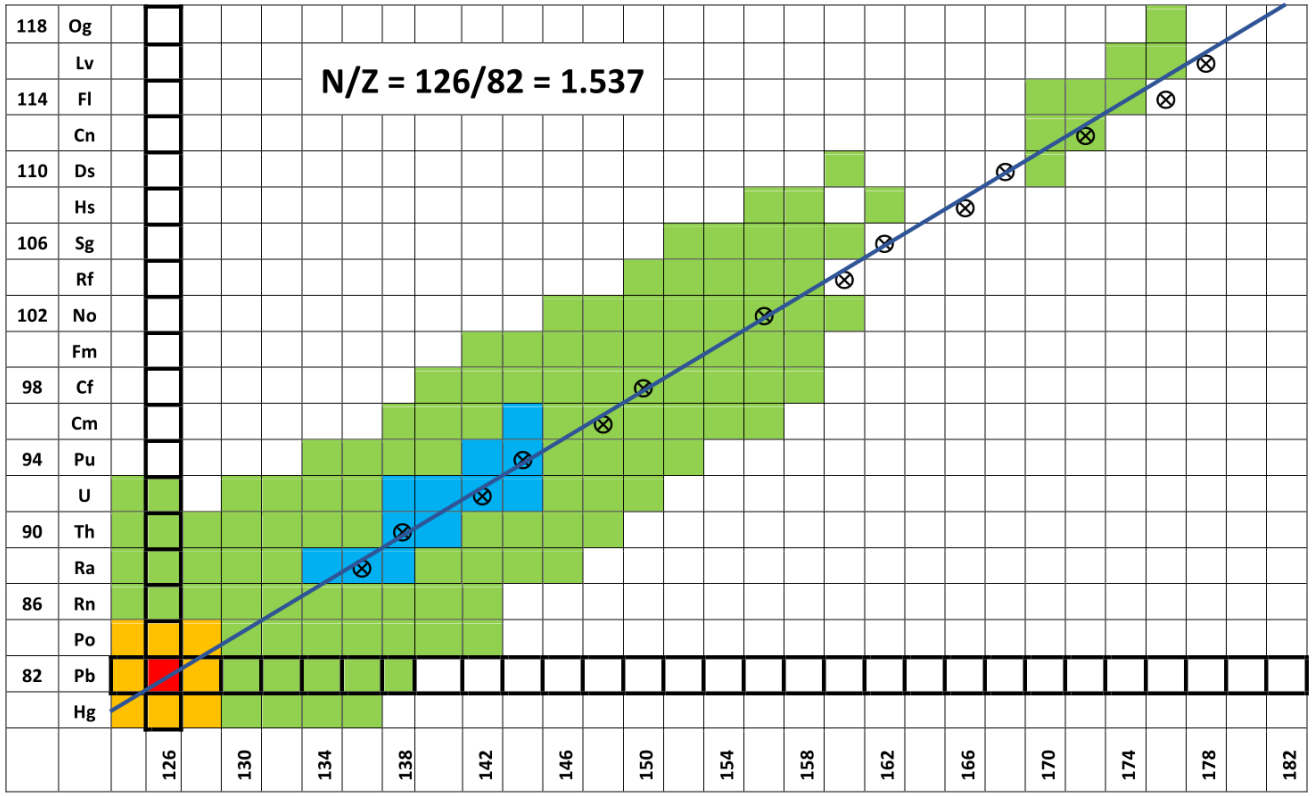

Chart of SH nuclides

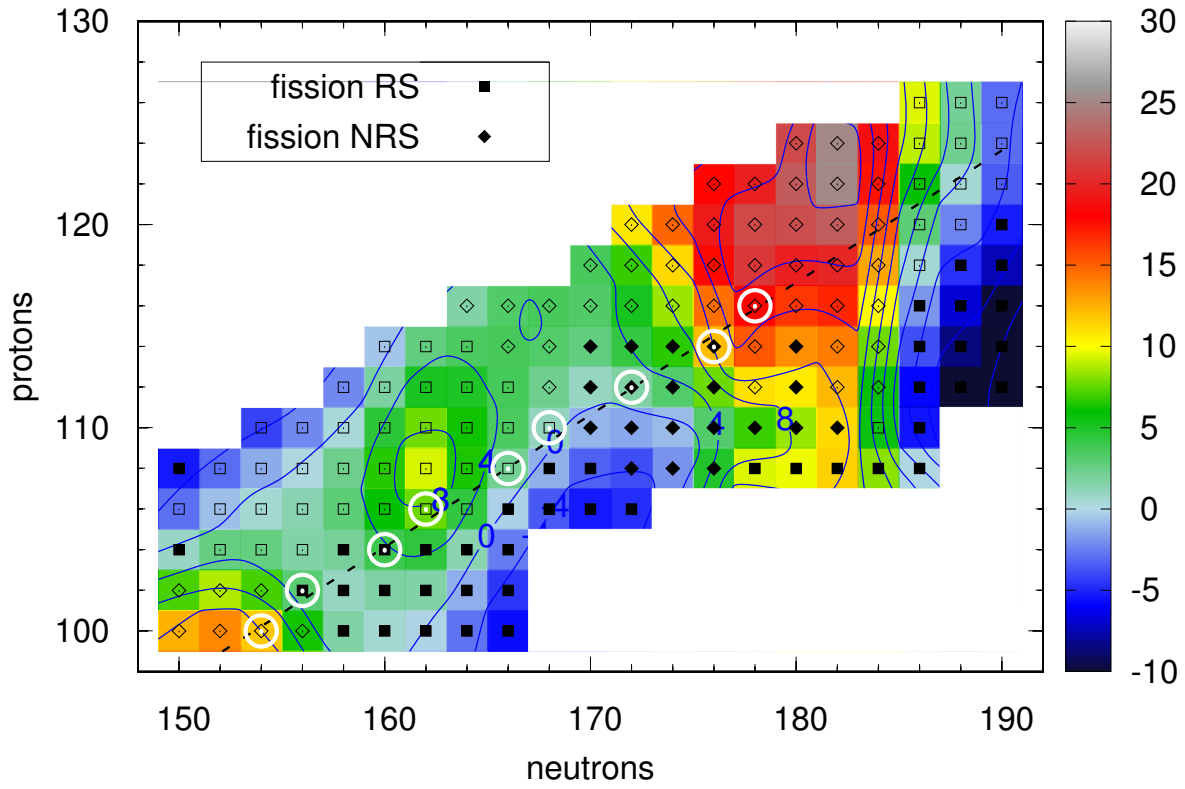

M. Warda, J.L. Egido, Phys. Rev. C 86 (2012) 014322
A. Baran, M. Kowal, P.G. Reinhard, L.M. Robledo, A. Staszczak, M. Warda, Nucl. Phys. A 944 (2015) 442

Fission barriers

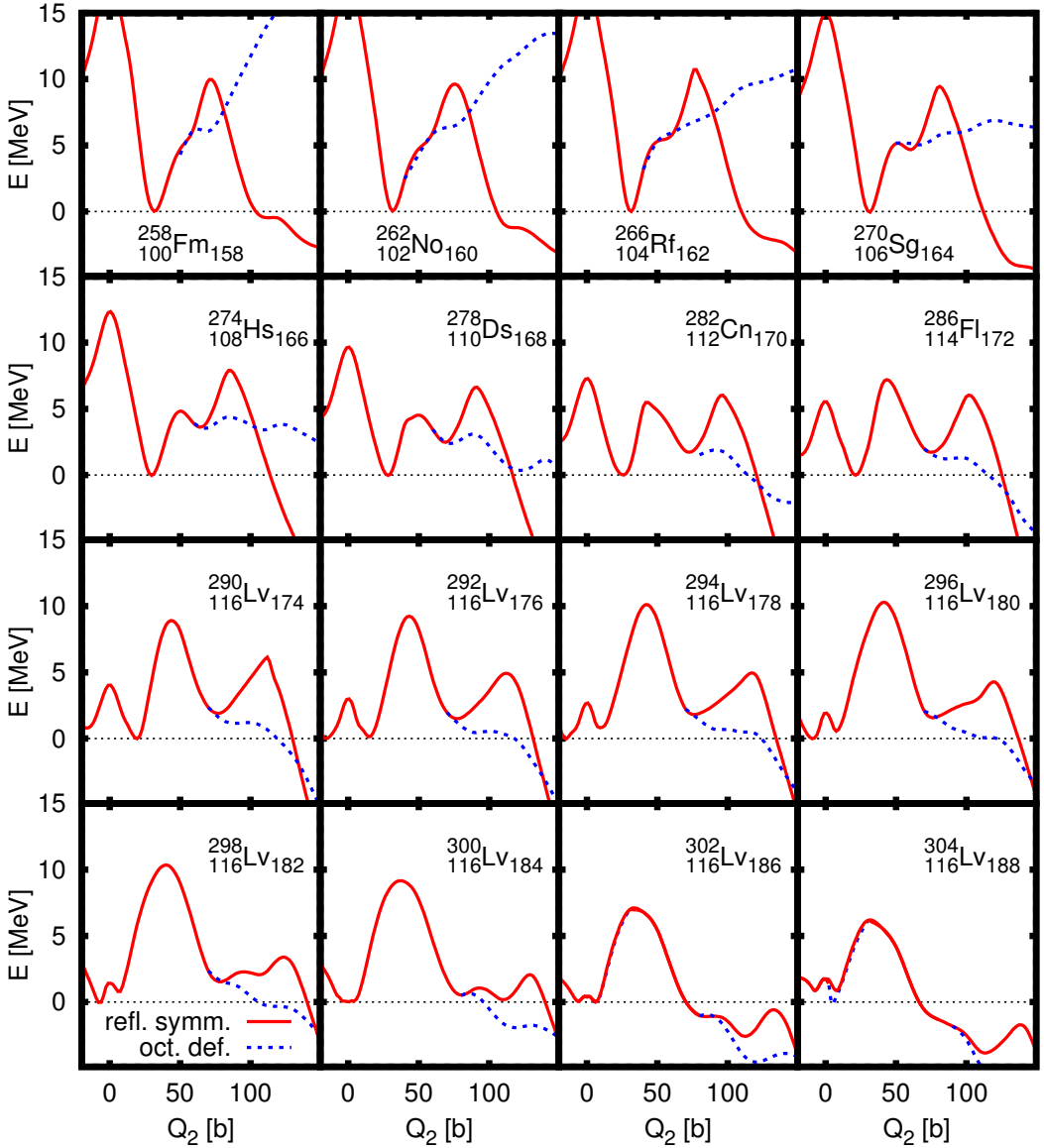

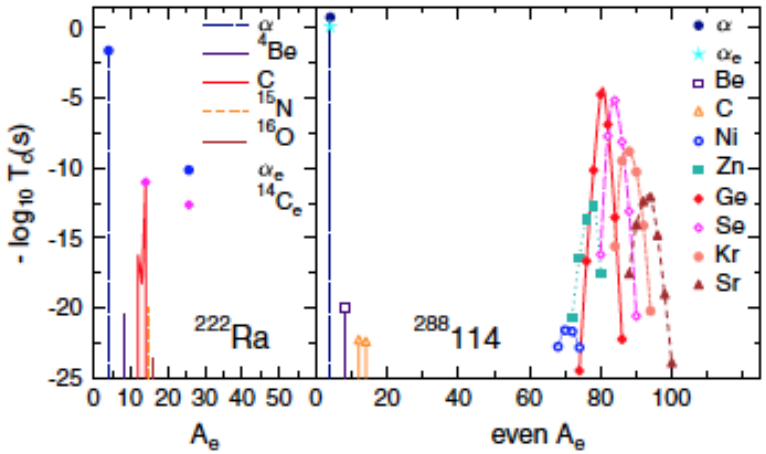

FIG. 1 (color online). Time spectra of different cluster emissions from ^{222}Ra (left panel) and from the superheavy nucleus ^{288}114 (right panel). The most probable emitted clusters from ^{222}Ra and ^{288}114 are ^{14}C and ^{80}Ge, respectively, both leading to ^{208}Pb daughter nucleus.

D. N. Poenaru, R. A. Gherghescu, and W. Greiner
Phys. Rev. Lett. 107, 062503 (2011); Phys. Rev. C 85, 034615 (2012)

Cluster radioactivity - chart of nuclides

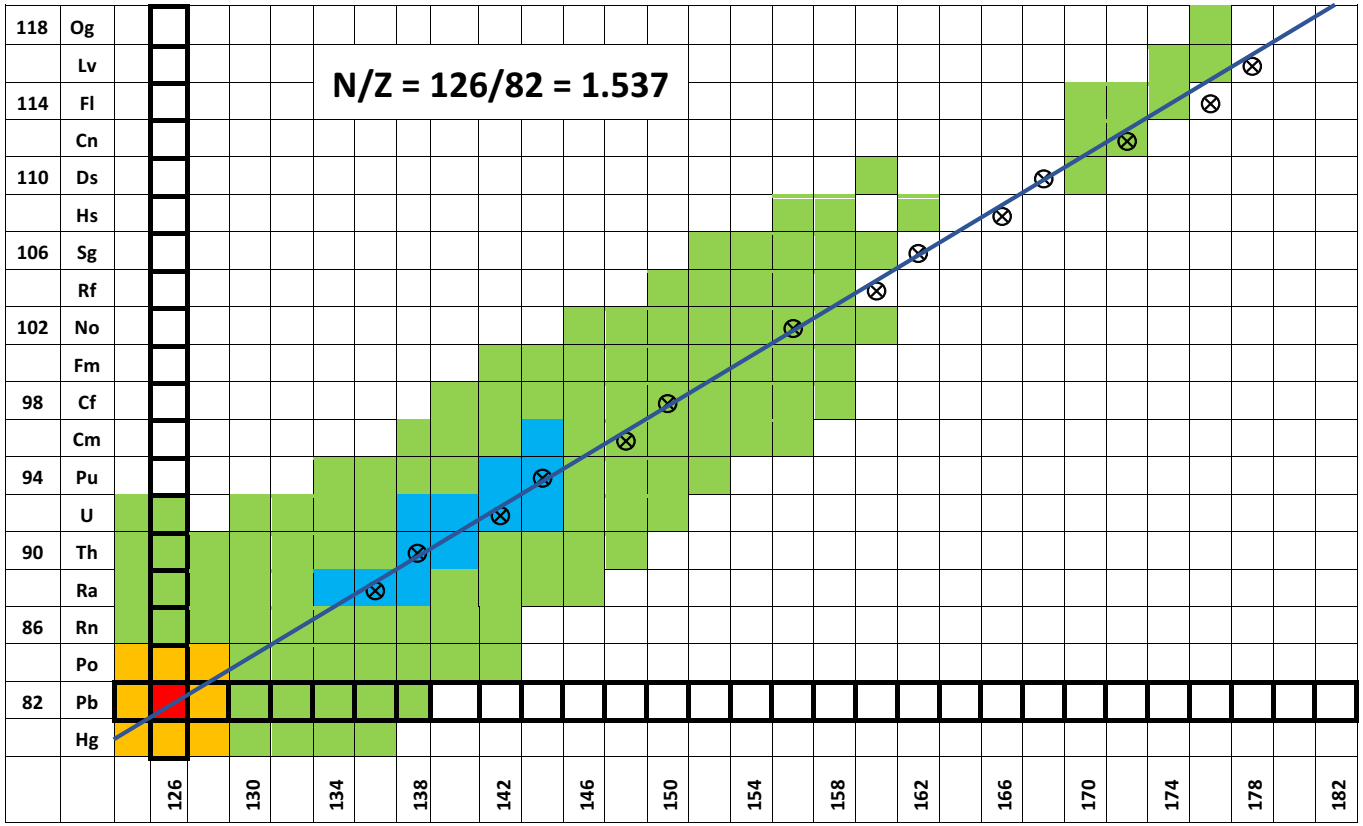

^{224}Ra

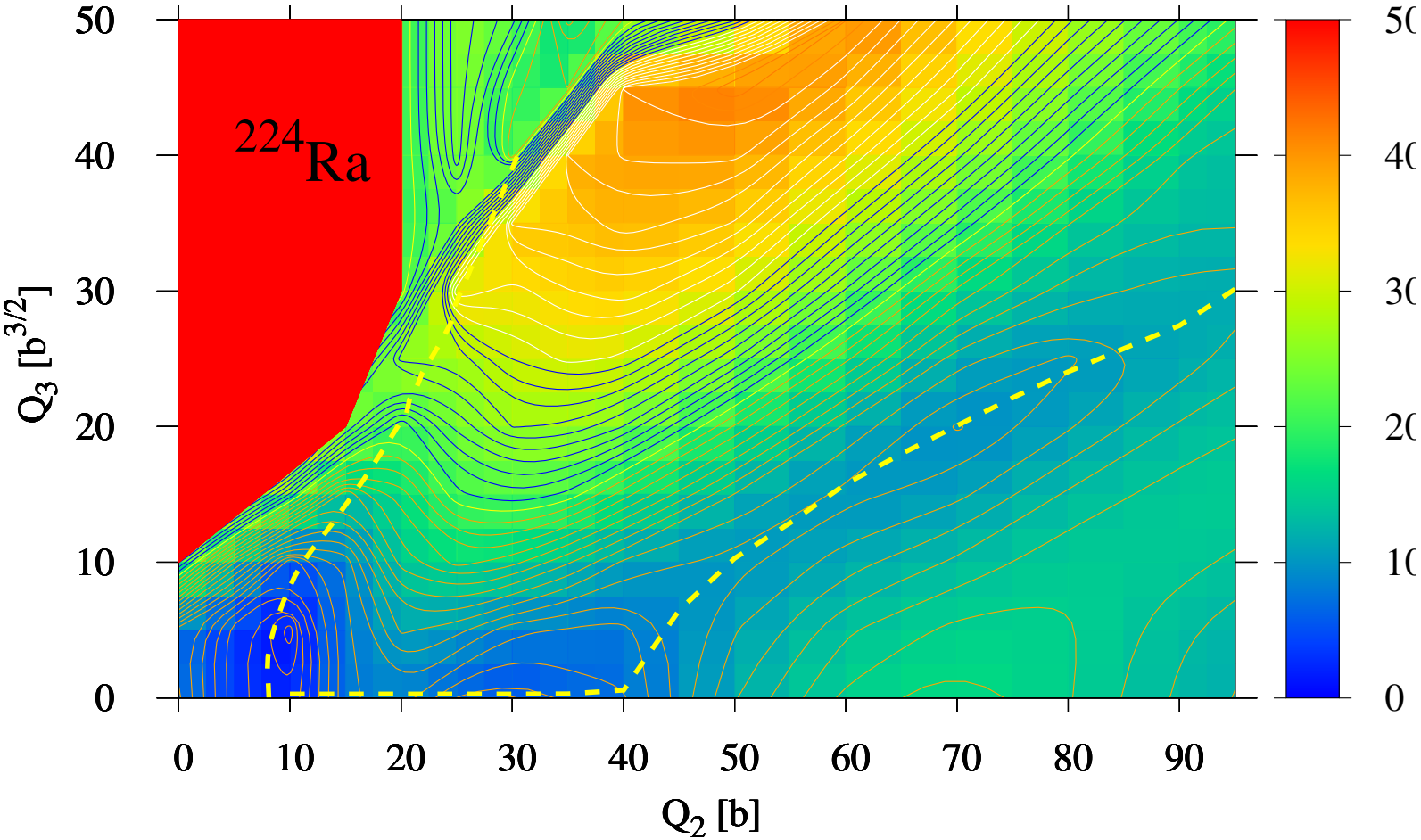

^{228}Th

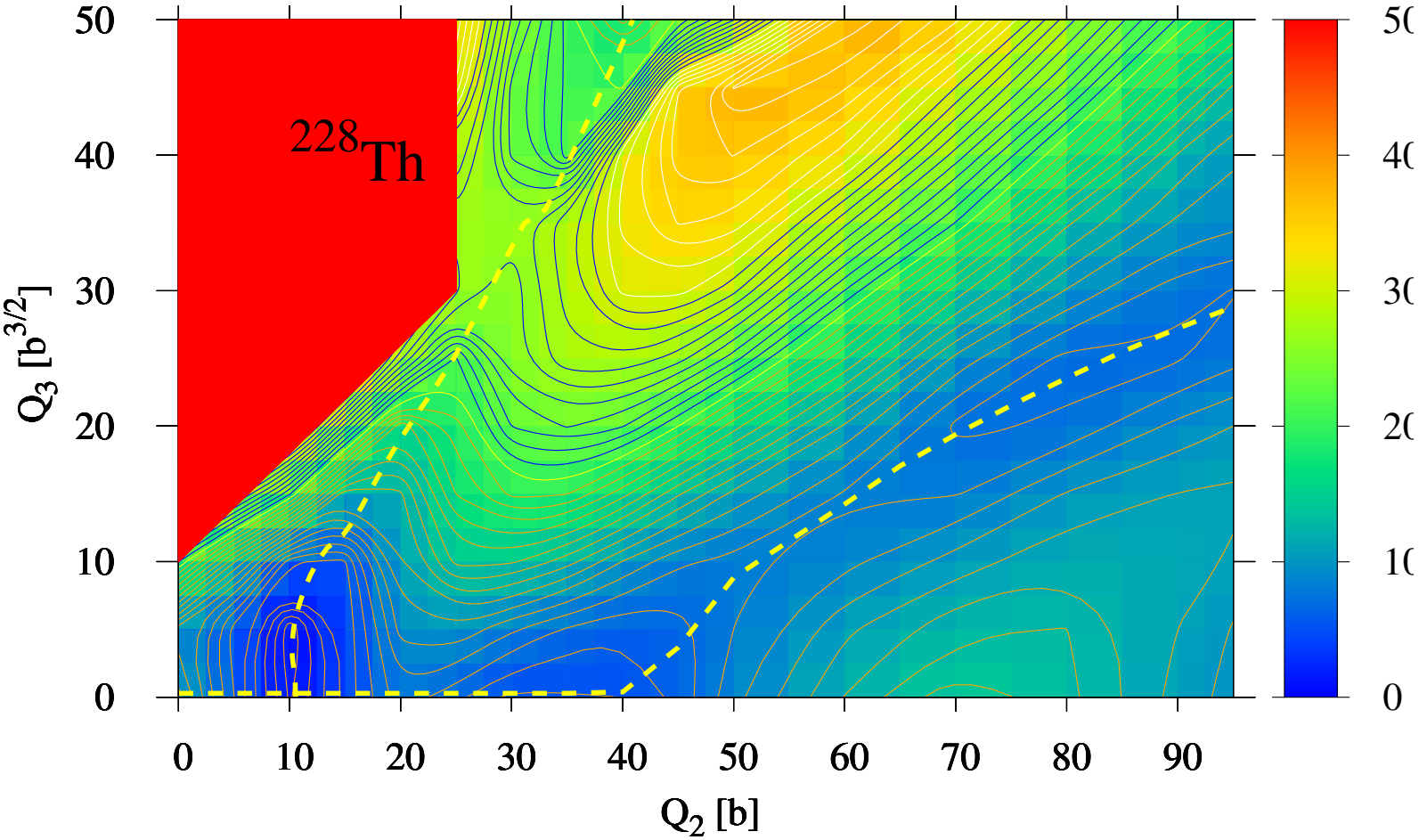

^{234}U

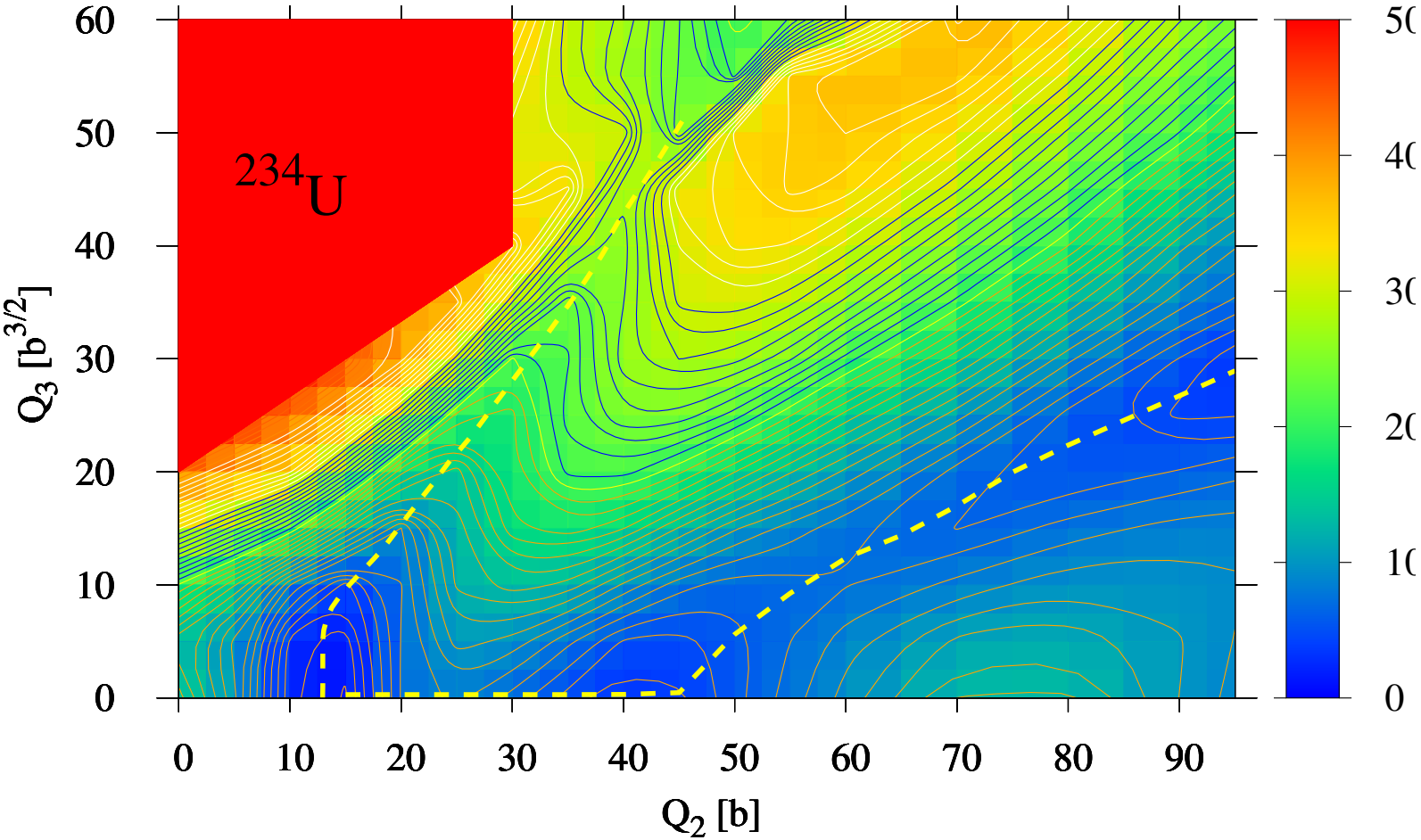

^{238}Pu

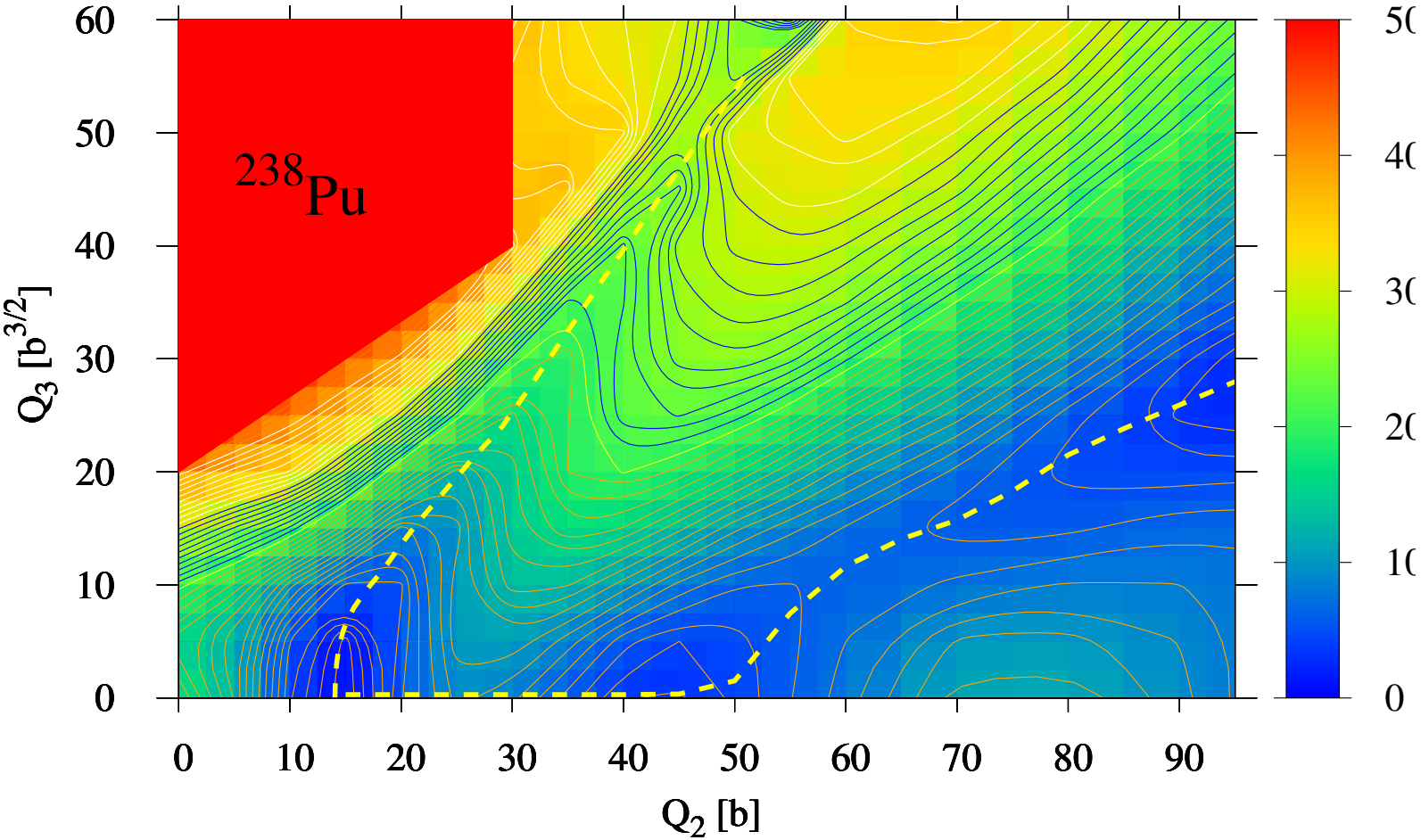

^{244}Cm

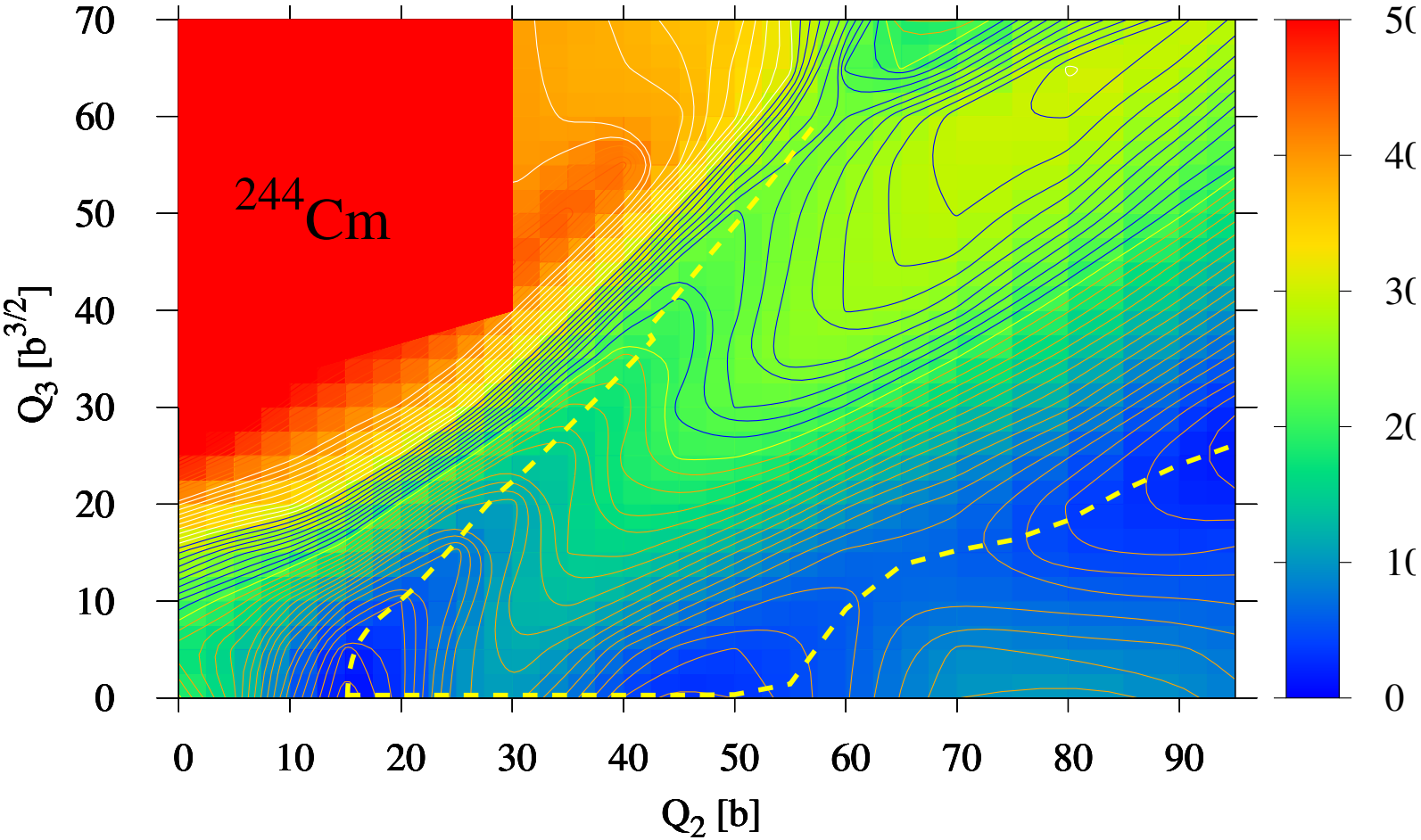

^{248}Cf

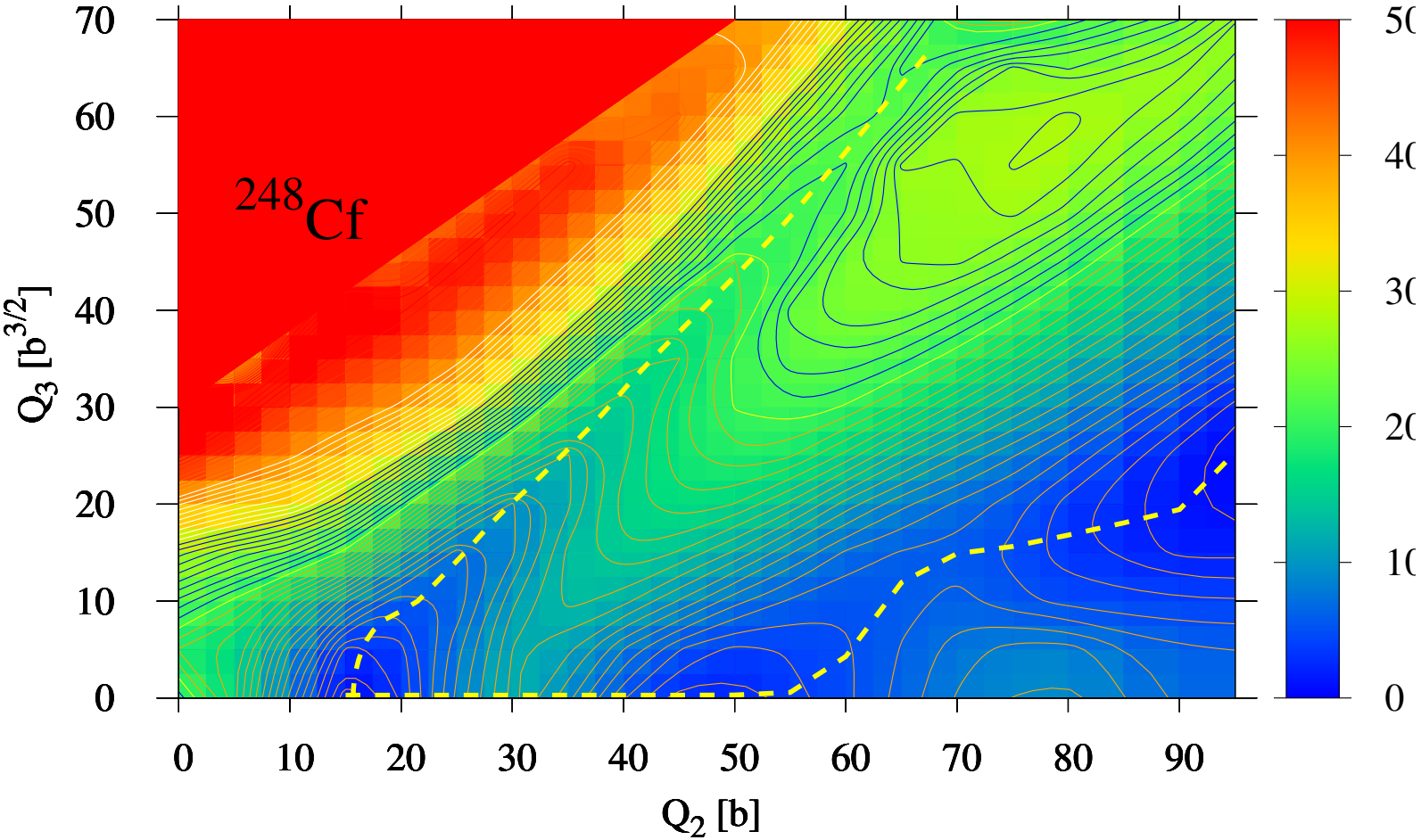

^{254}Fm

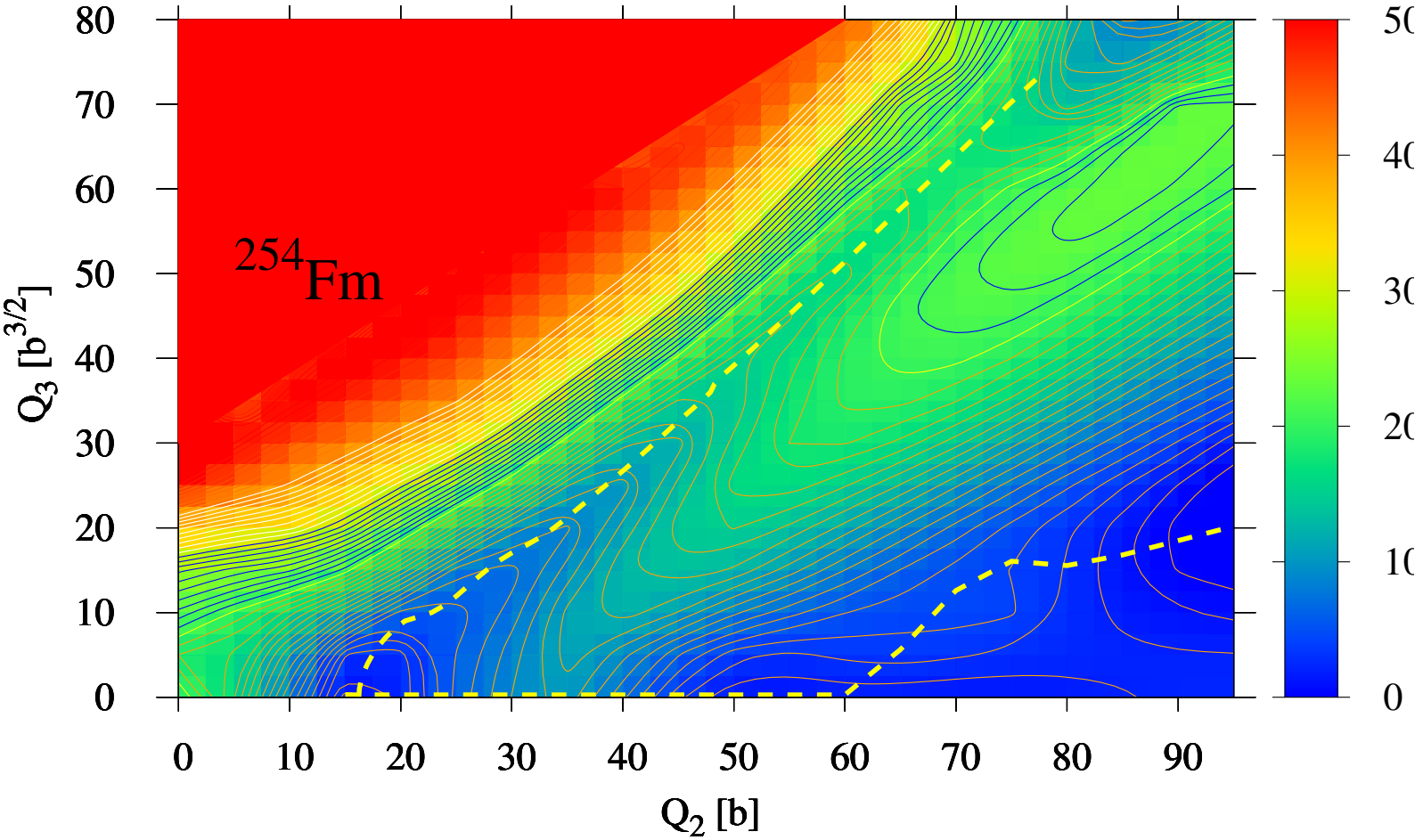

^{258}No

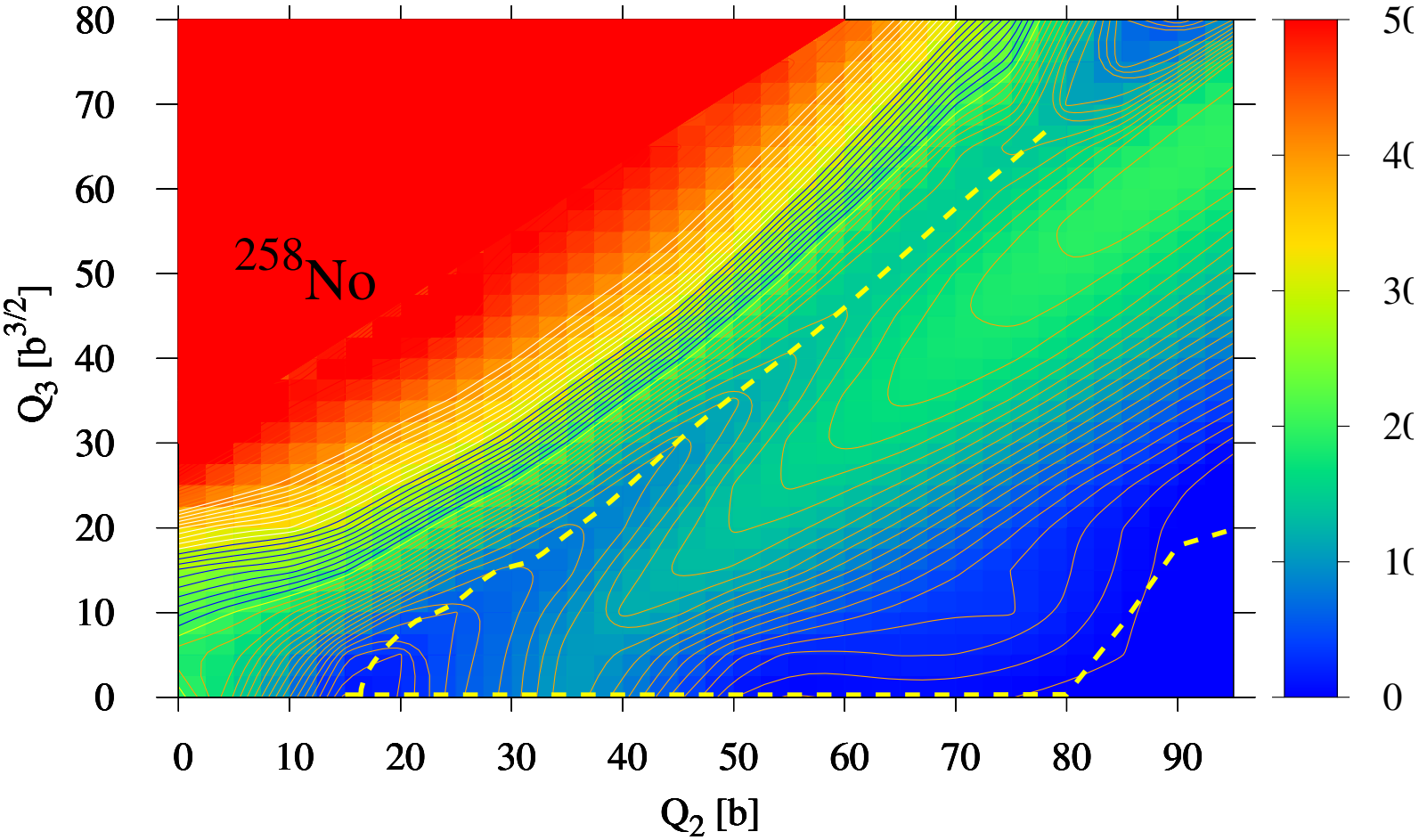

^{264}Rf

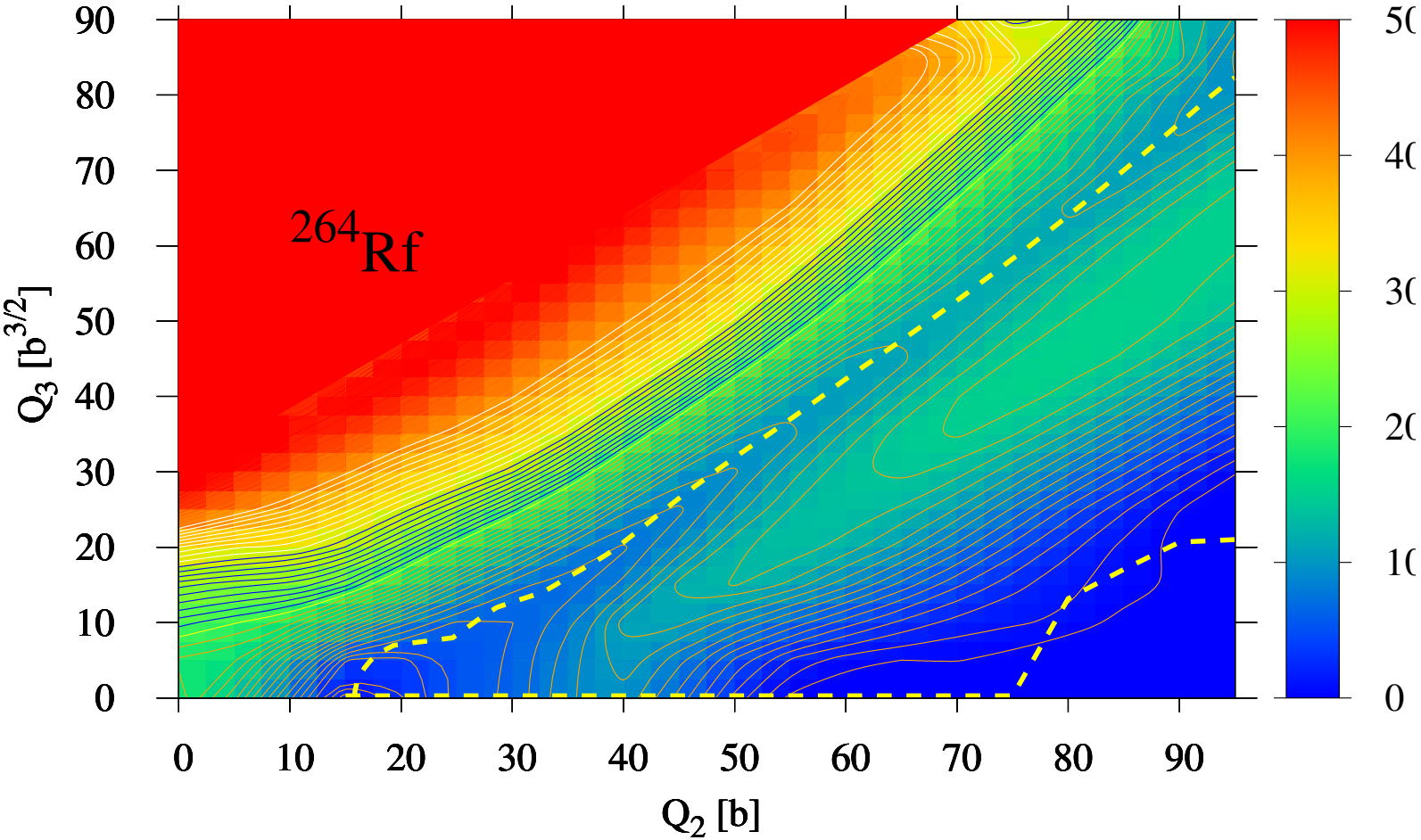

^{268}Sg

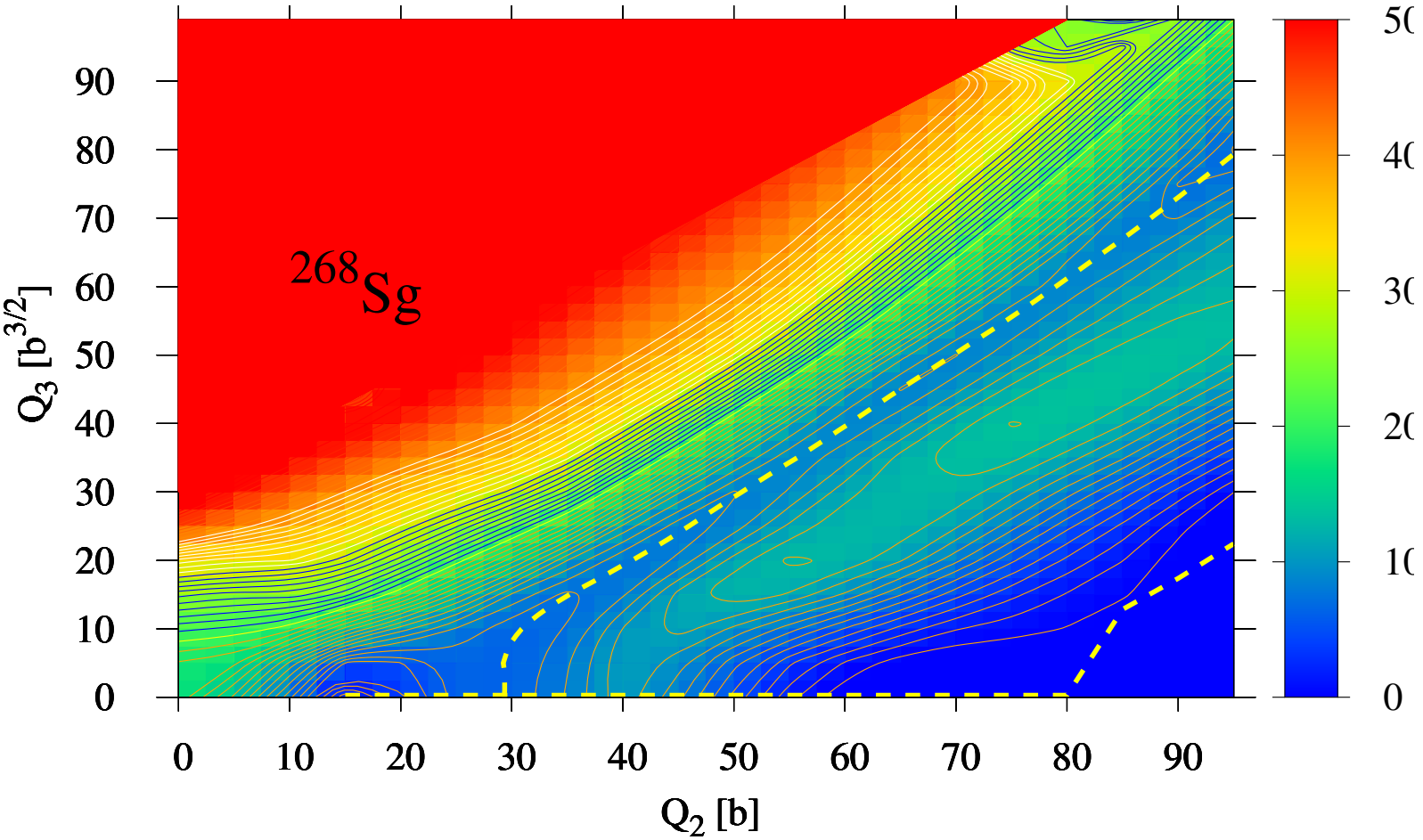

^{274}Hs

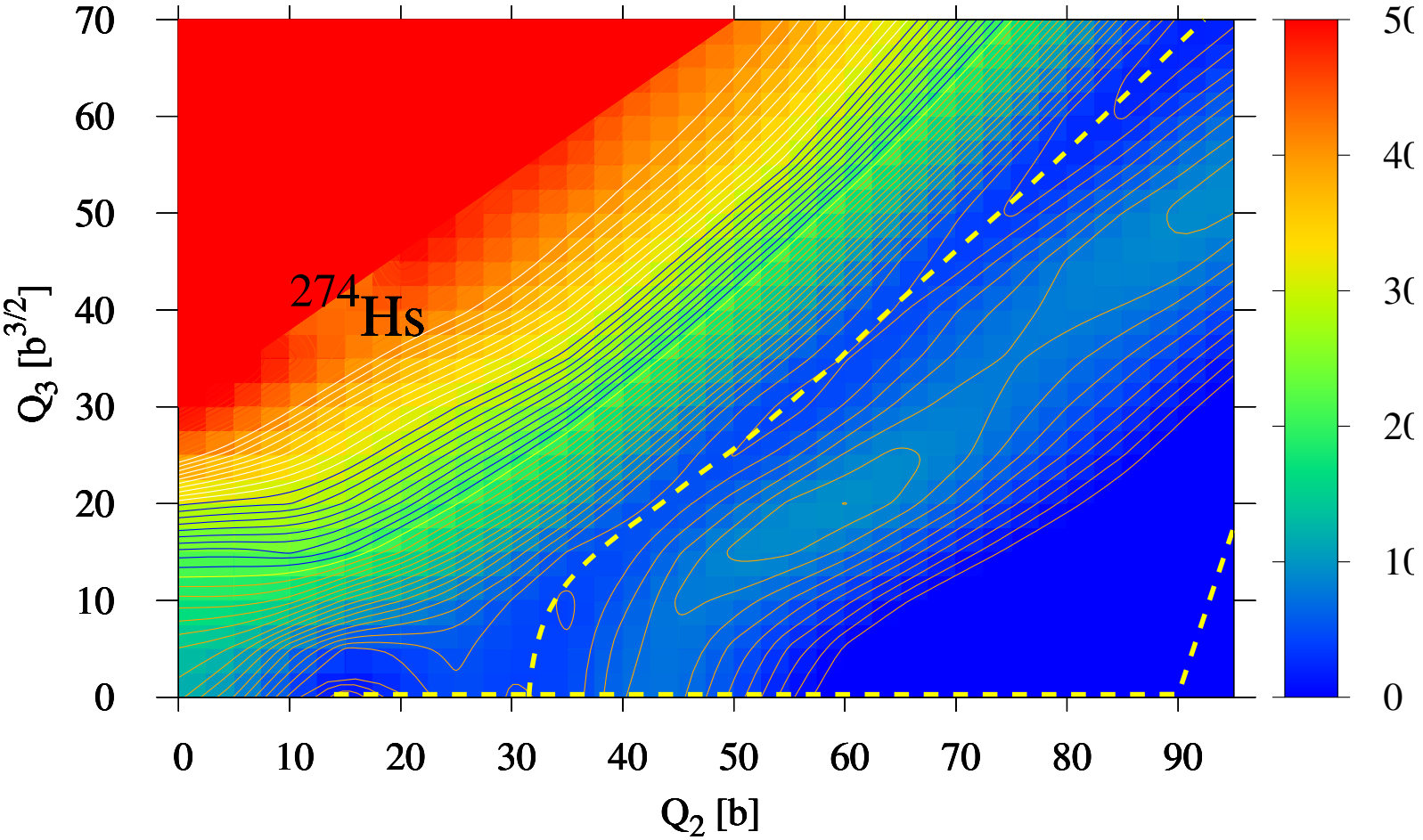

^{278}Ds

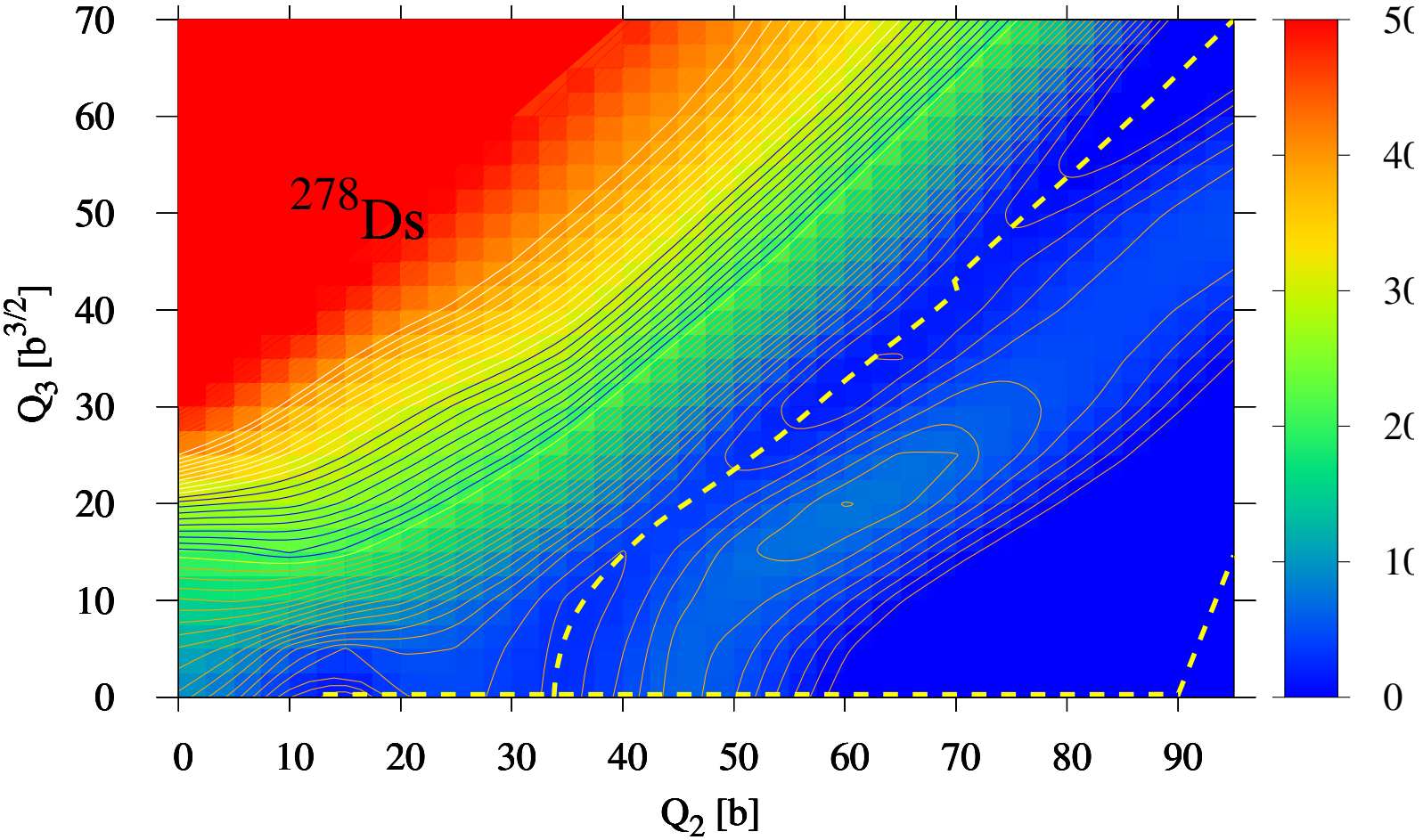

^{284}Cn

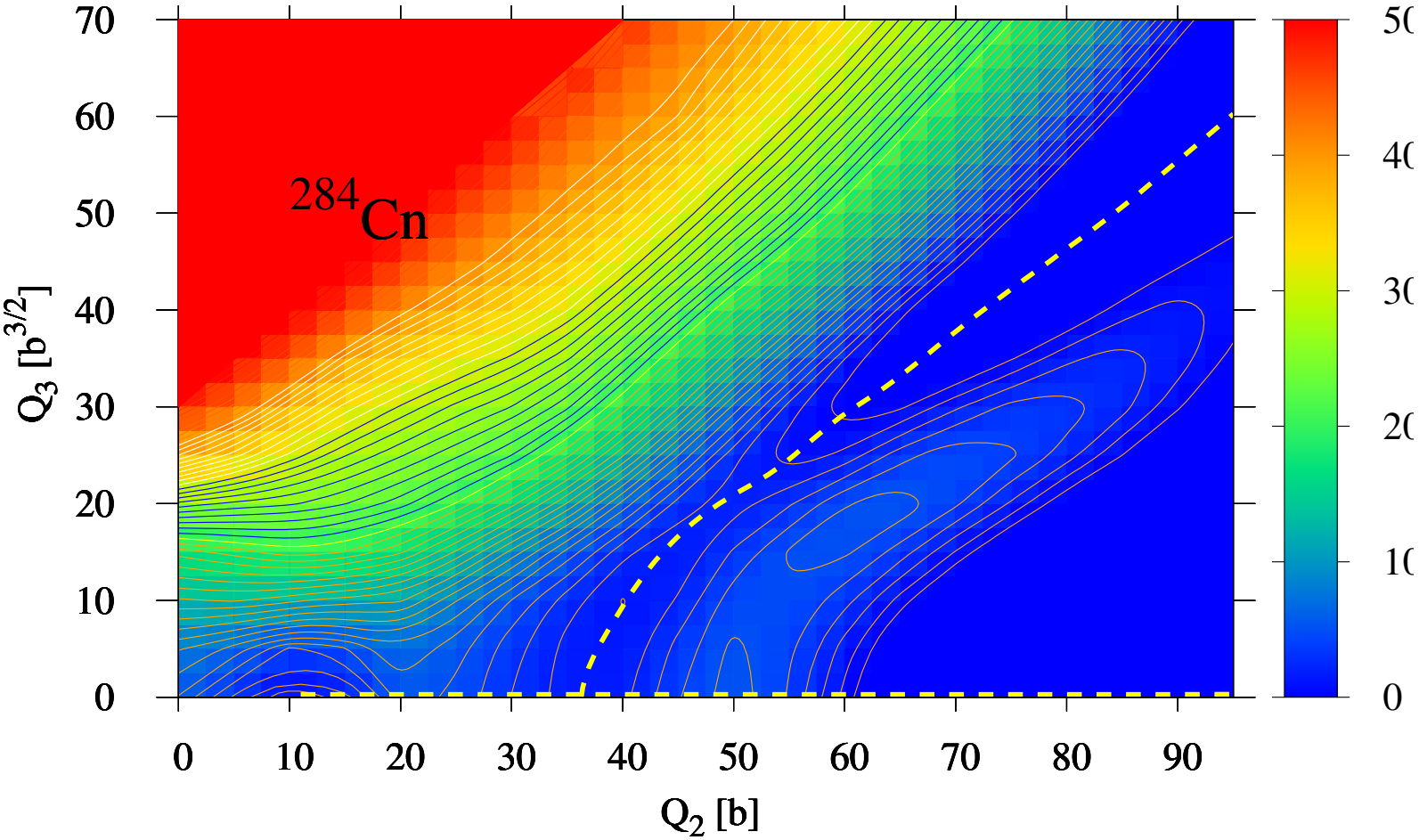

^{290}Fl

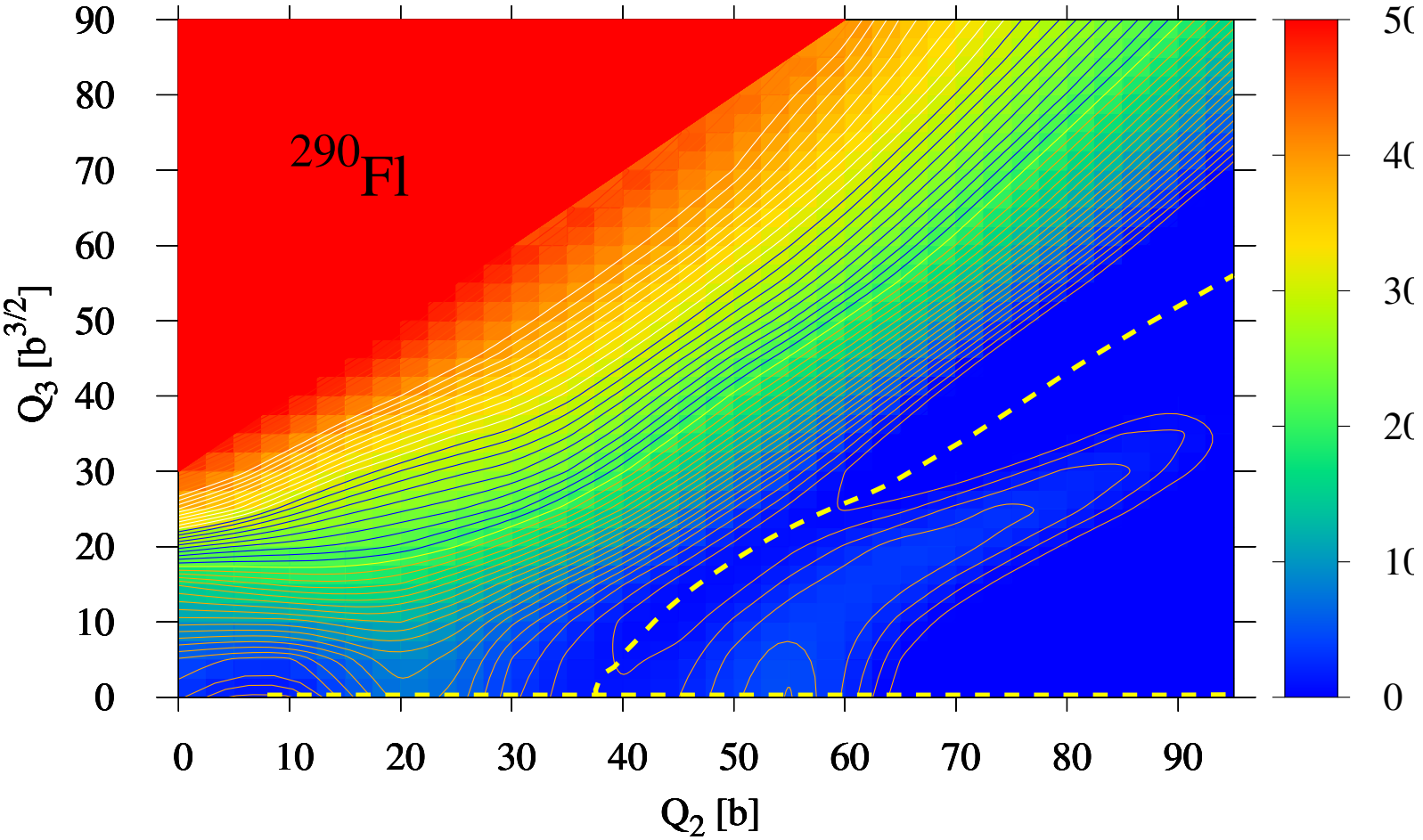

^{294}Lv

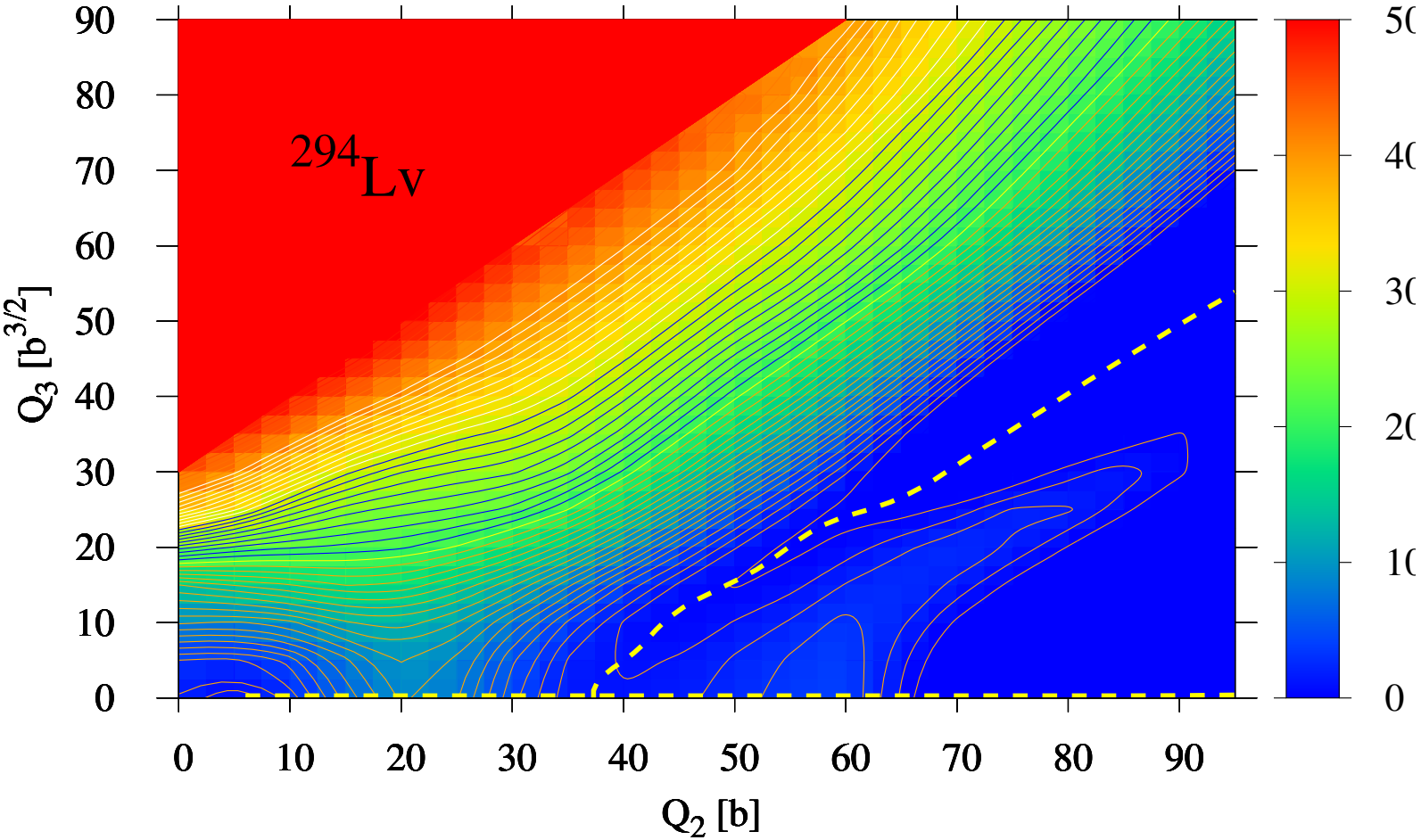

Cluster barriers

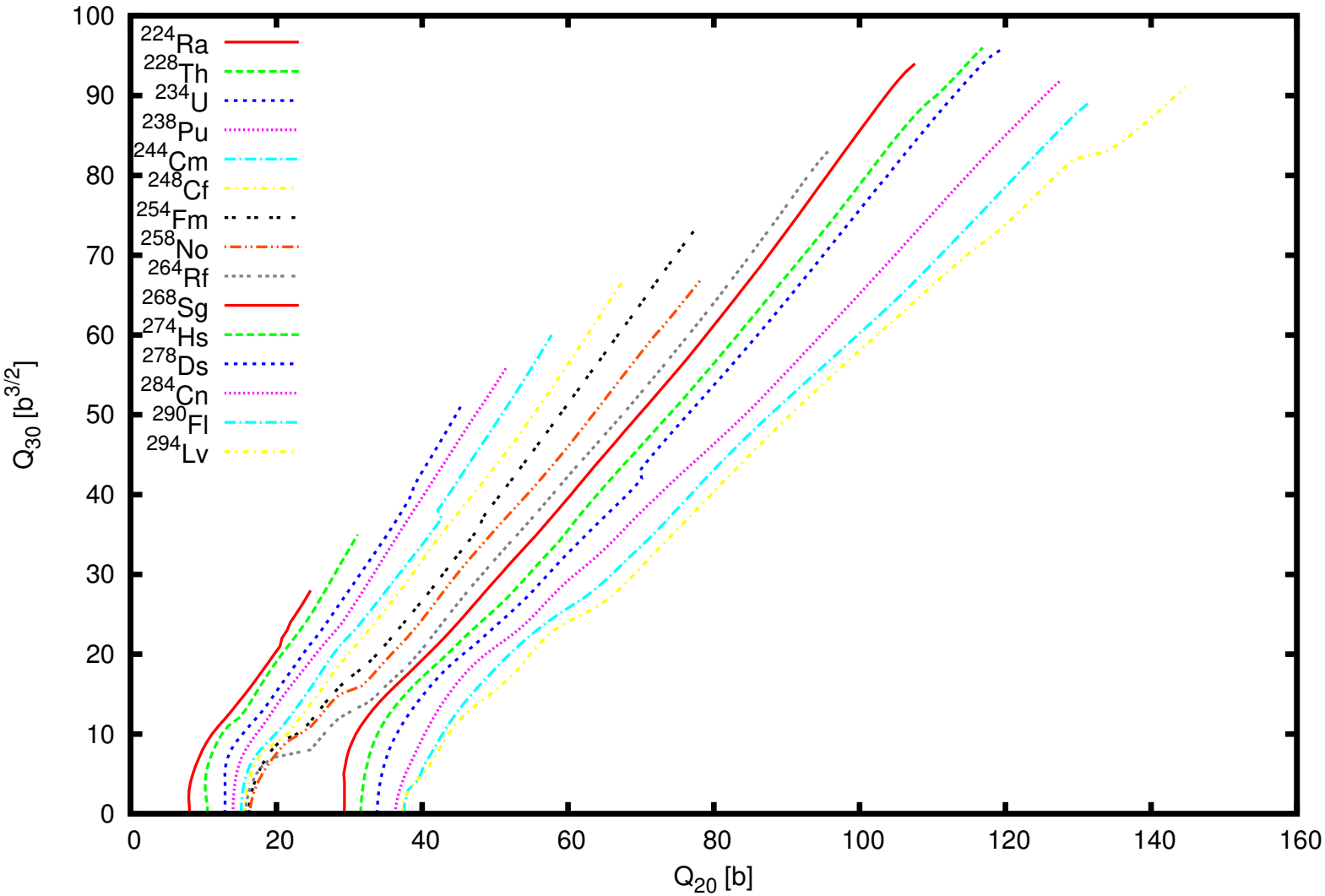

Cluster barriers

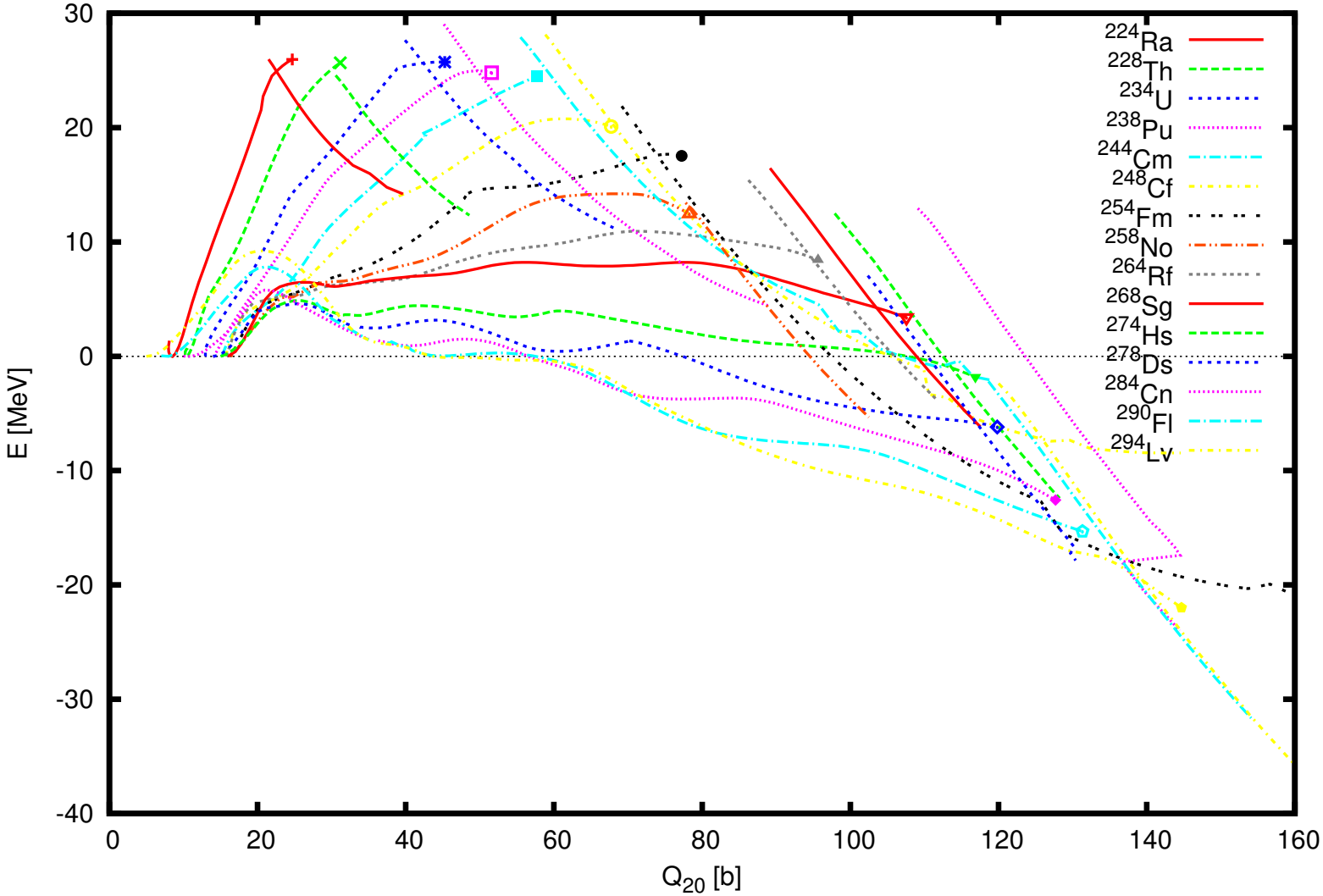

Cluster barriers

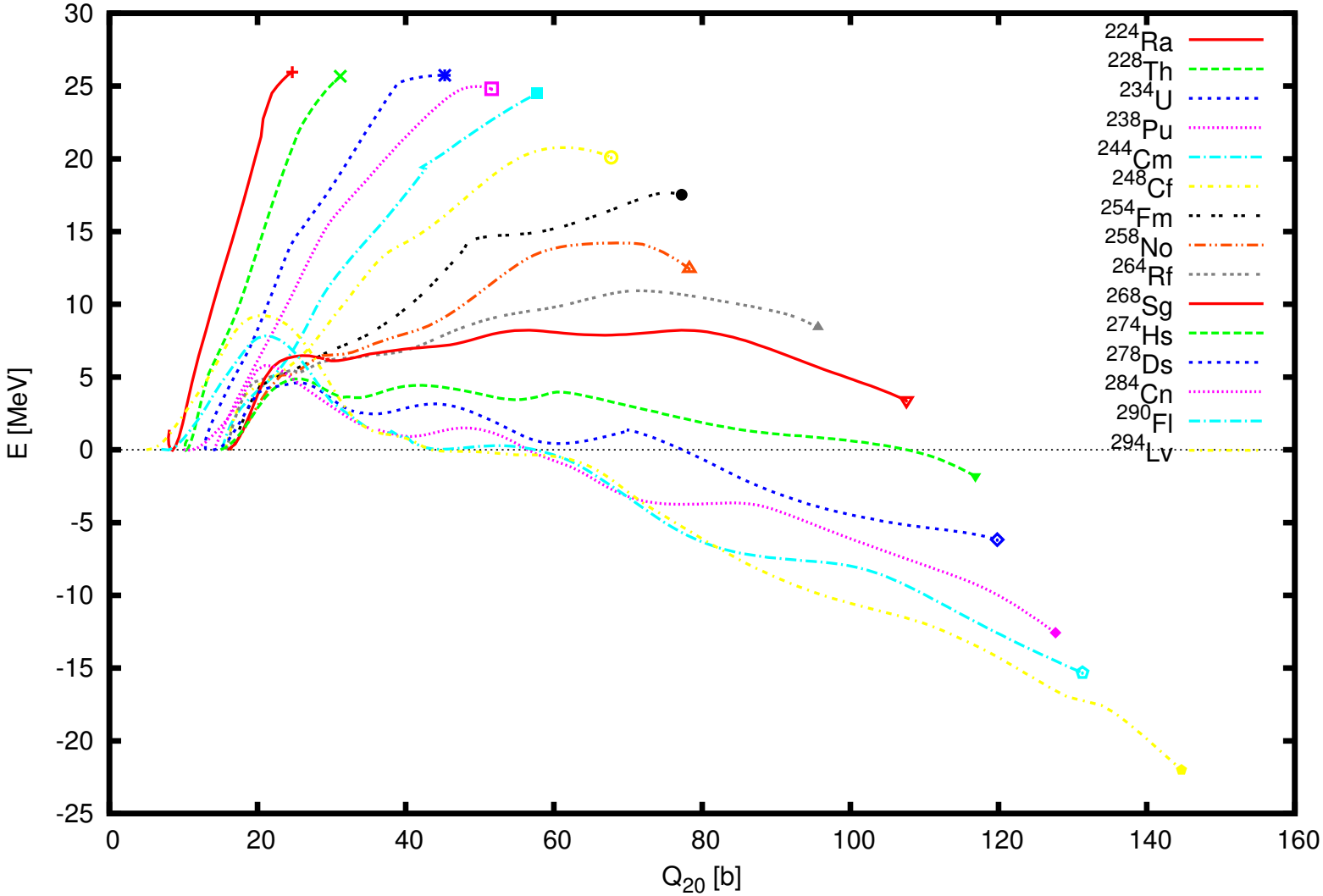

Pre-scission shapes

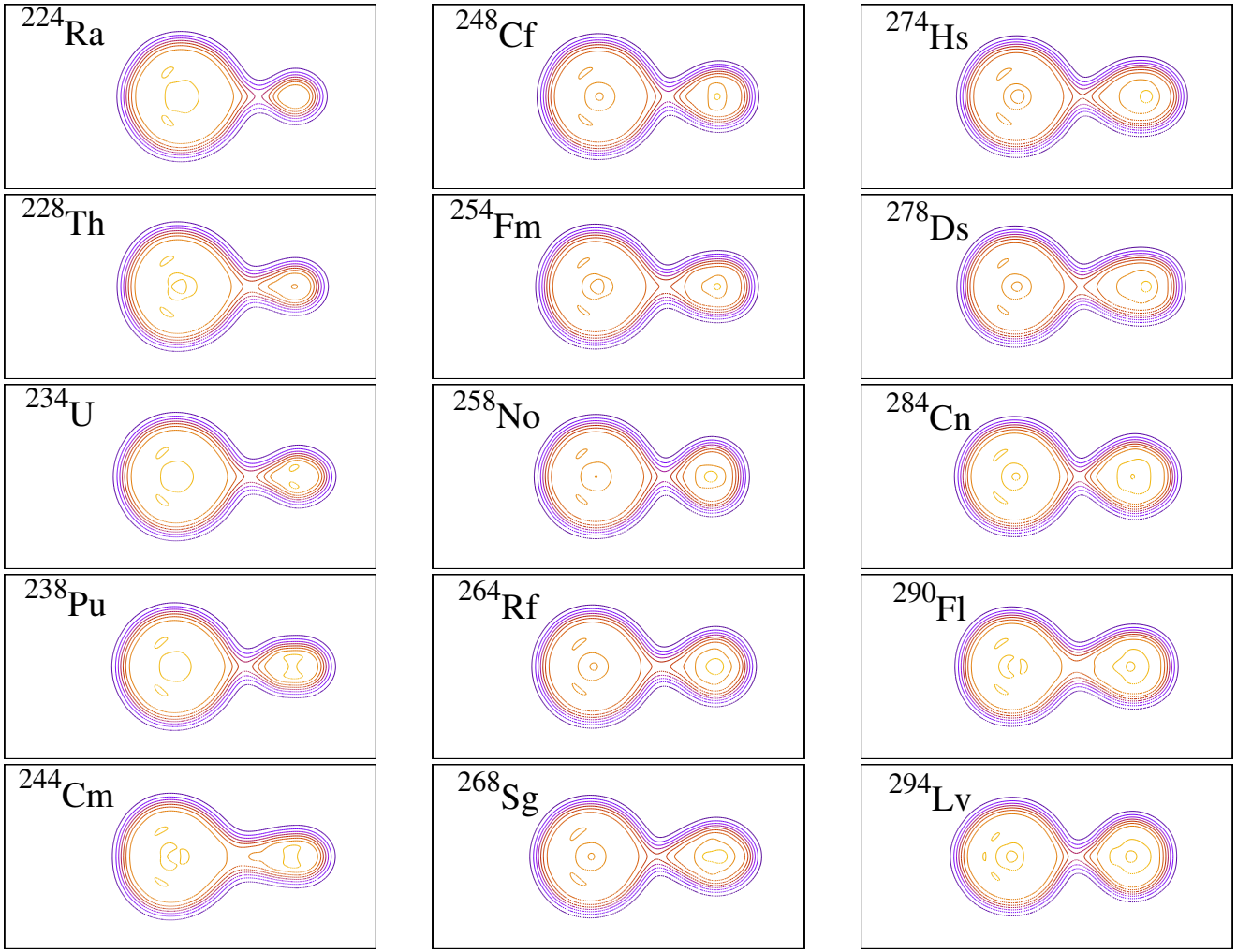

Post-scission shapes

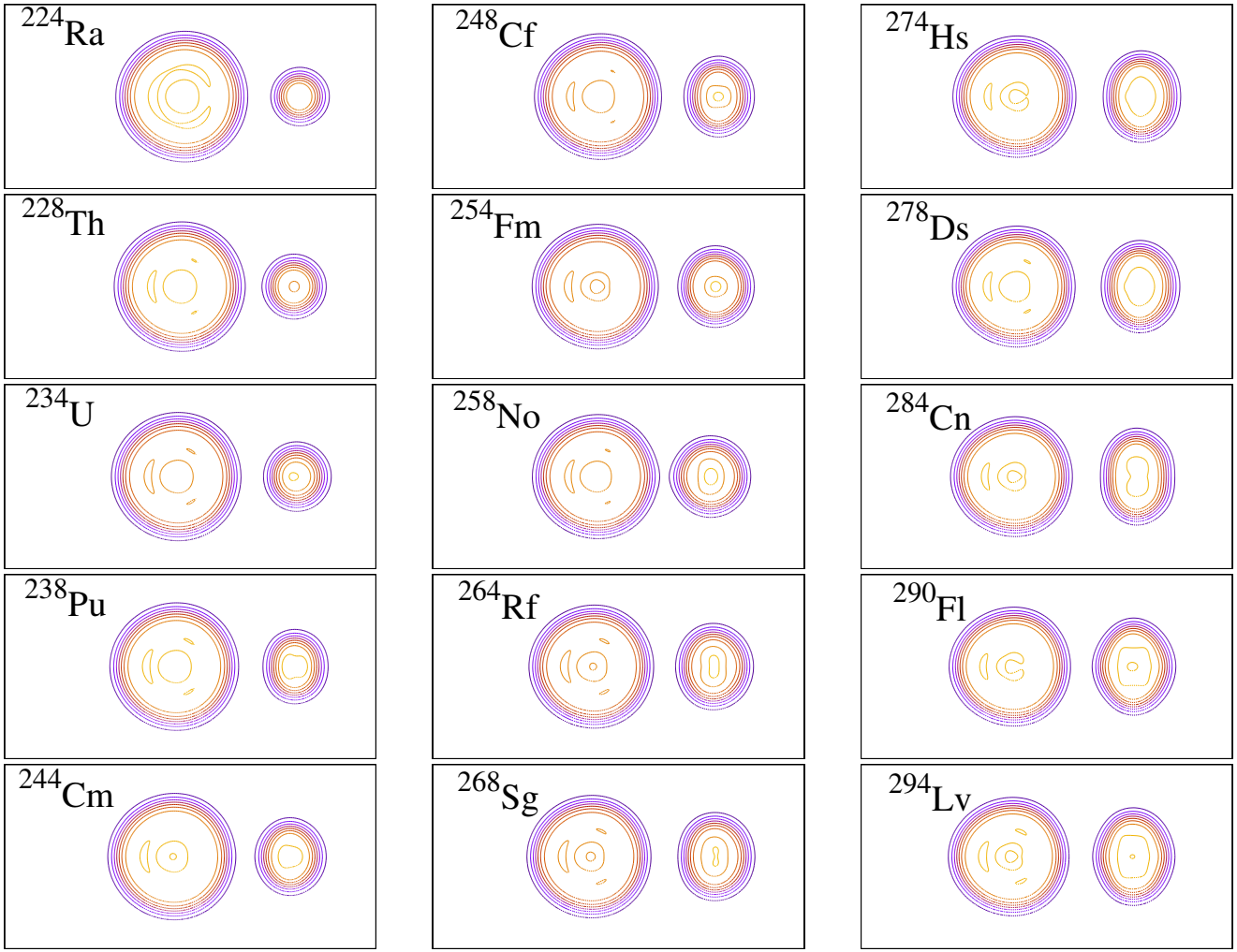

Cluster barriers

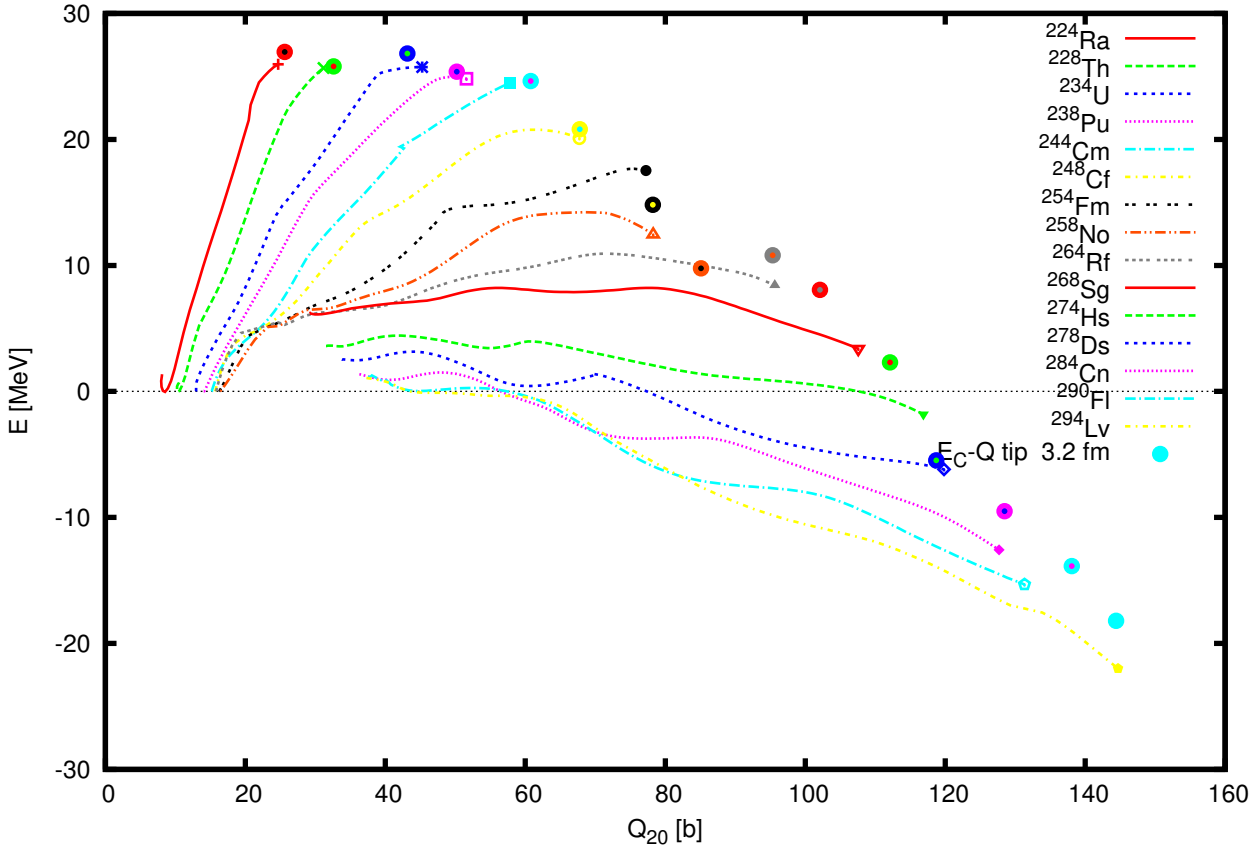

$$E = k\frac{82(Z-82)e^2}{r_{208}+r_{A-208}+d} - Q$$

Half-llives

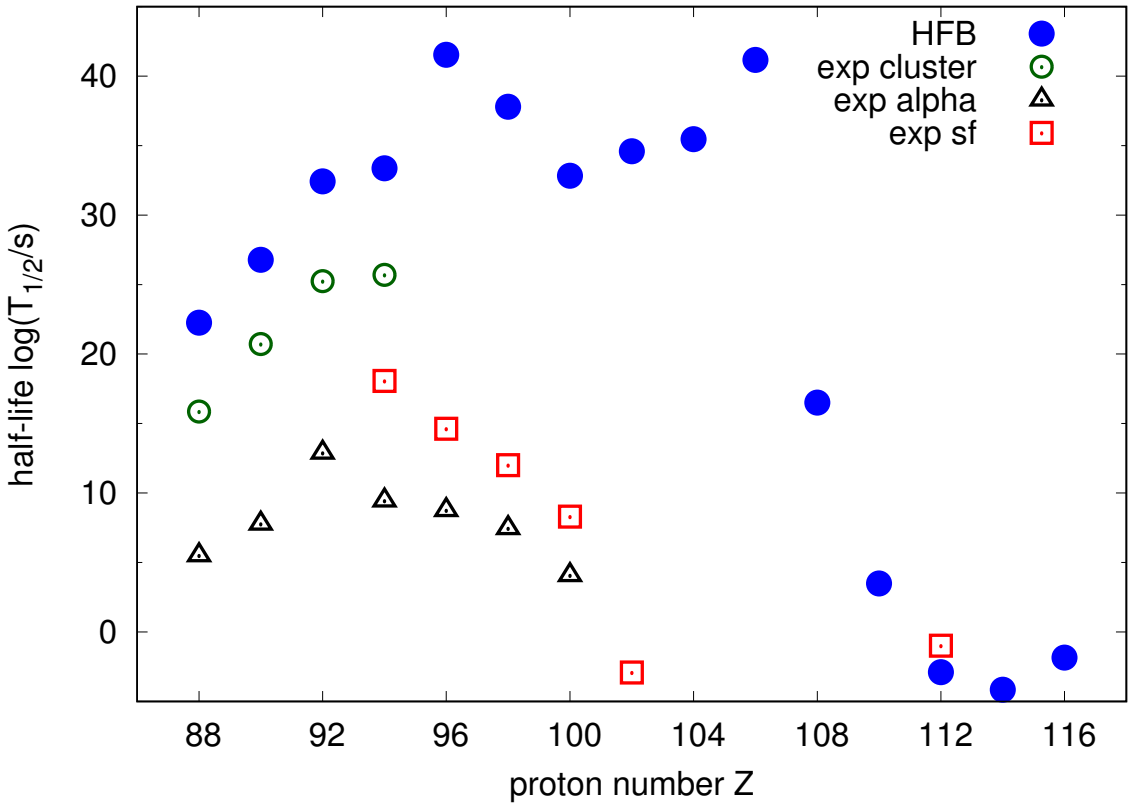
HFB
exp cluster
exp alpha
exp sf
half-life log(T1/2/s)
proton number Z
0
10
20
30
40
88
92
96
100
104
108
112
116

Experimental evidence in ^{284}Cn:

- GSI: 9 events
  Ch. Düllmann, at al., Phys.Rev.Lett. 104, 252701 (2010)
- Dubna: 19 events
  Yu. Oganessian, Radiochim.Acta 99, 429 (2011)
- lifetimes: 30 ms - 400 ms

^{284}Cn

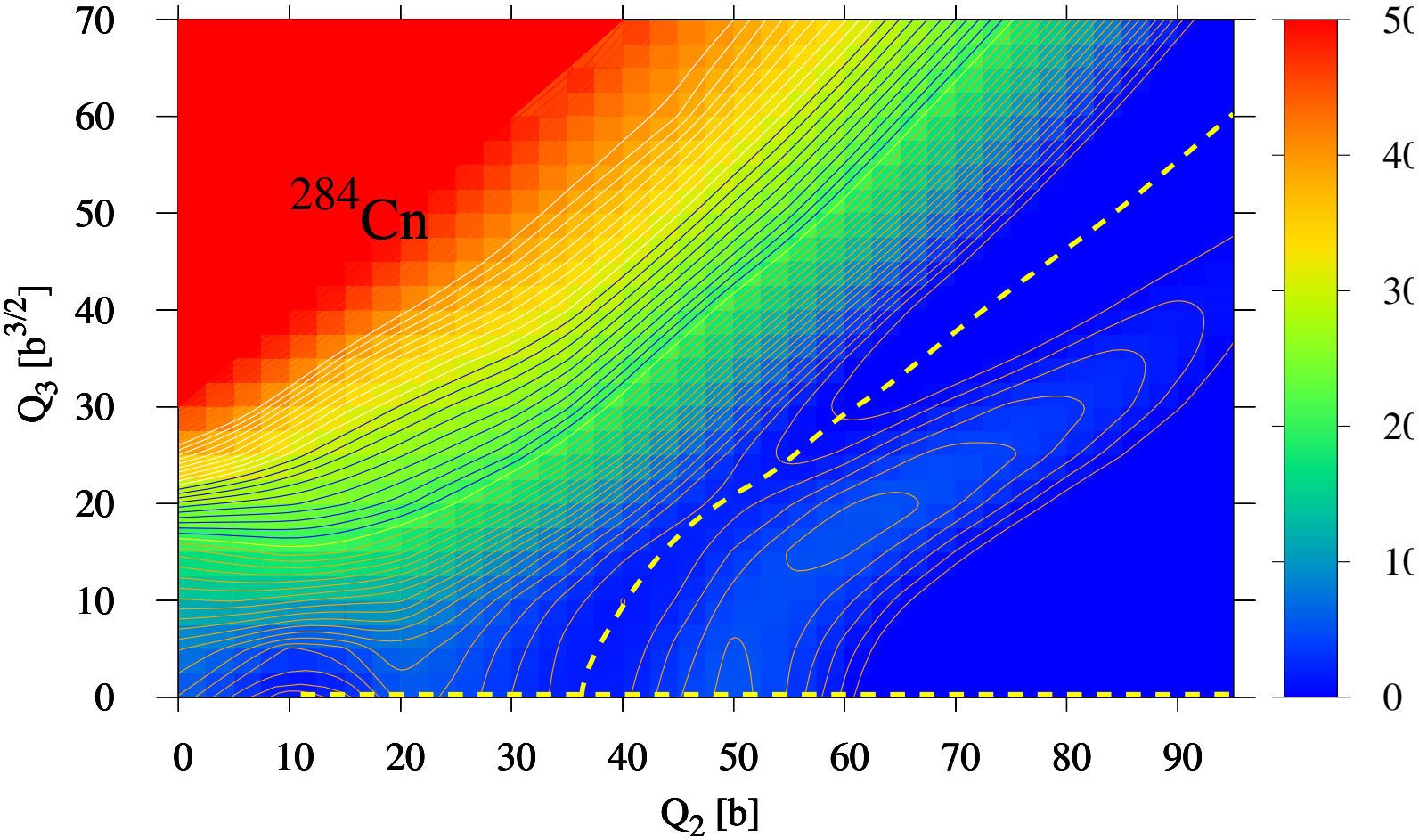

^{284}Cn

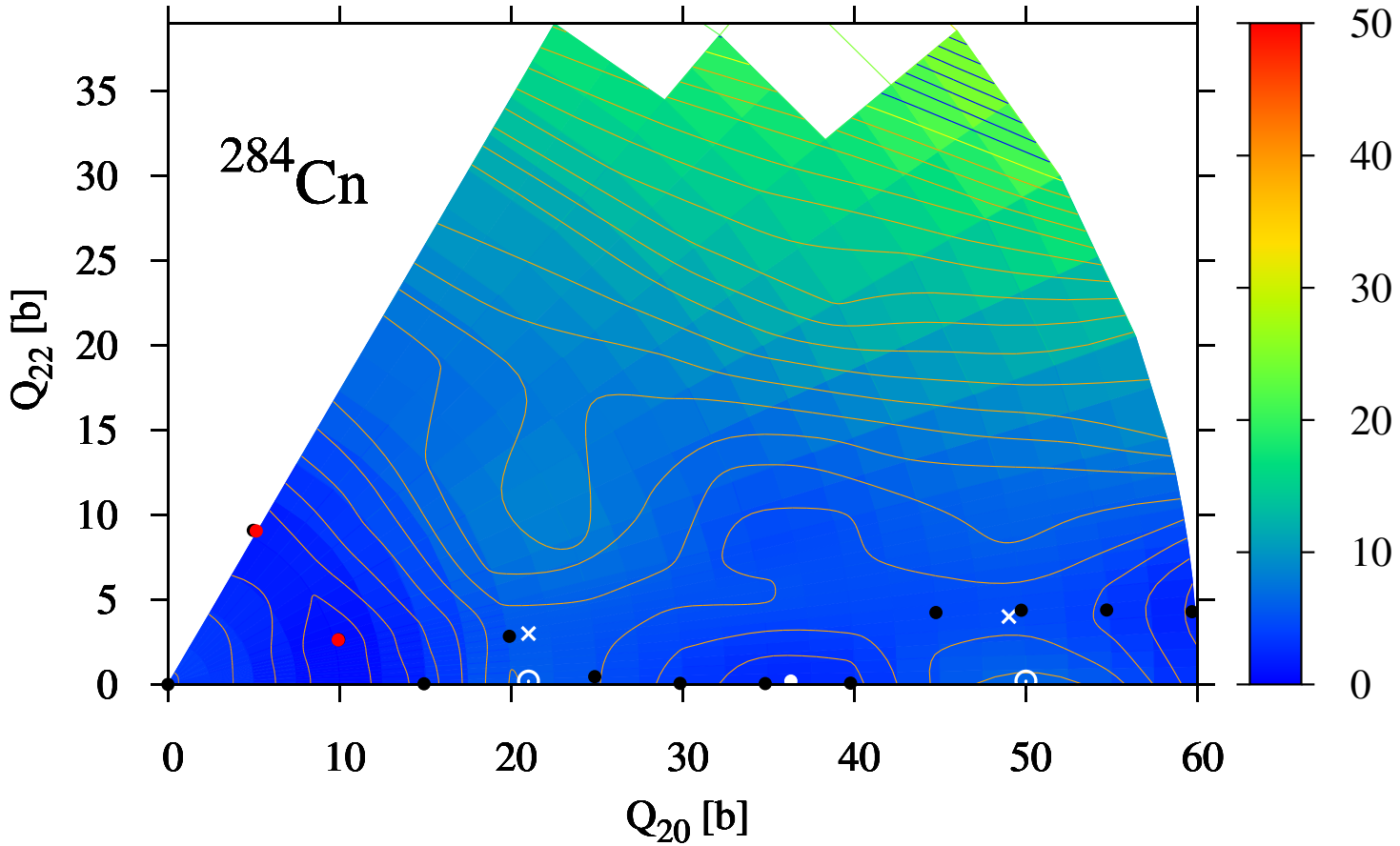
284Cn
Q22 [b]
Q20 [b]
0
5
10
15
20
25
30
35
0
10
20
30
40
50
60
0
10
20
30
40
50

^{284}Cn

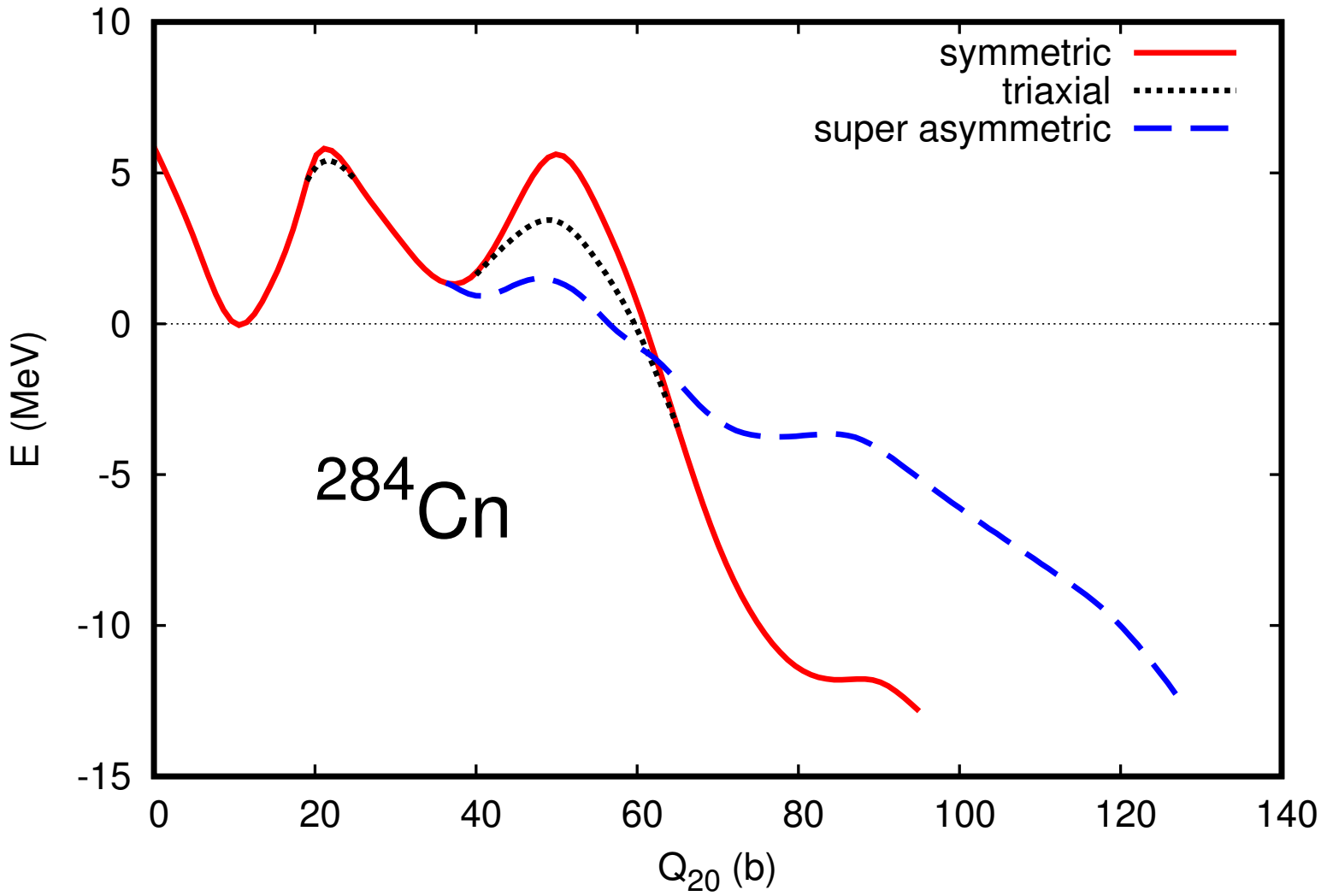
symmetric
triaxial
super asymmetric
^{284}Cn
E (MeV)
Q_{20} (b)
10
5
0
-5
-10
-15
0
20
40
60
80
100
120
140

Chart of SH nuclides

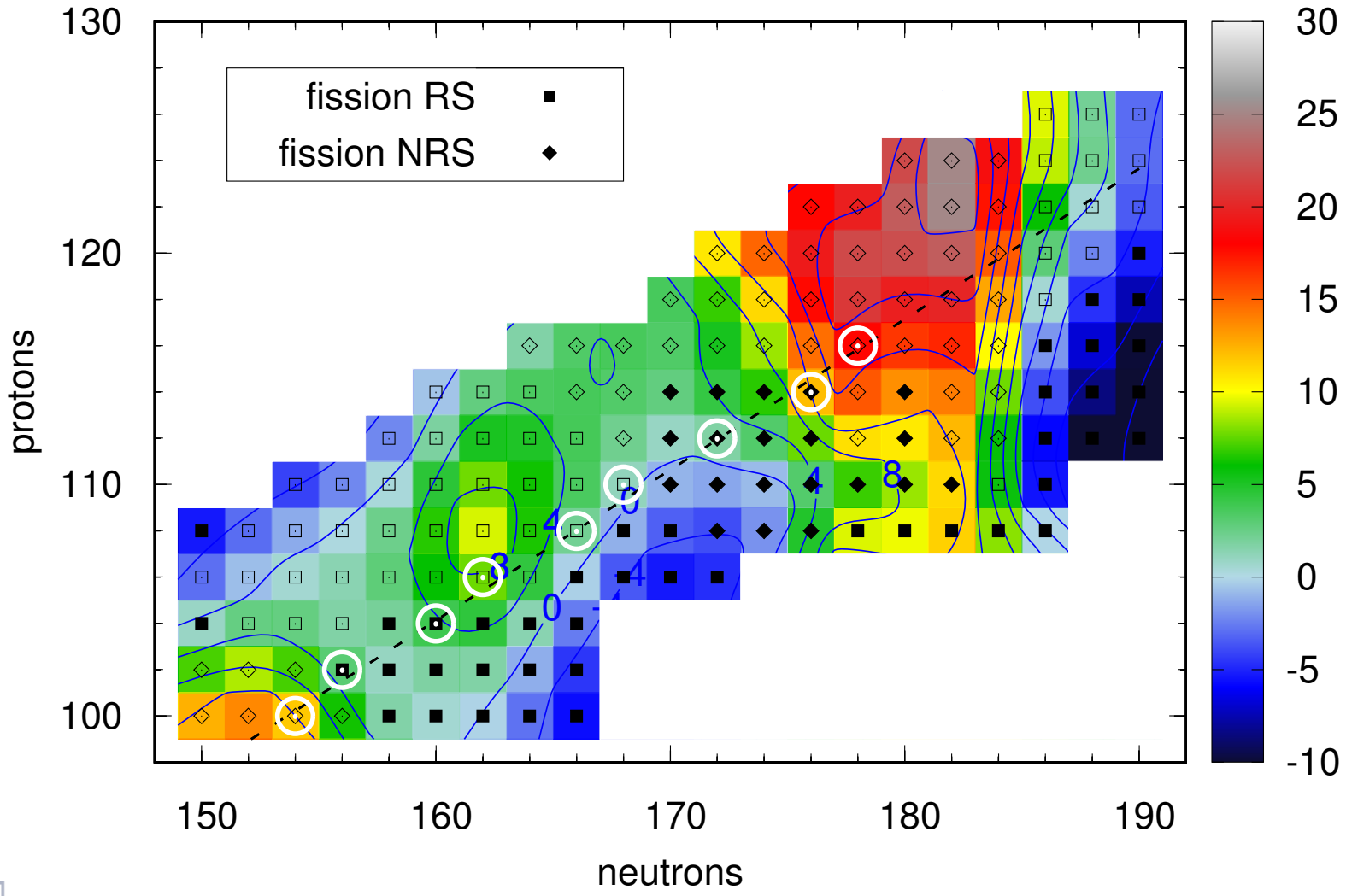

Actinides and superheavies

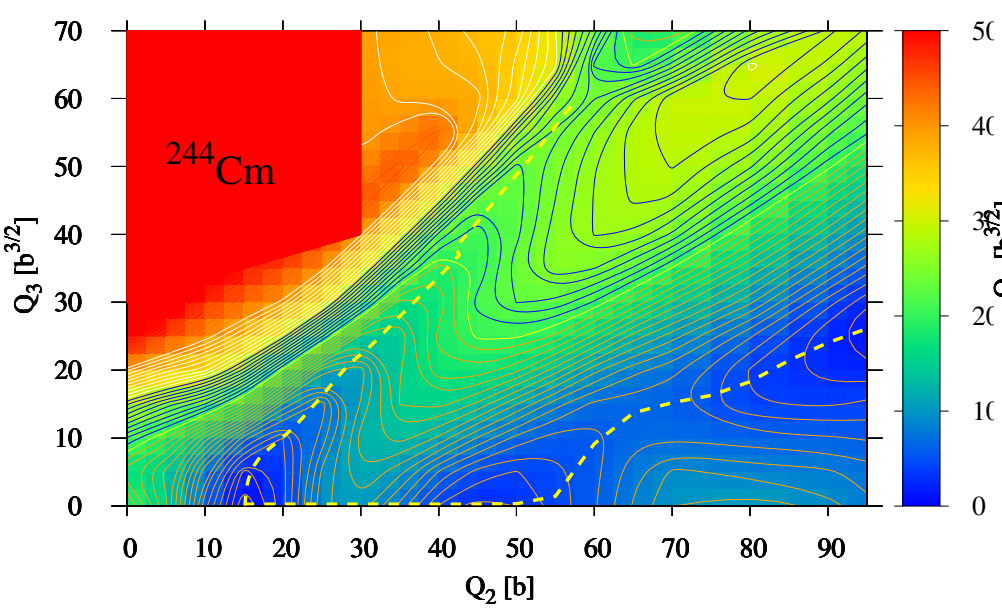

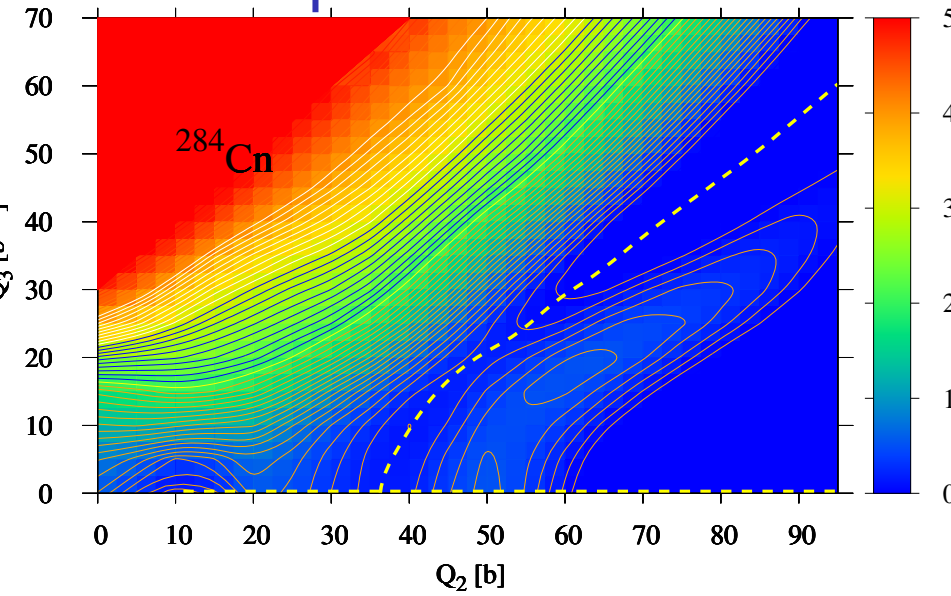

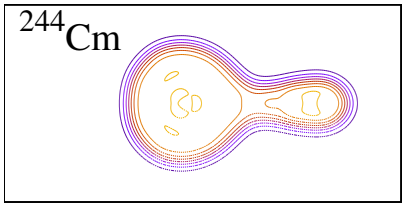

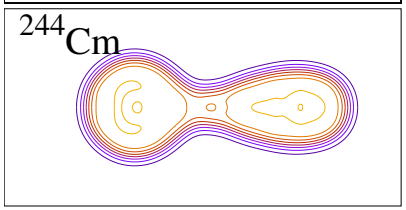

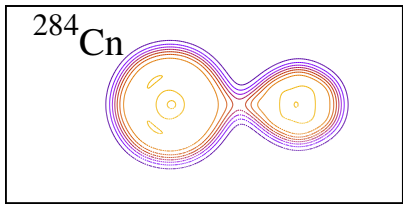

Actinides and superheavies

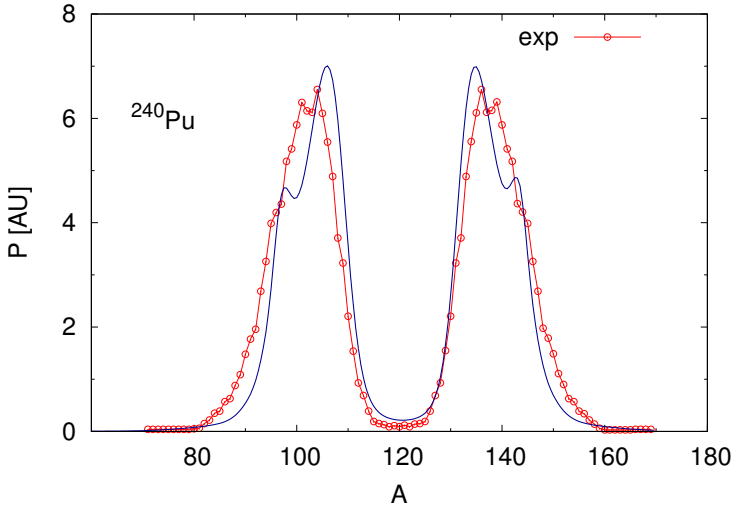

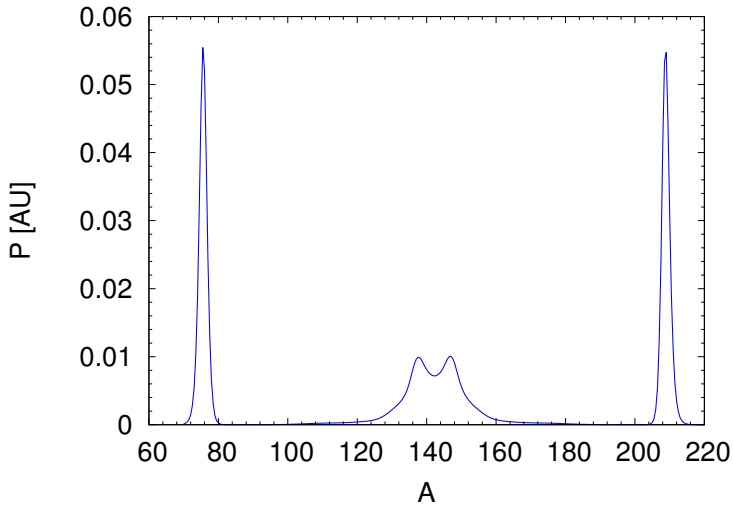

A. Zdeb, A. Dobrowolski, and M. Warda, Phys. Rev. C 95, 054608 (2017)

Mean fission fragment mass

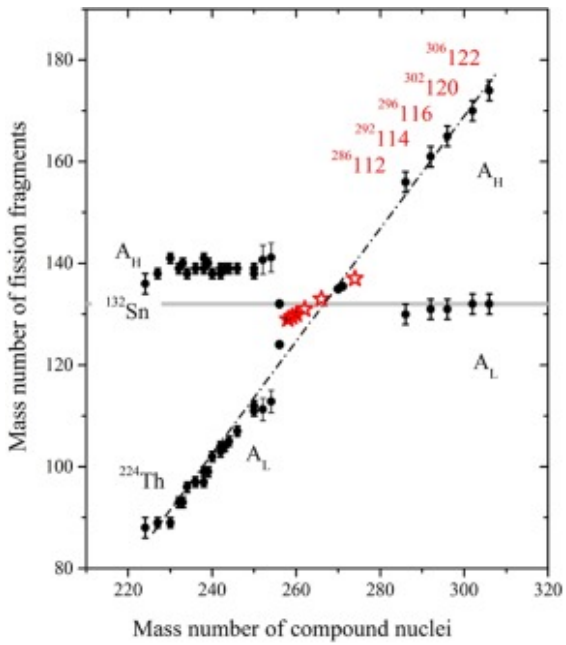

M.G.Itkis, E.Vardaci, I.M.Itkis, G.N.Knyazheva, E.M.Kozulin, Nuclear Physics A944 (2015) 204

Mean fission fragment mass

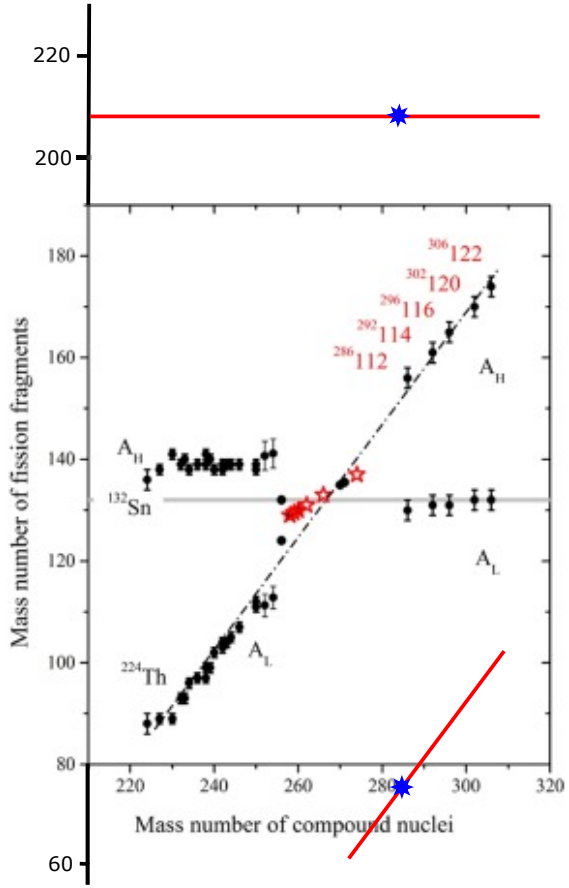

M.G.Itkis, E.Vardaci, I.M.Itkis, G.N.Knyazheva, E.M.Kozulin, Nuclear Physics A944 (2015) 204

Isotopes and isobars

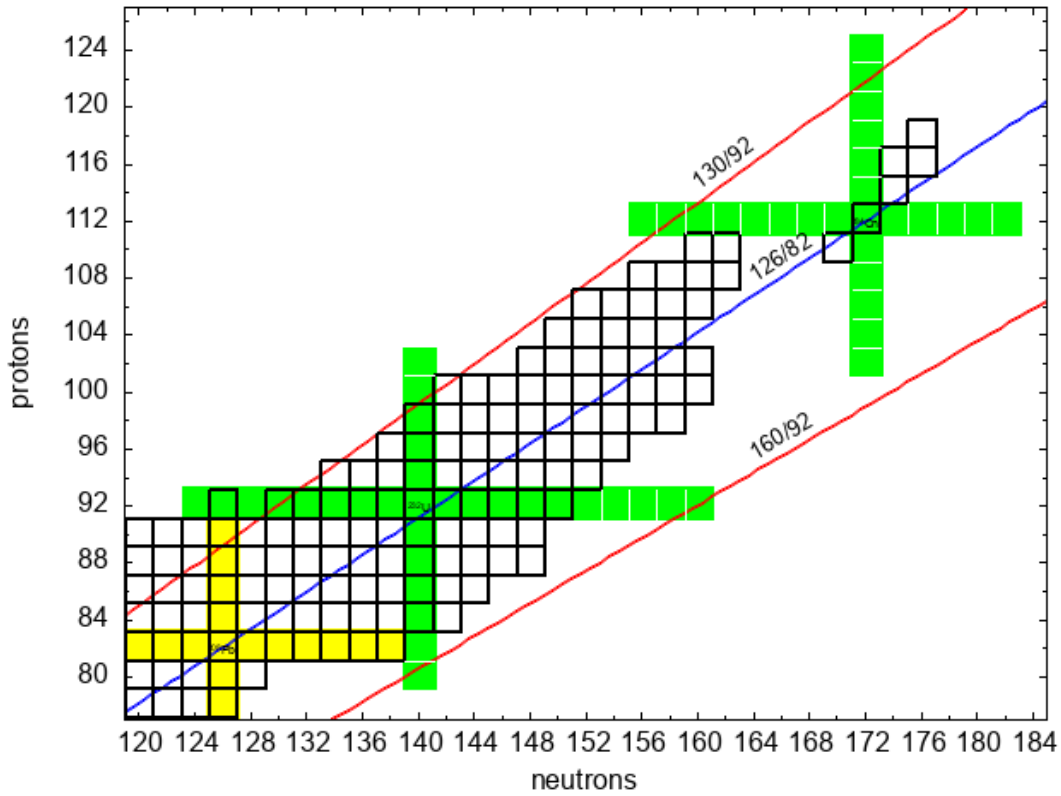

M. Warda, A. Zdeb, and R. Rodrguez-Guzmn, Phys. Rev. C 113, 034619 (2026)

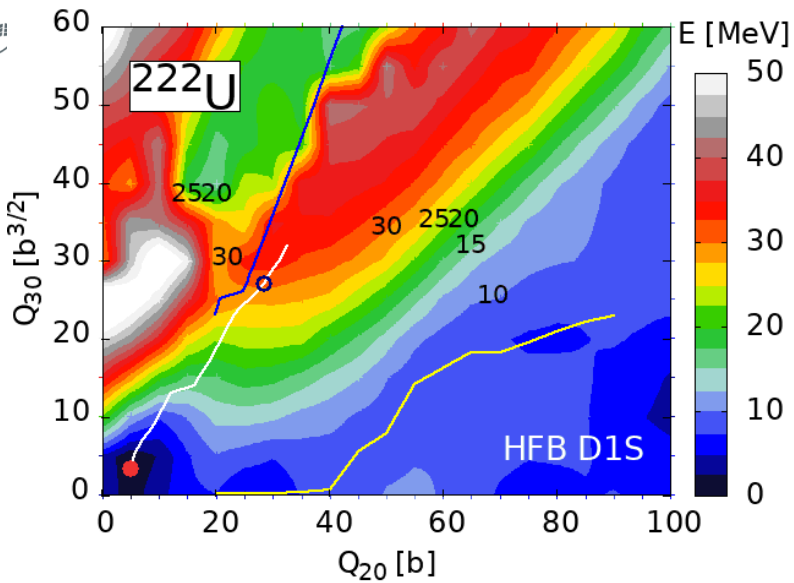
222U
HFB D1S
Q30 [b3/2]
Q20 [b]
E [MeV]
2520
30
15
10

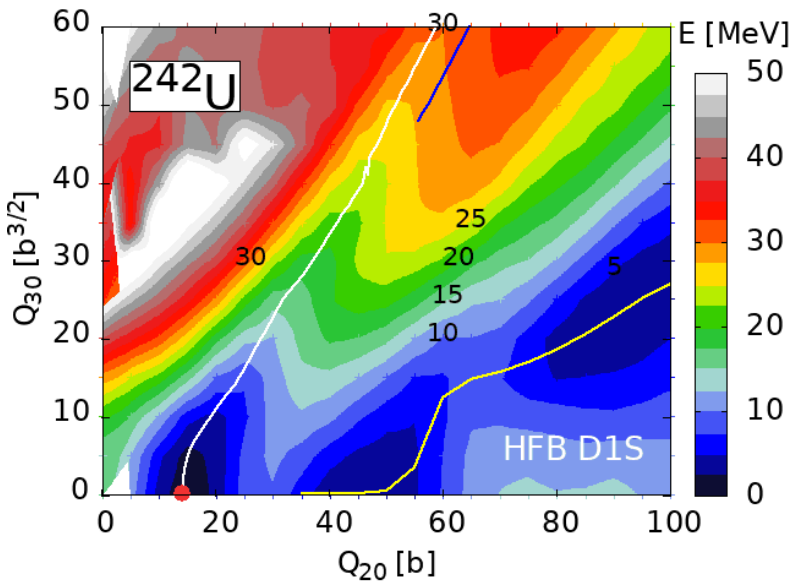
242U
HFB D1S
Q30 [b3/2]
Q20 [b]
E [MeV]
30
25
20
15
10
5

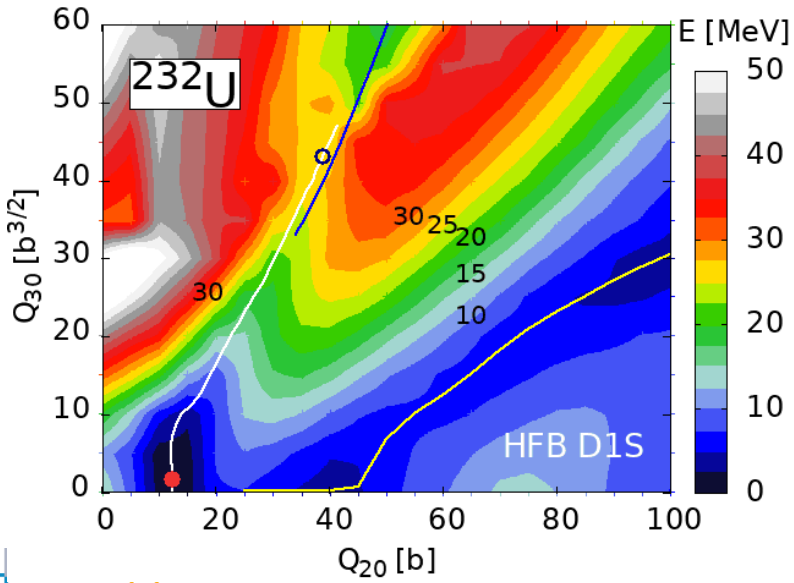
232U
HFB D1S
Q30 [b3/2]
Q20 [b]
E [MeV]
30
25
20
15
10

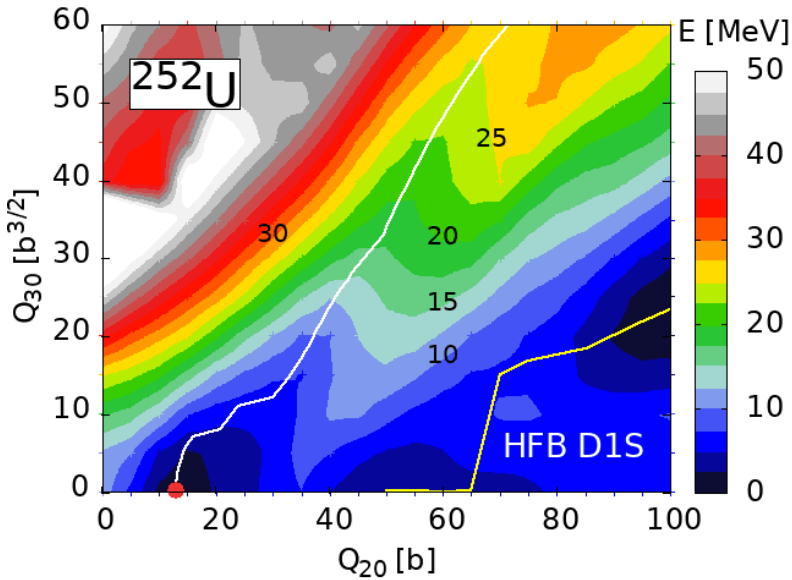
252U
HFB D1S
Q30 [b3/2]
Q20 [b]
E [MeV]
30
25
20
15
10

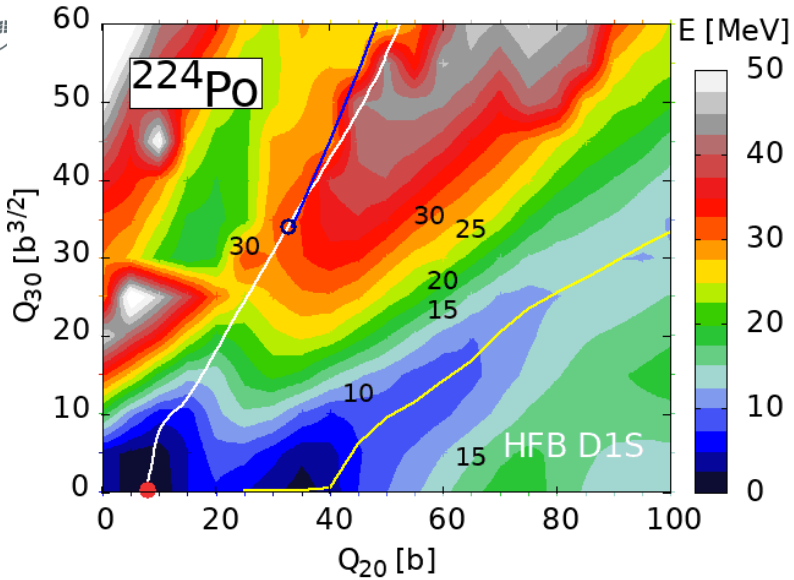
224Po
HFB D1S
Q30 [b3/2]
Q20 [b]
E [MeV]

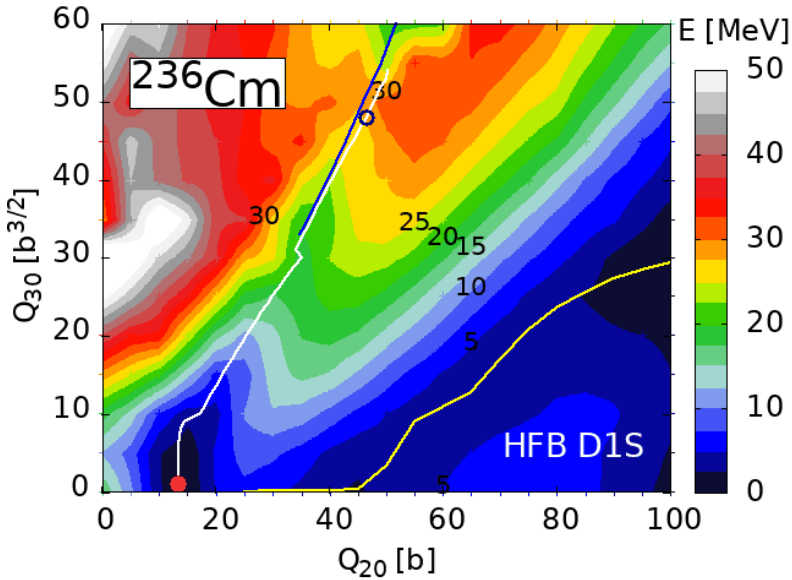
236Cm
HFB D1S
Q30 [b3/2]
Q20 [b]
E [MeV]

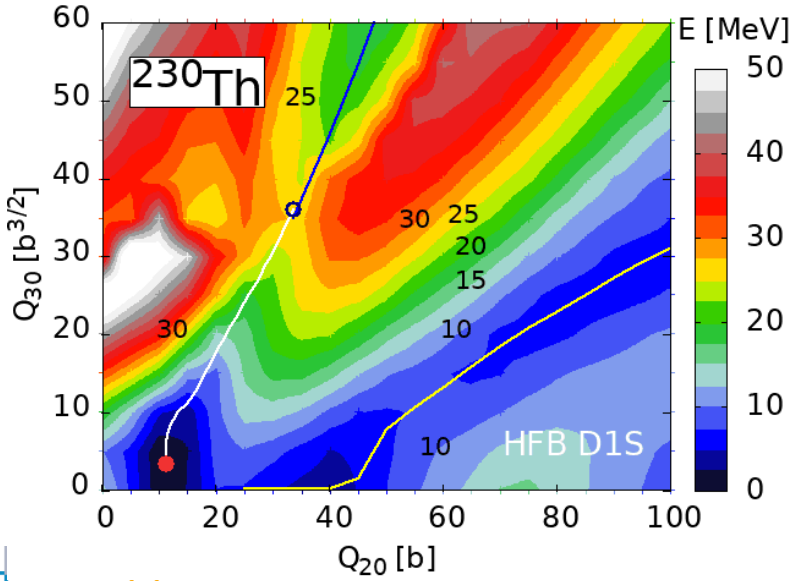
230Th
HFB D1S
Q30 [b3/2]
Q20 [b]
E [MeV]

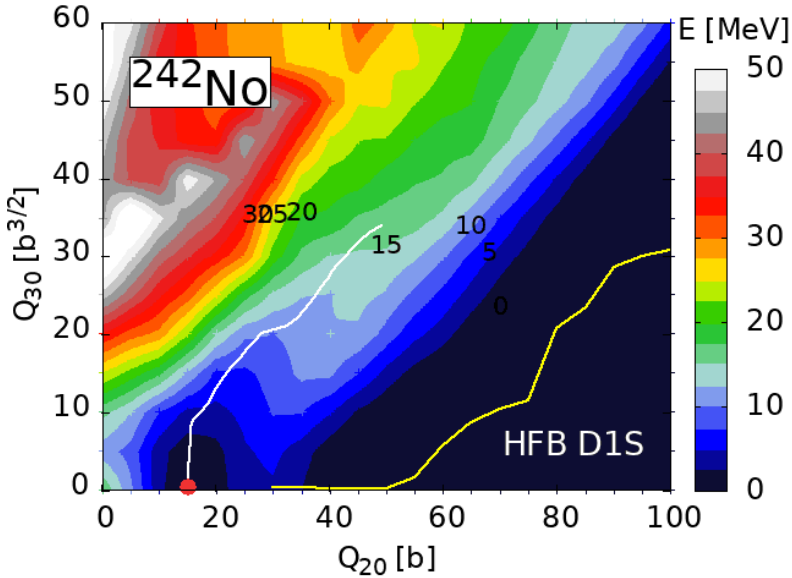
242No
HFB D1S
Q30 [b3/2]
Q20 [b]
E [MeV]

Fission paths around ^{232}U

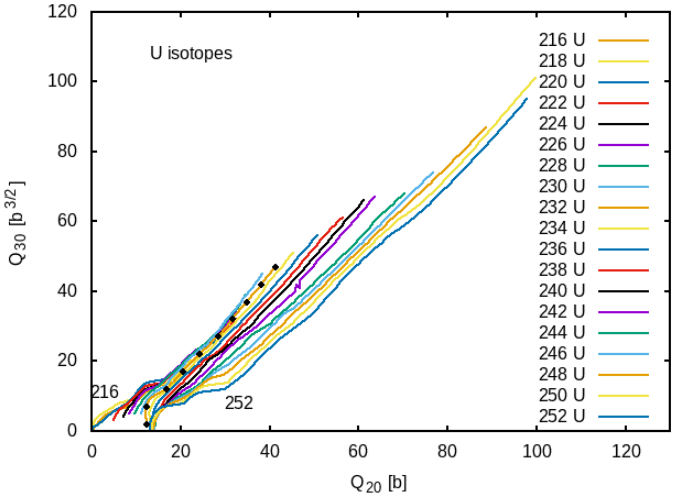

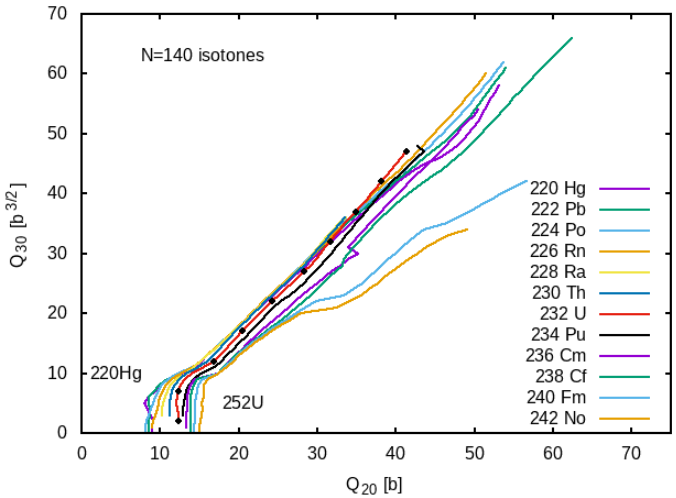

Fission paths around ^{232}U

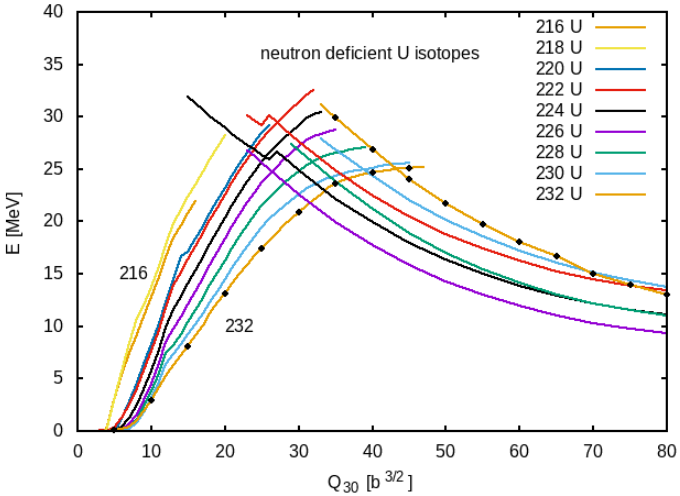

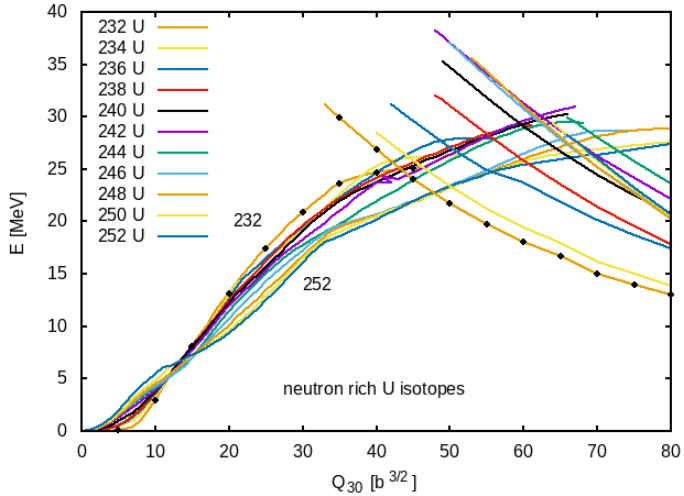

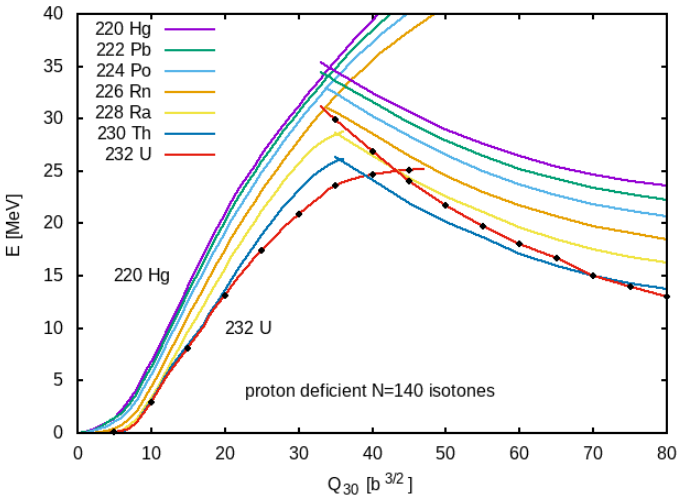

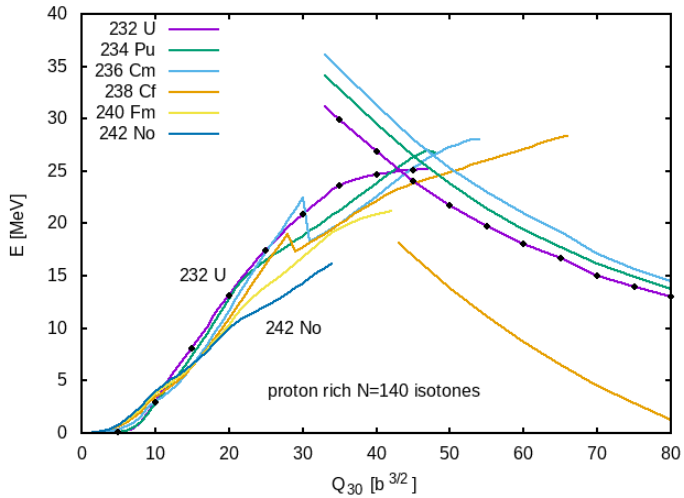

Fission paths around ^{232}U

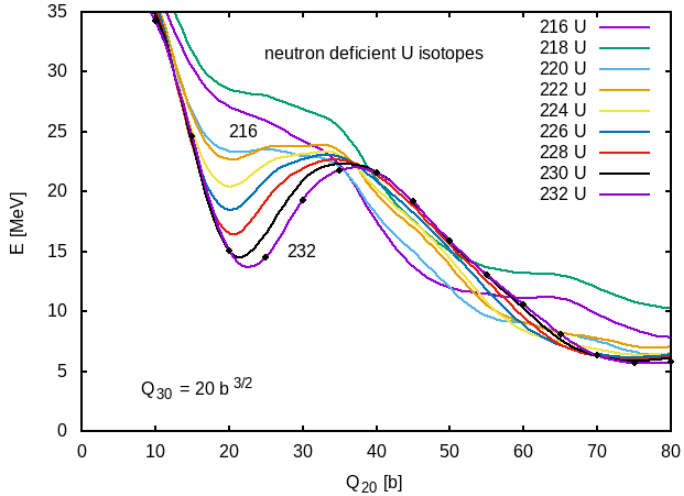

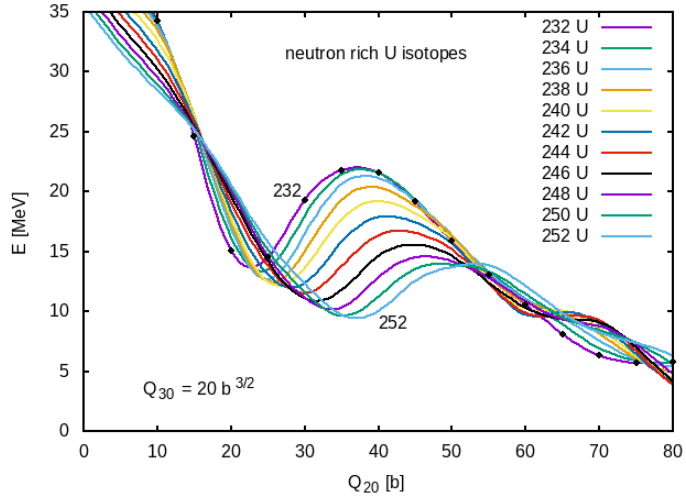

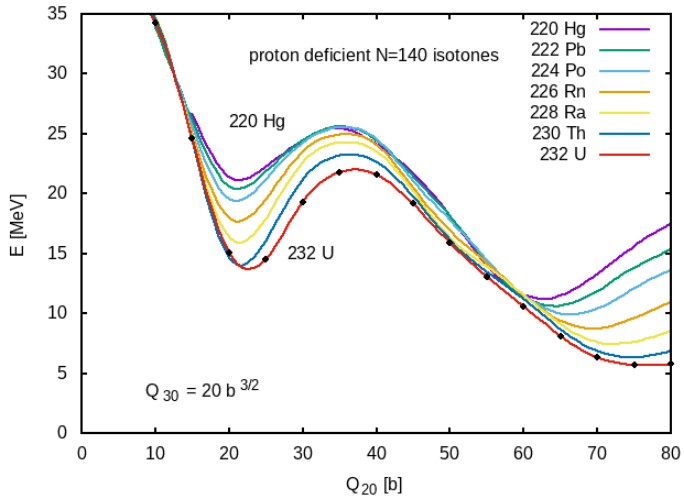

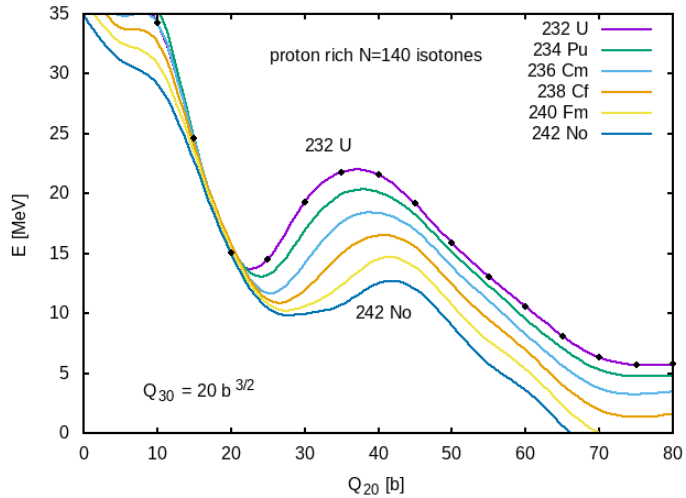

www.umcs.lublin.pl

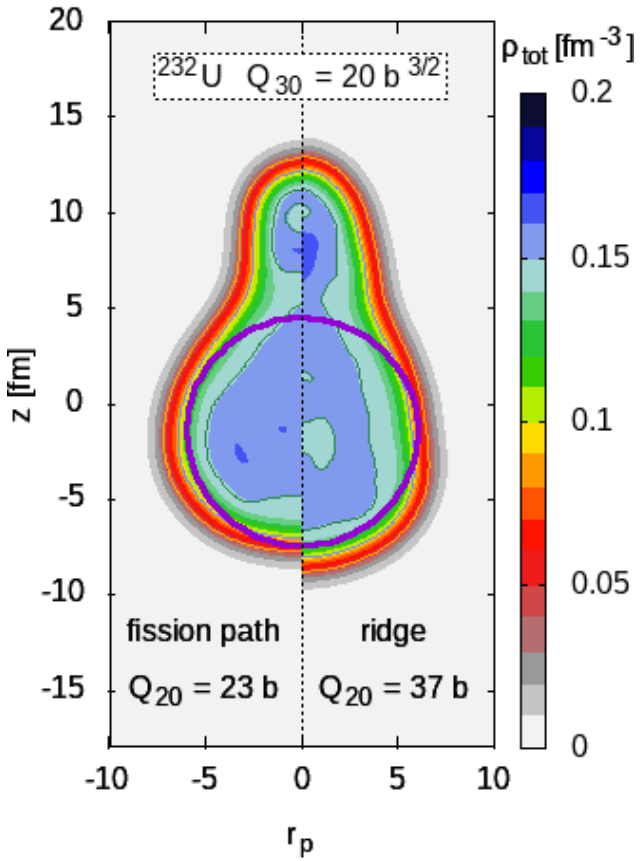
^{232}U Q_{30} = 20 b $^{3/2}$
ρ_{tot} [fm^{-3}]
0.2
0.15
0.1
0.05
0
z [fm]
20
15
10
5
0
-5
-10
-15
-10
-5
0
5
10
r_p
fission path
Q_{20} = 23 b
ridge
Q_{20} = 37 b

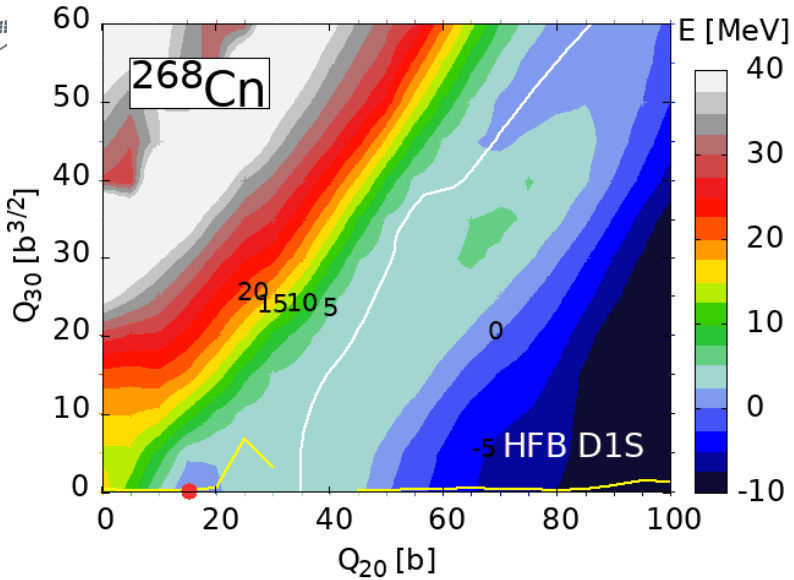
268Cn
HFB D1S
Q30 [b3/2]
Q20 [b]
E [MeV]

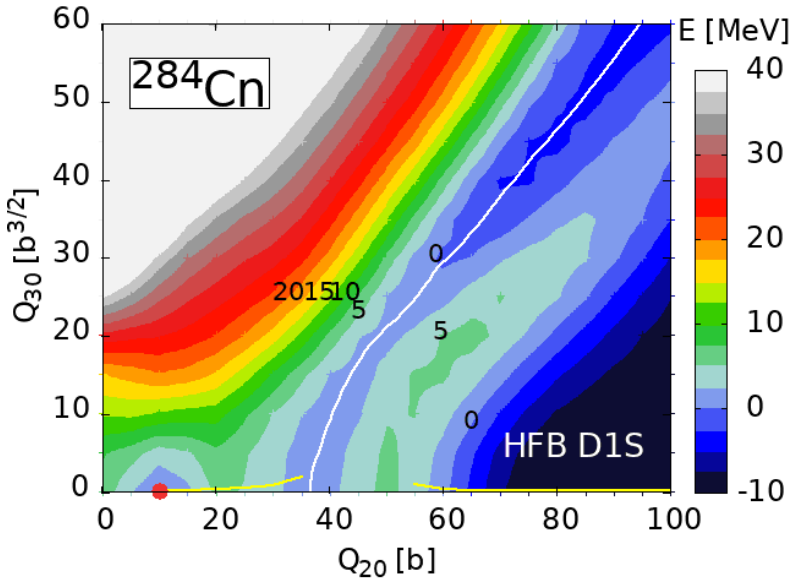
284Cn
HFB D1S
Q30 [b3/2]
Q20 [b]
E [MeV]

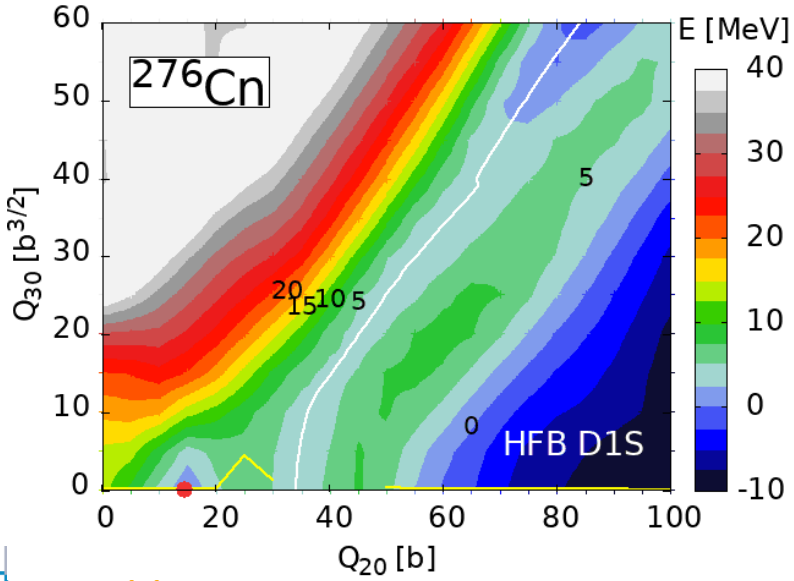
276Cn
HFB D1S
Q30 [b3/2]
Q20 [b]
E [MeV]

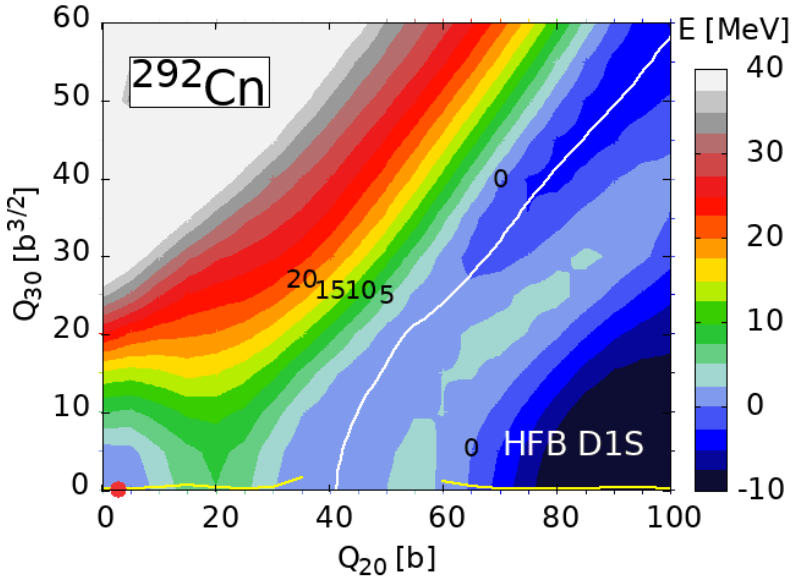
292Cn
HFB D1S
Q30 [b3/2]
Q20 [b]
E [MeV]

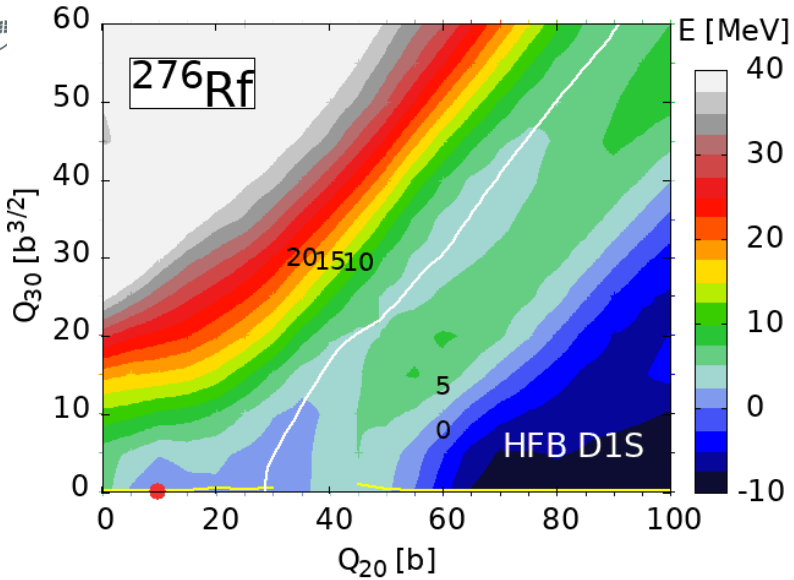
276Rf
HFB D1S
Q20 [b]
Q30 [b3/2]
E [MeV]

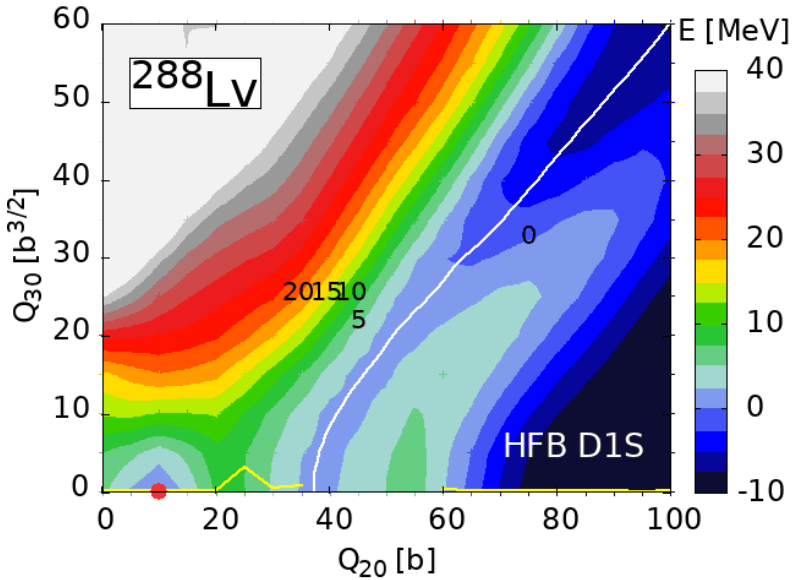
288Lv
HFB D1S
Q20 [b]
Q30 [b3/2]
E [MeV]

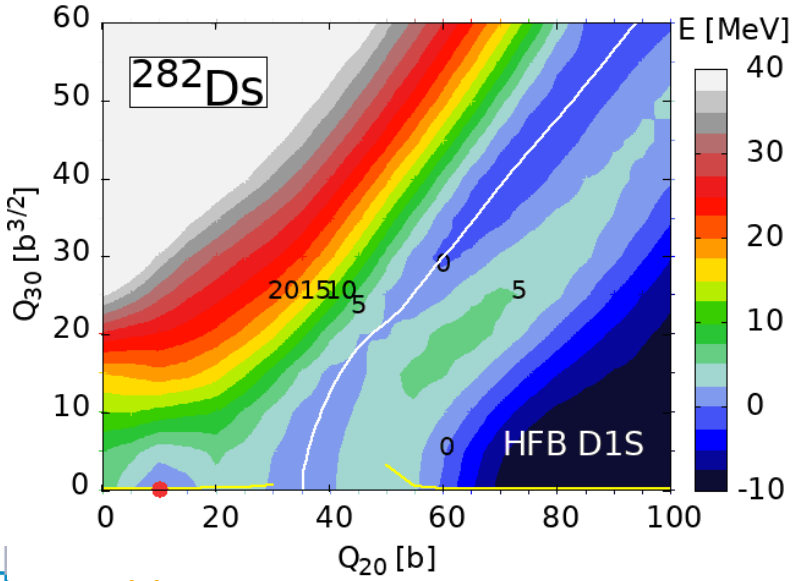
282Ds
HFB D1S
Q20 [b]
Q30 [b3/2]
E [MeV]

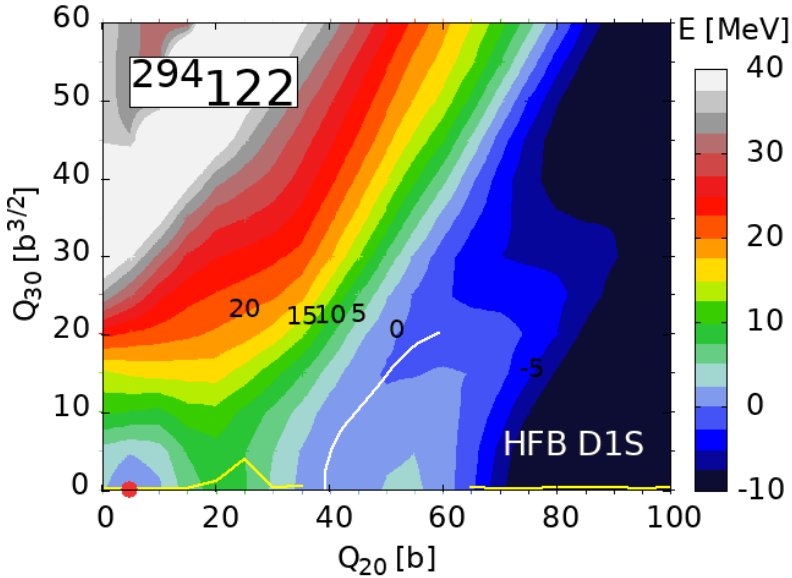
294122
HFB D1S
Q20 [b]
Q30 [b3/2]
E [MeV]

Fission paths around ^{284}Cn

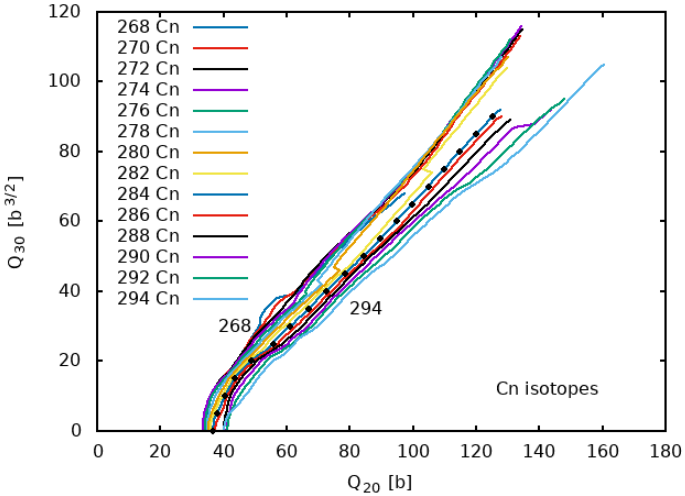

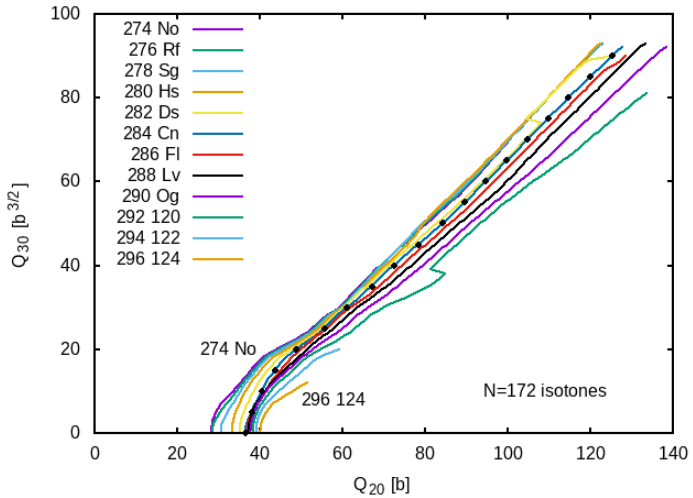

Fission paths around ^{284}Cn

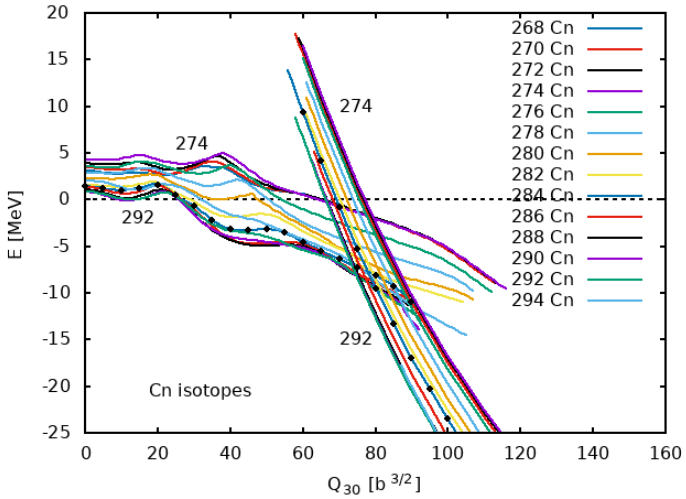

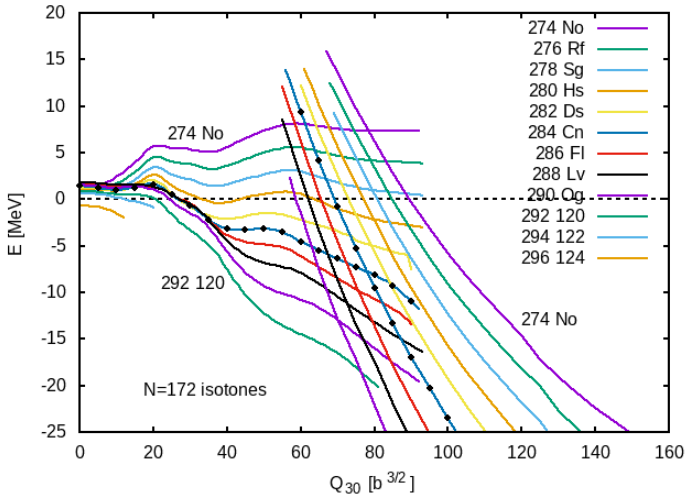

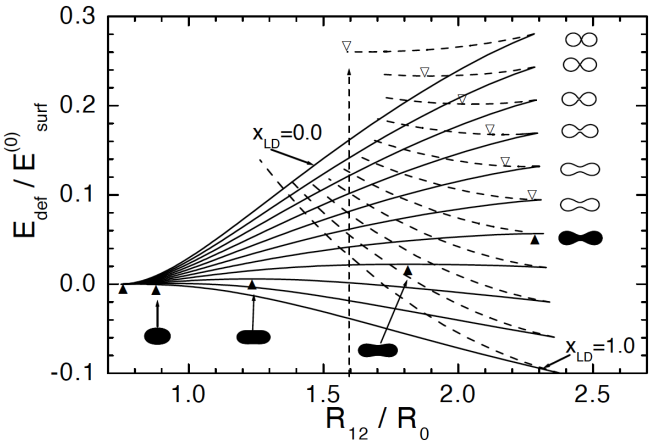

F. Ivanyuk, K. Pomorski, Phys. Rev. C 79, 054327 (2009).
F. Ivanyuk, K. Pomorski, Int. J. Mod. Phys E 19, 514 (2010).

Fission paths around ^{284}Cn

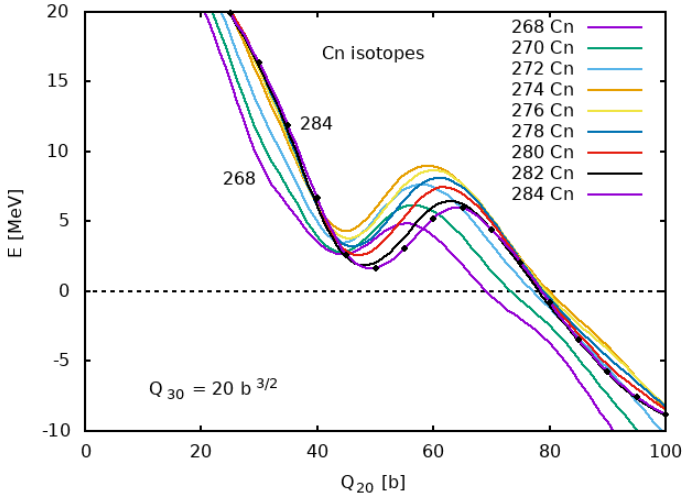

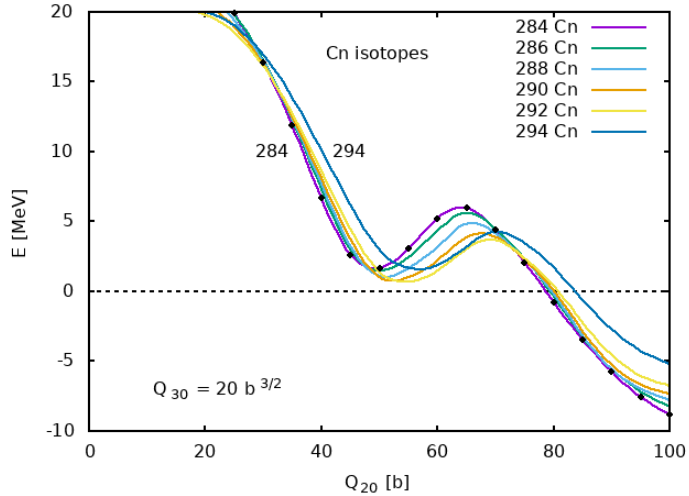

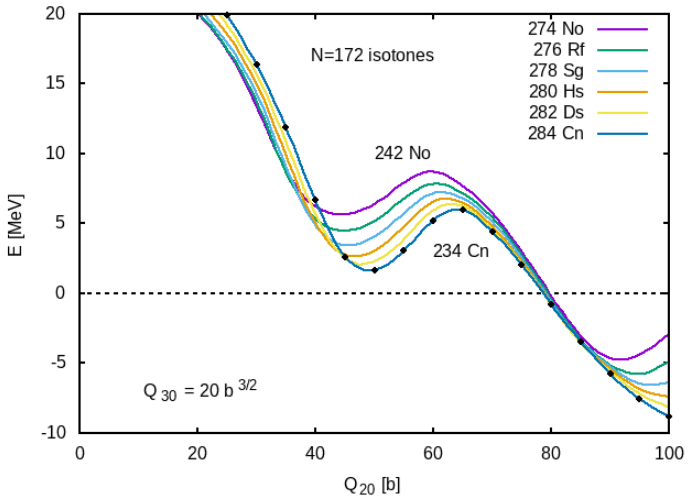

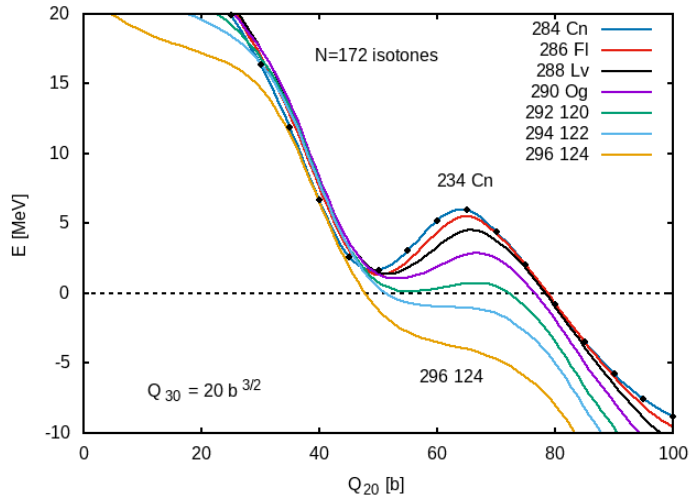

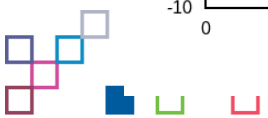

Isotopes and isobars

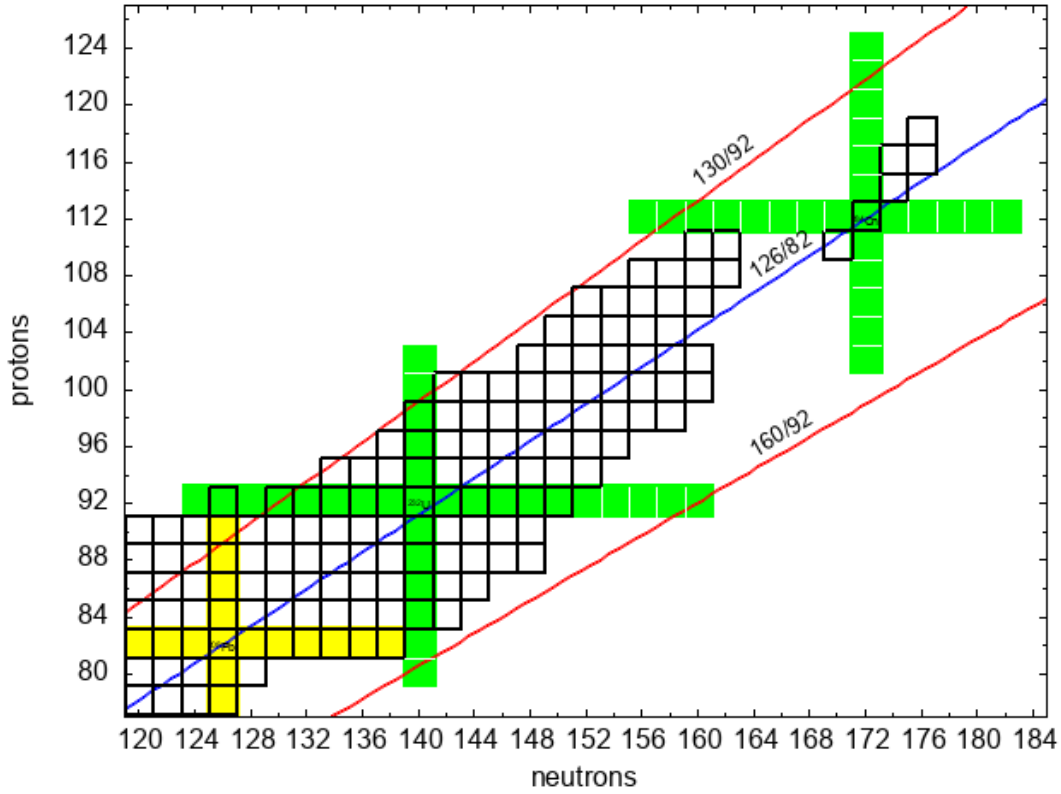

Conclusions

- Cluster radioactivity described as super-asymmetric fission in actinides and super-heavy nuclei
- This decay may be dominant decay channel in some super-heavy nuclei
- Shell correction of doubly-magic ^{208}Pb and symmetry energy plays the crucial role in the enhancement of this decay channel
- super-asymmetric fission valley is observed in quite wide range of heavy and super-heavy nuclei

Further investigations

- Shapes and sizes of pre-fragments
- Influence on magic numbers on mass asymmetry

UMCS

32nd Nuclear Physics Workshop

28-30 September 2026
Lublin, Poland

Nuclear physics: structure, excitations, decays

TOPICS

- Nuclear fission and other decay reactions
- Heavy ion collisions
- Effective nuclear interactions
- Symmetries and symmetry breaking in nuclear physics
- Nuclear structure:
  - collective modes in nuclei
  - isomeric states
  - nuclei far from stability

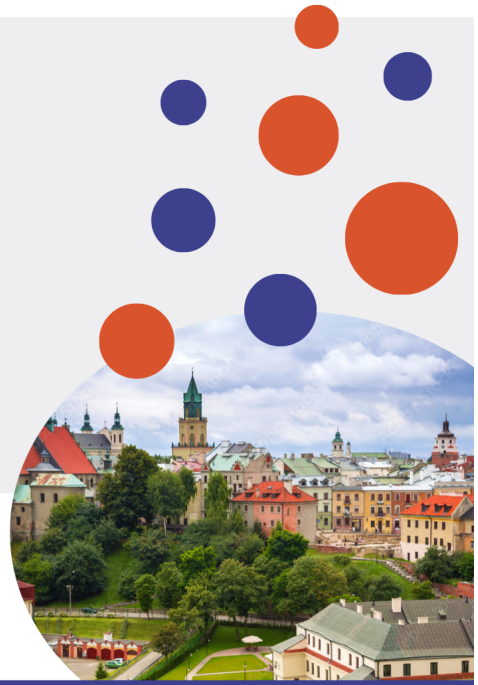

ORGANIZERS

- Department of Theoretical Physics
  Maria Curie-Skłodowska University in Lublin
- National Centre for Nuclear Research in Świerk/Warsaw

IN COOPERATION WITH

- Lublin Branch of the Polish Physical Society
- Nuclear Physics Section of the Polish Physical Society.

https://indico.umcs.pl/event/3/

UMCS UNIWERSYTET MARII CURIE-SKŁODOWSKIEJ

NATIONAL CENTRE FOR NUCLEAR RESEARCH ŚWIERK

POLSKIE TOWARZYSTWO FIZYCZNE 1920

www.umcs.lublin.pl

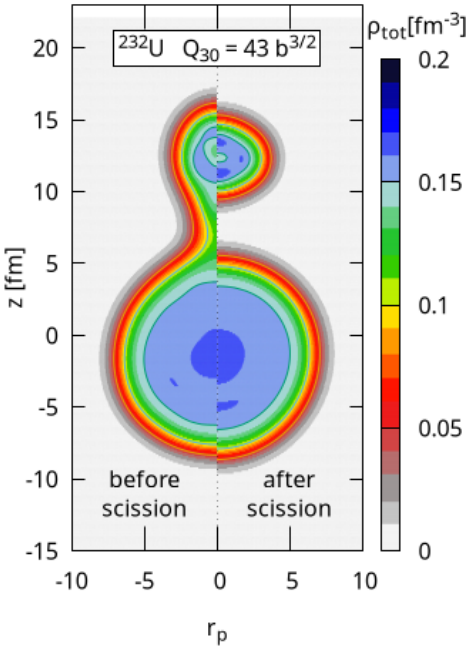

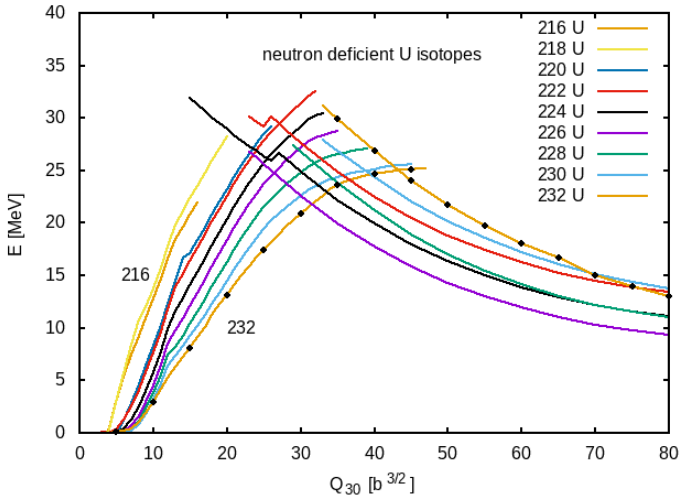

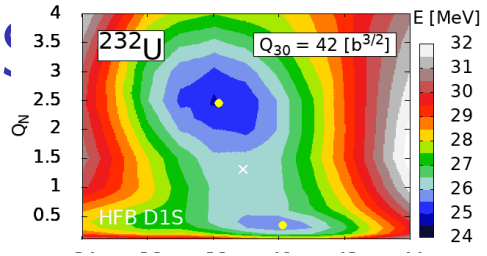

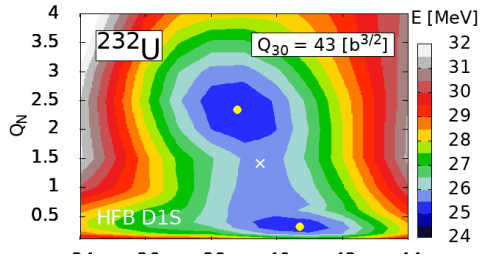

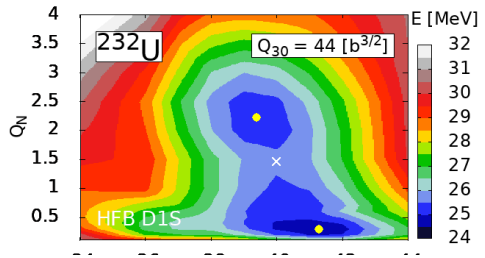

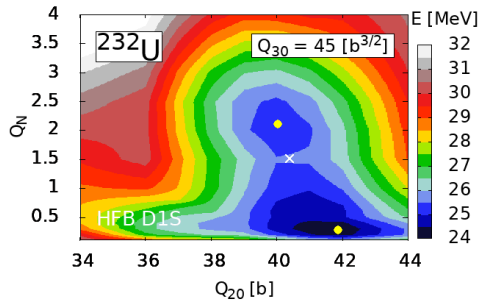

www.umcs.lublin.pl

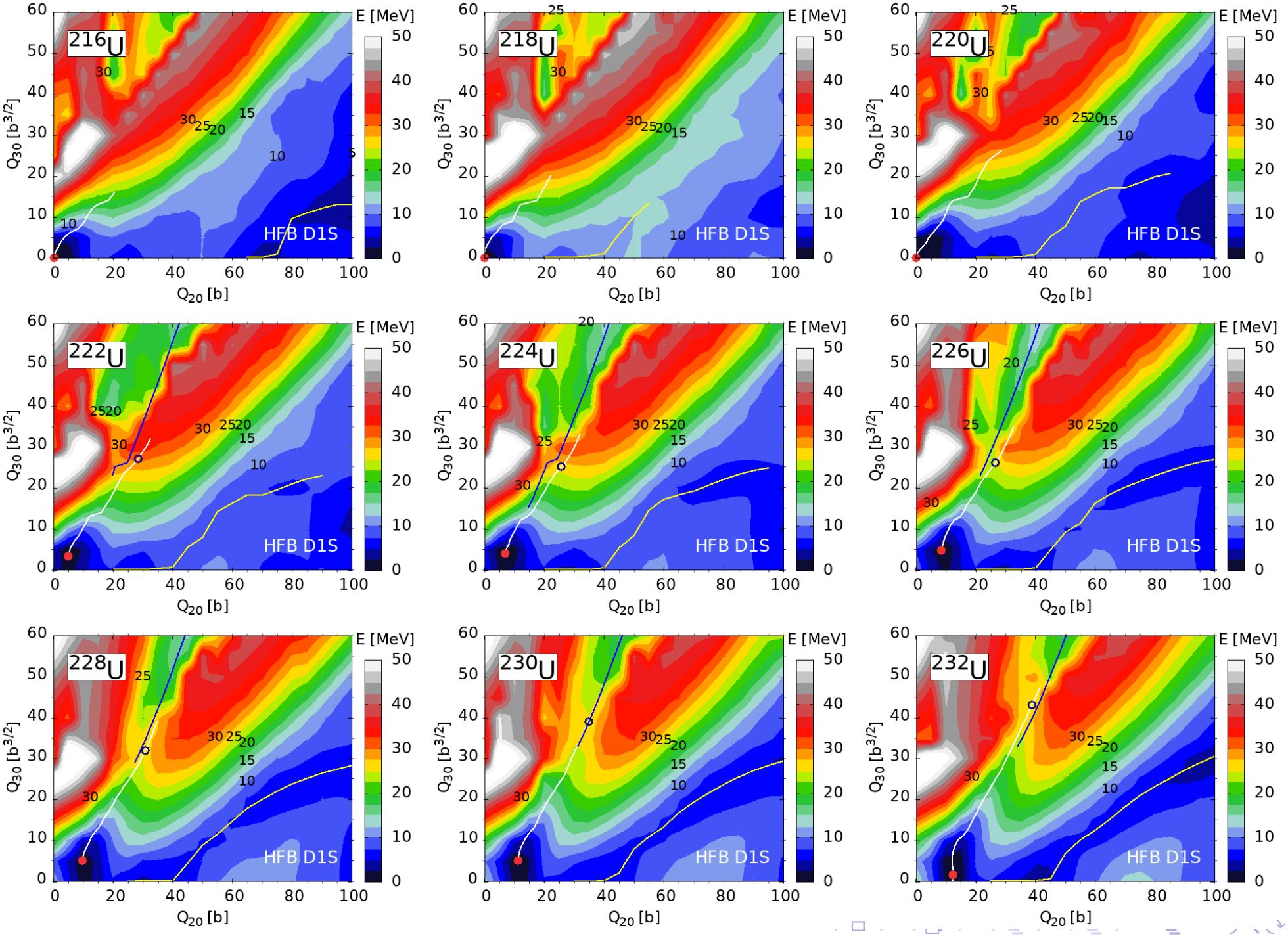
216U
218U
220U
222U
224U
226U
228U
230U
232U
HFB D1S
E [MeV]
Q20 [b]
Q30 [b3/2]

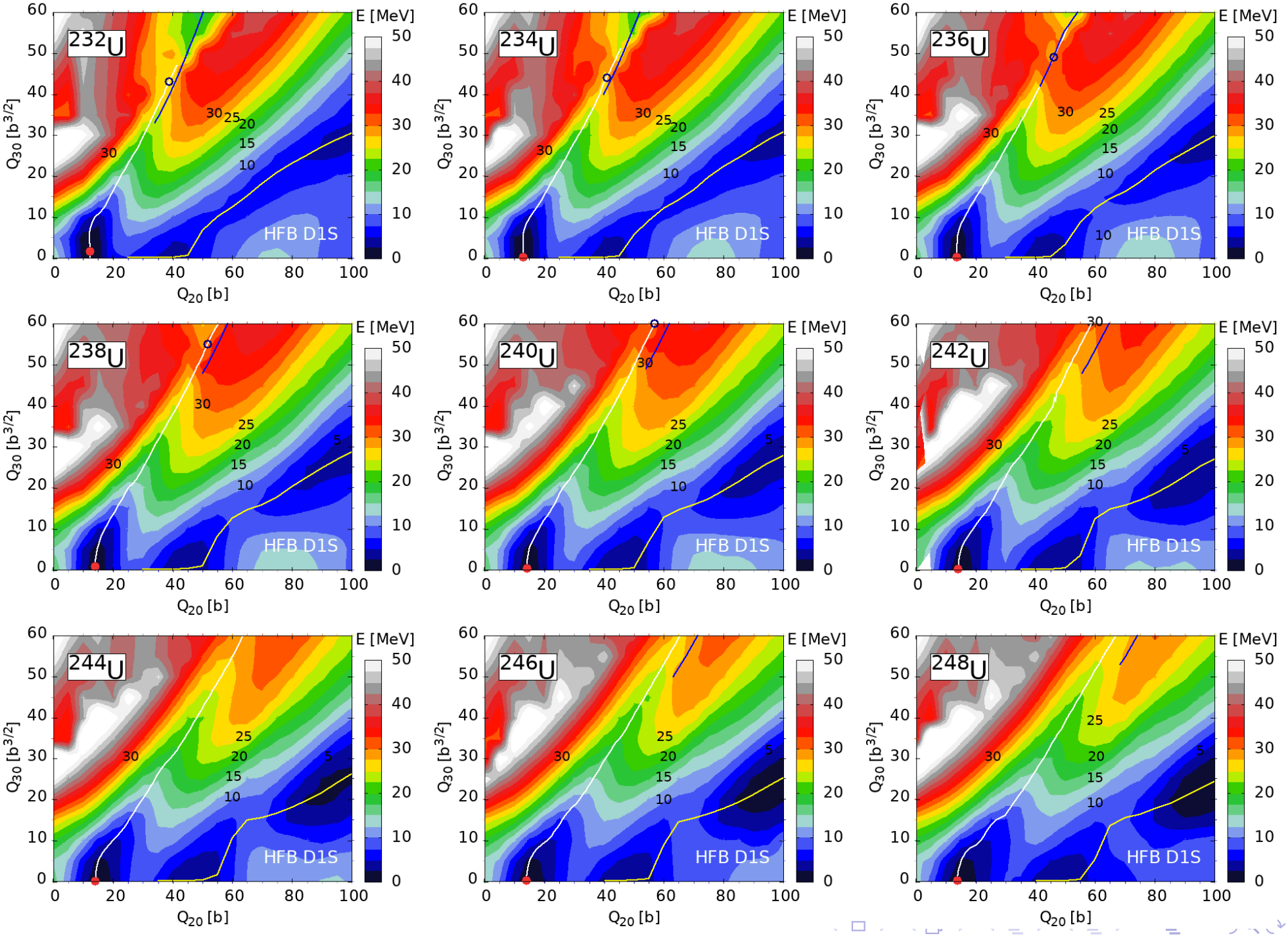
232U
234U
236U
238U
240U
242U
244U
246U
248U
HFB D1S
E [MeV]
Q20 [b]
Q30 [b3/2]

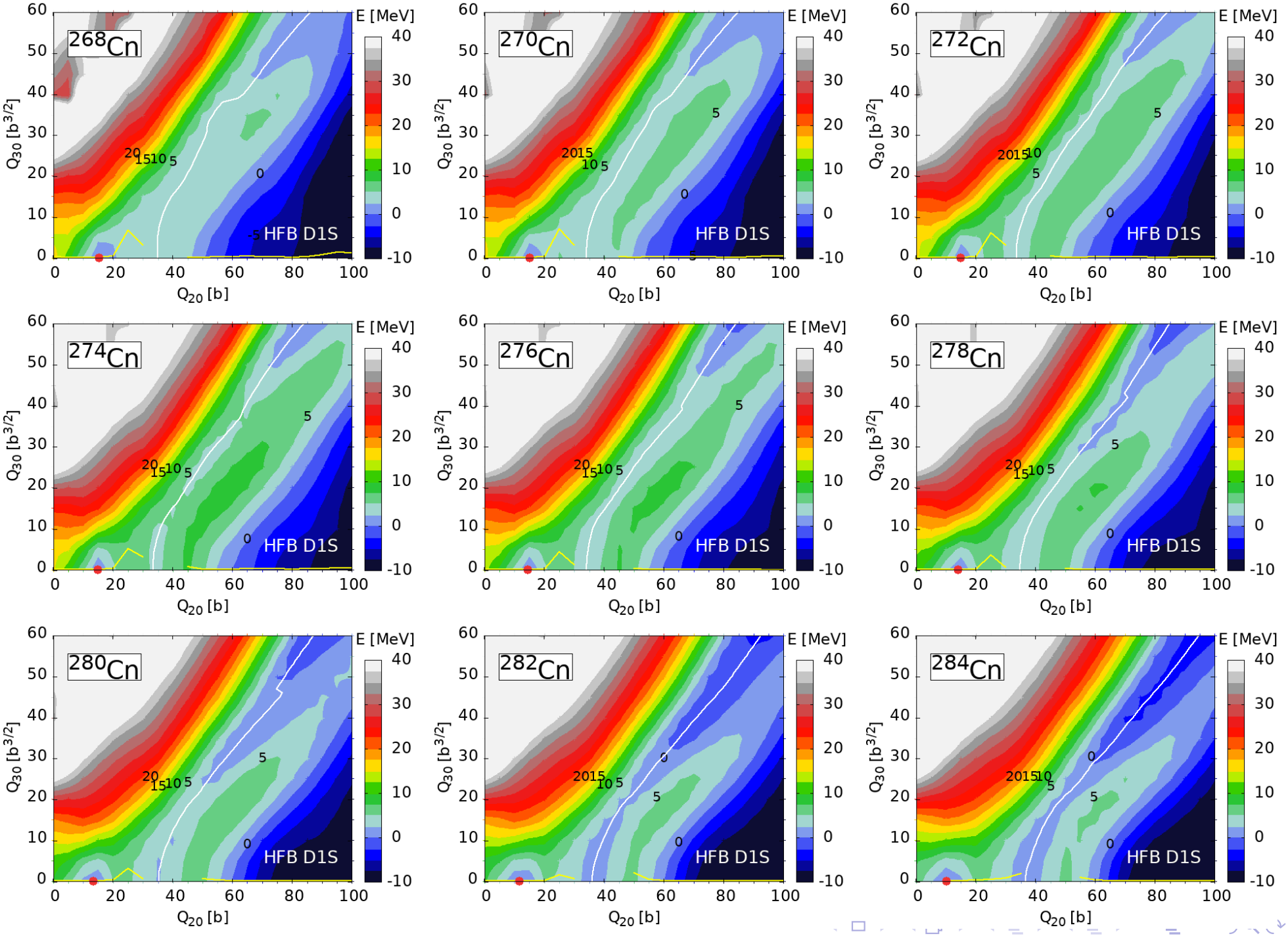
268Cn
270Cn
272Cn
274Cn
276Cn
278Cn
280Cn
282Cn
284Cn
HFB D1S
E [MeV]
Q20 [b]
Q30 [b3/2]

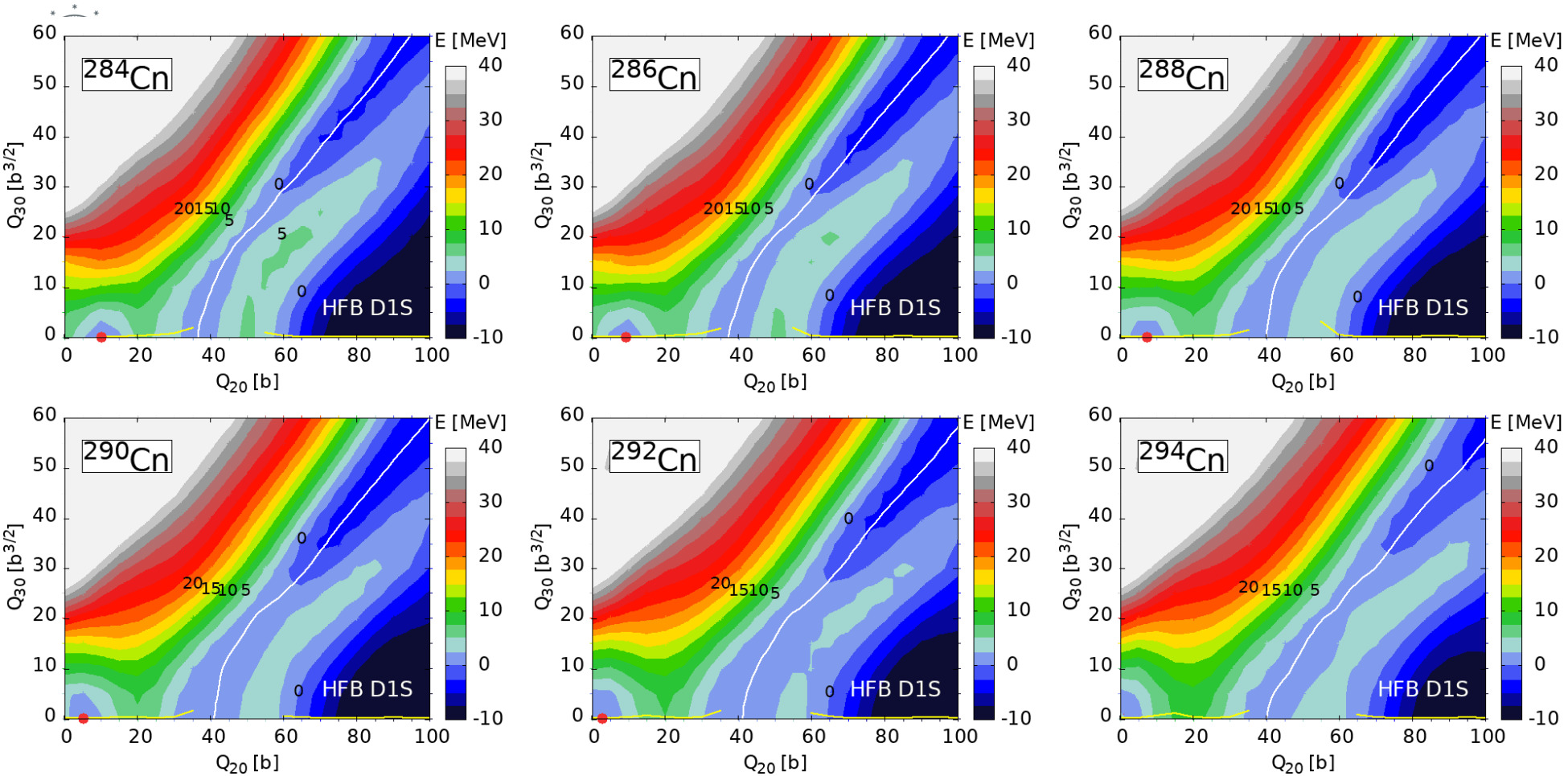
284Cn
286Cn
288Cn
290Cn
292Cn
294Cn
HFB D1S
E [MeV]
Q20 [b]
Q30 [b3/2]